Decoupled Modelling and Controller Design for the Hybrid Autonomous Underwater Vehicle: MACO

by

Jeff Kennedy
B. Eng., University of Victoria, 2002

A Thesis Submitted in Partial Fulfillment of the
Requirements for the Degree of

MASTER OF APPLIED SCIENCE

in the Department of Mechanical Engineering

Supervisor: Dr. Colin Bradley

Abstract

The autonomous underwater vehicle (AUV) MACO was developed at the University of Victoria, in partnership with Defence Research and Development Canada (DRDC) as part of a feasibility study. DRDC was interested in investigating the use of an AUV to support rapid deployment of acoustic element arrays. The requirements on the AUV to stop and hover, while triggering a low frequency sound source, lead to the multiple thruster, hybrid design of MACO.

This thesis presents the development of MACO with the primary focus on the AUV dynamics modelling and its controller design. The project commenced with the development of the vehicle's mechanical and software systems, followed by the collection of the open-loop experimental data. This data was used to produce drag and inertial parameters, which were used during the dynamics modeling process for each degree of freedom (surge, yaw, heave, and pitch). Next, discrete controllers based on PID, feed forward, and velocity feedback were added to each model along with discretely represented sensors in the feedback loop. The closed loop responses of each simulated controller were then compared with experimental response data collected during lake testing for model validation. Finally, the overall AUV mission performance was evaluated based on an analysis of path deviation error during sea trials.

Supervisor: Dr. C. Bradley, (Department of Mechanical Engineering)

Table of Contents

List of Tables

List of Figures

Acknowledgements

Many people helped make this effort a success and I would like to express my appreciation to them here. First of all, I would like to thank my supervisor Dr. Colin Bradley who gave me total freedom during the development of MACO, but ensured the project kept moving as a whole when I would get focussed on small details. I couldn't have asked for a better supervisor and mentor. Many thanks to Emmett Gamroth who put in countless hours and sleepless nights developing the software for MACO. Not to mention his loyalty during the lake testing in the rain and wind storms in our 13-foot boat; sorry about your cell phone and your calculator. Rodney Katz for all of his expert machining work and our various design discussions. Thank you for the double o-rings Rodney. Kevin Jones for helping me with various electronic conundrums and making the emergency system on such short notice. Garry Heard for his enthusiasm for the project and his patience during its completion. Pan Agathoklis for lending his control theory expertise freely. And finally my family, who probably cannot believe I am actually finished.

Dedication

I would like to dedicate this thesis to my two precious sons Ethan and Benjamin.

1 Introduction

1.1 *Unmanned Underwater Vehicle Classification*

Unmanned underwater vehicles (UUVs) are playing an ever-increasing role in oceanic exploration. The use of manned submersibles is limited, due to the very high operational cost and issues related to pilot fatigue and personal safety. UUVs generally fall into two major categories: (i) remotely operated vehicle (ROV) and (ii) autonomous underwater vehicle (AUV).

ROVs are hard-tethered to a surface support vessel by means of an umbilical cable. The umbilical cable provides a link for transferring power, communication and video between the ROV and the surface. The high number of conductors, fibres, and strength members, combined with the durable armoured jacketing required for the harsh service that they endure, results in large diameter umbilical cables. In order to be useful, the umbilical cable is several hundred metres to several kilometres in length. The combined effect produces a large drag load on the vehicle. ROVs are typically used as underwater work platforms for robotic arms, welding tools, cutters and related tools. Hence, they are designed to be maneuverable and stable; however, this results in a box-like design with very little dynamic streamlining (fig. 1). All of these limitations make ROVs unsuitable for survey work where sensors must sweep large areas.
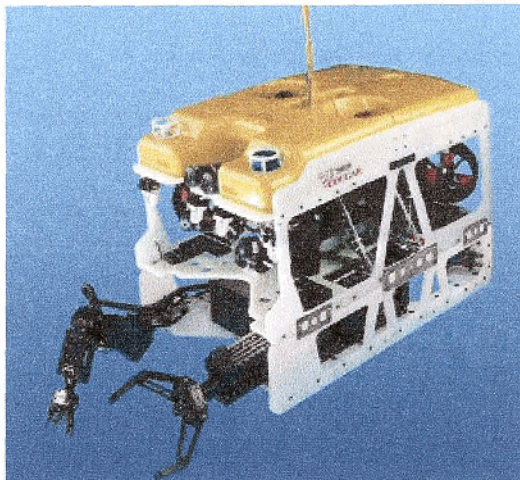
Fig. 1. The box-shaped geometry typical of an ROV [1].

The AUV was developed to meet the demand for long-range survey vehicles, principally for oil and gas exploration. Initially, AUVs were very large vehicles shaped like an

unmanned submarine, as in the example of the 35-foot AUV shown in fig. 2. These vehicles were capable of travelling hundreds of kilometres and were equipped with elaborate navigations systems, including six degree of freedom (DOF) inertial measurement units (IMU), three-dimensional Doppler velocity loggers (DVL), and a suite of other precise and expensive sensors. For example, the AUV Theseus, which laid a 190 km fibre-optic cable in 500 m depth under a 2.5 m ice pack, was equipped with: a Honeywell MAPS 726 inertial navigation unit, EDO 3050 Doppler sonar, ORE LXT low-frequency acoustic homing, and a Sonatech STA-013-1 forward-looking sonar used for obstacle avoidance [BUTLER].
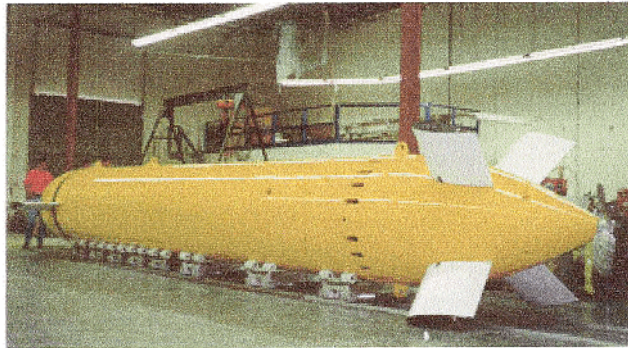
Fig. 2. The Theseus AUV used for cable laying is 10.7 m long [2].

Over the past decade, all sizes of AUVs have undergone a great deal of development for many diverse applications. Currently, AUVs fall under four main categories: survey AUVs, gliders, micro AUVs, and inspection or hybrid AUVs.

Survey AUVs are designed around a very efficient torpedo-style hull with a single tail-mounted propeller and make use of hydroplanes for control. Although they all share this configuration, survey AUVs are further subclassified by size: large, medium, and small. Large survey AUVs such as the Hugin 3000 [MARTHINIUSSEN], Autosub [STEVENSEN], and Theseus [THORLEIFSON] are in the order of 1m in diameter and 10 m long. They have design depths ranging from 1000 m to 3000 m and have long-range endurance capabilities in the hundreds of kilometres. Large survey AUVs are most commonly used for detailed mapping involving side scan sonar, cable laying, and pipeline tracking operations.
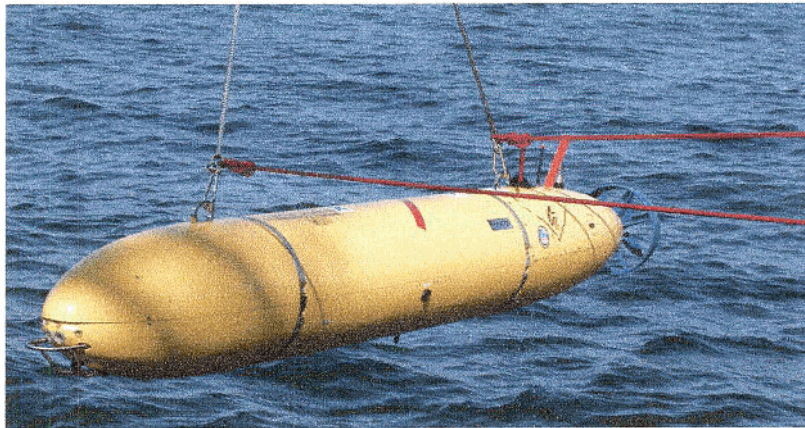
Fig. 3. The Dorado, medium-size survey AUV being deployed from a vessel of opportunity [3].

Medium survey AUVs such as the Dorado [SIBENAC], BPAUV [RISH], and Odyssey III [DAMUS], are in the order of 0.5 m in diameter and 2 m long. These are also designed for deep-water operations. The Dorado as shown in fig. 3, for example, has a working depth rating of 4500 m and the capability of going to 6000 m with special payloads. The medium-size survey class of AUVs are used in similar applications to their larger counterparts; however, they tend to have much less range. The size reduction does allow launch and recovery from a vessel of opportunity, obviating the necessity of the much larger designated ship required by the large class. As the academic and scientific interest in AUVs began to grow, a new class of smaller vehicle was developed, even easier to deploy. Small survey AUVs such as the Remus [ALLEN], Gavia [9], and Fetch [PATTERSON] are in the order of 15 to 20 cm in diameter and just over 1 m long, depending on the configuration. This category of AUV has reached a size that permits deployment and recovery by a crew of two from a small vessel, as seen in the photograph in fig. 4.
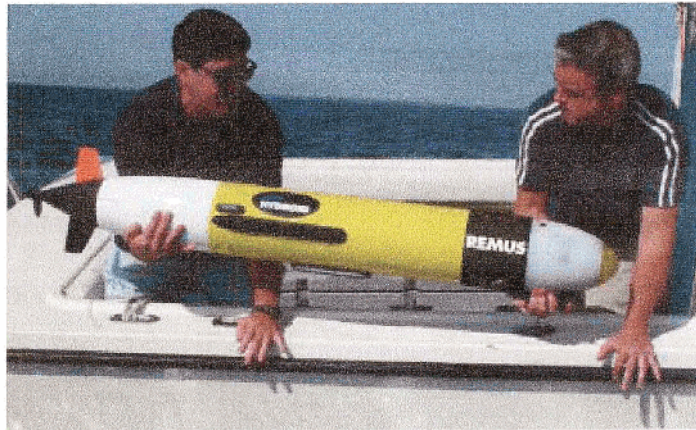
Fig. 4. The REMUS AUV being manually deployed from a small vessel [4].

These small AUVs are manufactured in limited production quantities and are proving extremely useful in numerous areas such as mapping chemical plumes [FLETCHER], military reconnaissance and mine countermeasures [STOKEY], search and rescue [TRIPP], and profiling the water column for scientific measurements of conductivity, temperature, density, and sound speed and other acoustic measurements.

Gliders such as the Spray [SHERMAN], Seaglider [ERIKSEN], and the Slocum [WEBB] are quite distinct from typical underwater vehicles in that they use buoyancy engines and ballast shifting rather that thrusters and dynamic control surfaces to navigate. They are in the order of 15 cm in diameter and up to 2 m long with hull- or tail-mounted wings of fixed attack angle (fig. 5). Gliders are designed to travel up and down through the water column over enormous distances. The Slocum, for example, was designed to glide with a 40 000 km operational range.
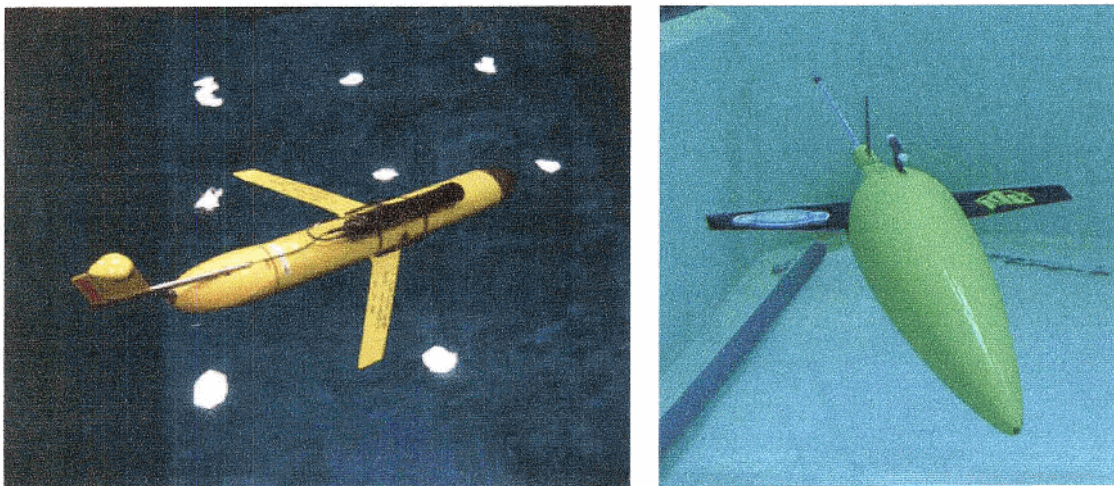
Fig. 5. Gliders a) Slocum [5] and b) Seaglider [6] during pool testing.

Micro AUVs such as the Ranger [HOBSON] and the USNA-1 [WICK] are very small, but fully capable, AUVs in the order of 9 cm in diameter and less than 1 m in length. They share a similar mechanical design to survey AUVs. The main research focus around the use of micro AUVs is swarm behavior. The goal is to use a group of micro AUVs in synchronicity to increase the spatial resolution of sampling or to track chemical plumes.

For many years, the torpedo-inspired hull design has provided hydrodynamic, and therefore energy-efficient, UUVs. However, some emerging applications require a vehicle to act as both an AUV (computer control and hydrodynamic) and ROV (3-D station keeping) during the course of a mission. For example, in some scientific applications it is desirable to vertically profile the water column at a discrete location in the mission path. The standard AUV (fig. 4) requires forward velocity for control and steering and, therefore, cannot meet these types of requirements.

Therefore, to facilitate station keeping, hovering, and vertical profiling, a new breed of UUV is emerging that integrates aspects of the AUV and the ROV. This type of vehicle is referred to in the literature as a hybrid AUV and is typified by vehicles such as Cetus [TRIMBLE], Alive [EVANS1], Swimmer [EVANS2], and the Seabed [SINGH]. Hybrid AUVs tend to be purpose built and incorporate as much, or as little, functionality from each vehicle style as required to suit the mission requirements, as demonstrated by the layout of the Cetus in fig. 6.
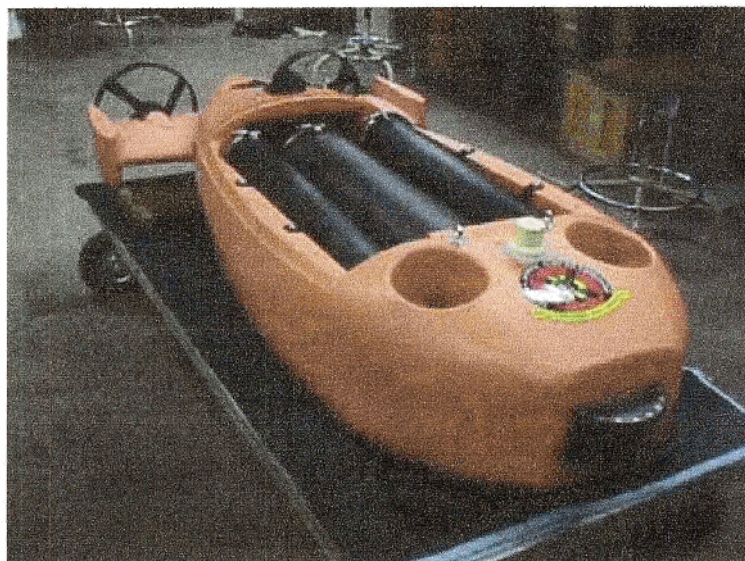
Fig. 6. Cetus hybrid AUV with two aft thrusters and two vertical tunnel thrusters in the nose [7].

A hybrid AUV has the full computing and navigation functionality of an AUV, but sacrifices hydrodynamic efficiency, and hence endurance, for increased manoeuverability. The necessary degree of manoeuverability is achieved through the addition of several thrusters to enable the type of motion found in a standard ROV (e.g., up, down, sideways and rotation).

The AUV MACO is a hybrid vehicle developed at the University of Victoria (UVic). MACO is an acronym for Multiple AUV Cooperative Operations and is derived from the research goal of developing small "fleets" of AUVs that can conduct missions collectively. As envisaged for micro AUVs, several MACO AUVs will be in communication and share common mission data related to navigation, control, communications and user requirements [BACCOU][KEMP][SINGH2][SOUSA]. MACO was initially developed in response to the expressed interest of Defence Research and Development Canada (DRDC) Atlantic in using an AUV to support their ongoing acoustics research program.

1.2 Project Motivation

DRDC Atlantic, located in Halifax, Canada, has expertise in sub-sea acoustics technology. One of their prominent research programs is the experimental validation of regularized array element localization (as described in [DOSSO]). DRDC has developed a system known as the CARBuoy, which is comprised of a self-surfacing pressure case containing a computer, batteries, and a suite of sensors and communication components. The case is part of a 200 m linear hydrophone array. The rapid deployment of the CARBuoy system involves laying the hydrophone array along the seafloor using a towed platform, followed by the release of the pressure case. The location of the array elements is not known precisely enough to allow for acoustic beam-forming and advanced signal-processing operations. To overcome this limitation a calibration routine, referred to as regularized array element localization, is performed on the deployed arrays. The current method for localization entails triggering a series of implosive sources (imploding light bulbs) in a raster scan pattern over the array. The source triggering is conducted onboard a moving ship (fig. 7).

Fig. 7. The Quest is specifically designed for open ocean acoustic research. The vessel is equipped with an ultra quiet turbine drive system to preserve the low-noise environment required during sensitive measurements [8].

The UVic hybrid AUV was proposed as the solution to the existing limitations of the DRDC research program. The vehicle was to be the "carrier" of a low-frequency (600 Hz) sound source. The vehicle and source would perform a localization mission consisting of full stops and source triggering along a predefined pattern, as illustrated in fig. 8. The benefits of utilizing an AUV for this mission are:

- logistical simplicity of deployment and recovery of an AUV.

  improved localization of the source (to within the navigational tolerance of the vehicle).

- time synchronization – having both the AUV and CARBuoy GPS time synchronized is very useful during localization calculations.

Not to scale: for a 200 m-long array, stay about 100 m on either side and 50 - 100 m past the ends. Several array crossings would be beneficial.
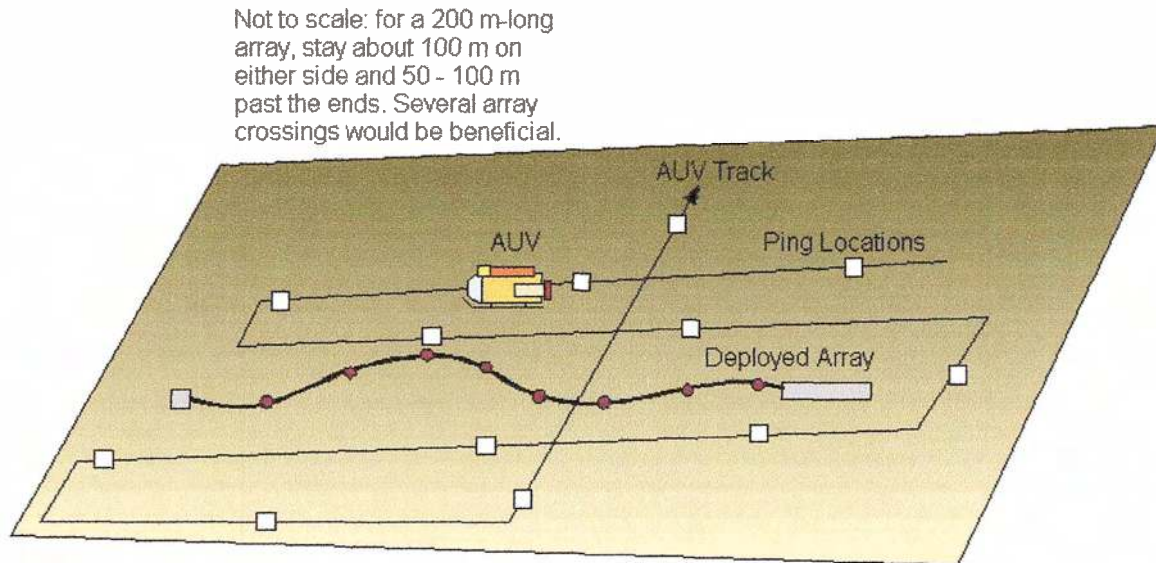
Fig. 8. The proposed AUV mission over the deployed array [9].

The enhanced localization method would be assessed during sea trials aboard the Quest, stationed in St. Margaret's Bay, Nova Scotia. The payload would be a low-frequency sound source, 0.5 m long with diameter of 13 cm and a dry weight of 8.5 kg. The mission length was to be 1500 m to 2000 m at a depth of 60 m. There would be approximately 20 full stops and a preferred completion time of less than one hour. In addition to the scheduled stops for sound source triggering, the AUV was to periodically stop and proceed to the surface to reacquire its absolute position using GPS. For this procedure to aid in navigation, it was essential that the vehicle have a minimal horizontal velocity component while moving through the water column.

1.3 Scope of Thesis

The scope of this thesis includes the development of an AUV system starting from the client's design criteria to the final sea trial evaluation in Halifax. However, the primary focus is on the process of modelling and controlling the AUV behavior. The remainder of the thesis is presented as follows and graphically depicted in fig. 9:

- Chapter 2: overview of the mechanical, hardware, and software systems
- Chapter 3: experimental determination of AUV model parameters
- Chapter 4: modelling of the AUV dynamics and individual subcomponents
- Chapter 5: utilization of the models to design continuous and discrete controllers
- Chapter 6: evaluation of the individual and overall AUV control system

• Chapter 7: conclusions and suggestions for future work
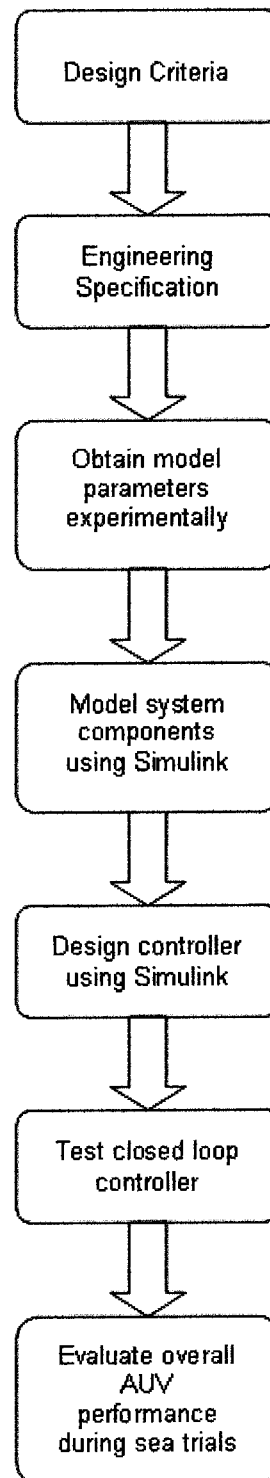
Fig. 9. Methodology for designing, modelling and testing the control system of the AUV.

2 Design of the Hybrid Autonomous Underwater Vehicle

The rationale for developing the hybrid autonomous underwater vehicle was explained in Chapter 1. The payload and typical mission characteristics, provided by DRDC, are essentially a statement of the "user" requirements to which the vehicle must conform. The application of standard engineering design techniques to the problem then requires that a design specification be created. This was not a linear process but involved consultation with DRDC to identify the needs and, thereby, produce an engineering specification that accurately reflected the requirement. In the interest of brevity, the design process is not described in this document; however, the resulting design specifications are presented in table 1.

The design specifications translate the qualitative needs of the user into quantitative engineering data wherever possible. The performance specifications provide detailed design goals and dictate important functional parameters. For example, the thrusters must be used to turn the vehicle, to any compass heading, while the vehicle is stationary. This is in contrast to traditional AUV designs where a single thruster and control surface (rudder) is used to turn the vehicle. Another important design goal to evolve from this process is the requirement that the vehicle hover (with no forward velocity) at any prescribed depth (in order to record the low-frequency sound source emitting a signal at a precise location). The resulting design has two vertical thrusters that enable hovering. Overall, this de-coupled thruster configuration is an important result of the design process.

The navigation system specifications are principally driven by the cost constraint of the user. A larger development budget would have enabled more accurate sensors to be employed to implement the dead reckoning method. For example, a Doppler velocity log could have been used to provide more accurate surge velocity readings, but a less expensive flow meter is employed.

The control and computer system specifications contributed to the most straightforward design decisions. They were based on the need and available components.

Table 1. Design specifications based on the user's requirements.

Performance Specifications	
Maximum Speed	1.5 m/s
Operating Depth	60 m
Endurance	Propulsion: 2.5 hours @ 0.9 m/s Computer: 10 hours
Mission Length	1500 m
Mission Patch Geometry	Raster scan path
Positional Accuracy (x y)	+/- 1% mission length
Positional Accuracy (z)	+/- 0.5 m
Payload Capacity	Low-frequency sound source Weight: 8.5 kg dry, 4 kg wet Size: 0.5 m long, 13 cm in diameter
Special Requirements	• Hovering without vehicle forward velocity • Turning without vehicle forward velocity

Navigation Specifications	
Type of Navigation Used	Dead Reckoning
Measured Position/Motion	Required Sensor
Surge Velocity/Displacement	Doppler Velocity Log (DVL) or Flow meter
Yaw Velocity	Gyro
Heading	Magnetometer
Pitch and Roll	Tilt sensors
Depth	Pressure transducer

Control System Specifications	
Controller Type	PID
Controlled DOF	Surge, Yaw, Heave, and Pitch
Type of Actuator	DC Thrusters
Number of Actuators	4
Cross Coupling	Heading + Surge, Pitch + Heave

Computer System Specifications	
Processor	Pentium (minimum)
Operating System	Real Time
I/O	Analog and digital
Serial Ports	3 (minimum)

The following sub-sections detail the mechanical, hardware and software systems of the hybrid vehicle. The sections each commence with an overview of the specific components and then provide a description of the techniques implemented to develop the vehicle. The chapter's objective is to provide a sufficient explanation of the vehicle development and manufacturing process in the context of the following, and more important thesis topic, of vehicle control.

2.1 Mechanical Design

The mechanical layout of MACO is shown in fig. 10. The overall vehicle geometry is based on the key requirement that hovering and turning must be possible independent of forward velocity. Typically an AUV design is similar to that of a torpedo, using a tail-mounted thruster to provide forward propulsion. The forces required for turning and diving are developed using control surfaces such as rudders and an arrangement of fore and aft hydroplanes. This configuration allows for a very streamlined, and therefore very hydrodynamically efficient, hull design. The drawback of this type of dynamic diving/turning system is its dependence on sufficient forward speed for operation.

A remotely operated vehicle (ROV) makes use of a multiple thruster configuration with significant physical separation between thrusters to maximize the available control torque. Using independent thrusters in effect decouples the association between the different degrees of freedom, but the large thruster separation usually results in a box-shaped vehicle with high drag characteristics.
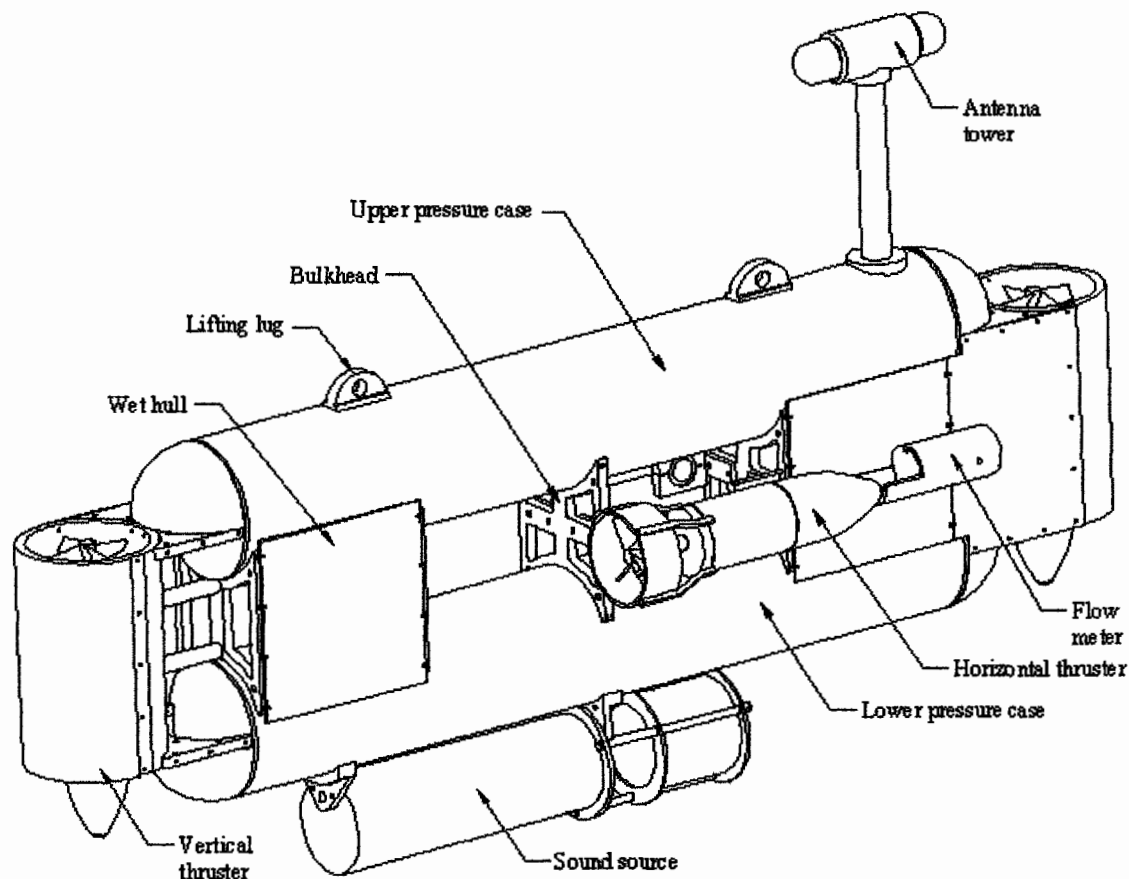
Fig. 10. Mechanical component layout.

MACO is a hybrid vehicle design that borrows attributes from both the traditional ROV and the AUV to meet its functional requirements. MACO implements a decoupled arrangement with two vertical thrusters used to control the pitch and depth of the AUV and two horizontal thrusters used to provide forward propulsion and the required turning torque. To minimize drag, MACO has a long slender hydrodynamic body with a 10:1 length-to-width ratio. Furthermore, the vertical thrusters are contained completely within the hull profile and the horizontal thrusters are located adjacent to the hull to minimize parasitic drag while still providing MACO with adequate turning capability. Table 2 contains details about MACO's physical size and construction as well as the key mechanical system components.

Table 2. MACO's physical characteristics and mechanical design information.

Size	1.5 m long, 0.41 m wide, 0.44 m high (excluding tower and sound source) Tower is 0.29 m high
Weight	70 kg dry, -0.25 kg wet (excluding payload) Sound source is 8.4 kg dry, 4 kg wet
Body	PVC construction throughout with the exception of anodized aluminum pressure case endcaps and thruster brackets
• Instrument housings	Provide 1 atmosphere environment for computer equipment, electronics, batteries, speed controllers, etc.
• Wet hull	Removable side panels provide hydrodynamics and access to add/remove flotation or payload.
• Bulkheads	Structurally connect pressure casings and provide mounting for thrusters and other peripherals
Thrusters	Aluminum housing, 1800 rpm, 100 mm 4-blade tunnel propellers
• Horizontal	Open thrusters with cowling, 35N forward thrust, 28N reverse thrust
• Vertical	Tunnel thrusters, 22N forward thrust (down), 28N reverse thrust (up)

2.2 Navigation and Control System Hardware

The internal hardware encompasses the PC-104 stack, sensors, and electrical components. Fig. 11 illustrates the basic association of hardware components.
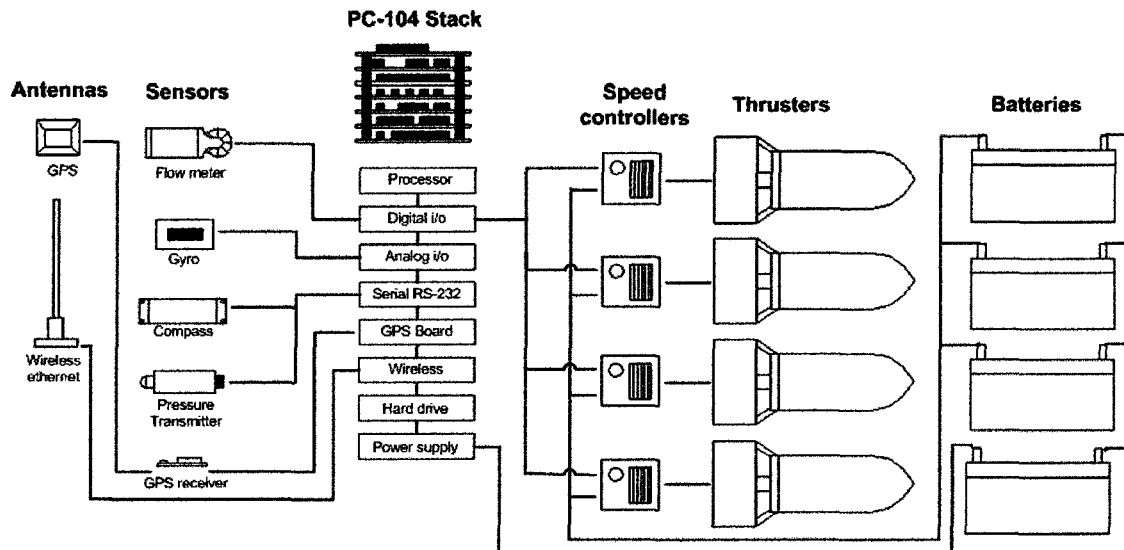
Fig. 11. Hardware connection diagram

For reference, table 3 contains the specifications for the hardware components.

Table 3. Electrical and electronic components used in MACO's navigation and control system.

Embedded Controller – PC-104 Stack	
Processor board	Advantech: PCM3350, AMD Geode CPU Module with VGA/ LCD, Ethernet & SSD
Digital i/o board	Diamond Systems Corporation: Quartz-MM, Advanced Counter/Timer and Digital I/O PC/104 Module
Analog i/o board	Diamond Systems Corporation: Diamond-MM-32-AT, 16-bit Analog I/O PC/104 Module With Autocalibration
RS-232 expansion board	Advantech: PCM-3643, 4/8 RS-232 COM Port Module
GPS carrier board	Tri-M: GPS104, GPS Compatible PC-104 Carrier Board
PCMCIA board	Aaeon: PCM-3115B, PCMCIA dual slot PC-104 Module
Wireless 802.11b	Lucent Technologies: Orinoco Gold (PCMCIA)
Hard drive	12 GB hard drive
Power supply	Tri-M: V104-512-16, PC/104 Vehicle Power Supply

Sensors	
Flow meter	Seametrcs: TX80, turbine-type flow meter, hall effect sensor, output 12VDC sinking, input: 12 VDC, polypropylene construction
Gyro	Systron Donner: Horizon, monolithic quartz sensing element, output: 0 to 5 VDC, input: 8 to 15 VDC, range: +/- 90 deg/s
Compass	Honeywell: HMR3000, magnetoresistive sensors, liquid tilt sensors, output: RS-232 at 20 Hz, input: 12 VDC, accuracy: 0.5°, resolution 0.1°
Pressure transmitter	Wika: D-10, strain gage type, output: RS-232 at 13 Hz, input: 12 VDC, range: 10 bar, linearity: 0.1% FS
GPS receiver	RoyalTek REB-12R Series

Electrical Components	
Batteries	Panasonic: LC-RA1212P, lead acid gel cells, 12 V, 12 Ah
Speed controllers	Robbe: 8423, output: 0 to 12 VDC 30 A continuous, input: 12 VDC and 1 to 2 ms pulse at 60 Hz
Thrusters	10 A @ 12 V

2.3 Software

The MACO software system is comprised of the following major sub-systems:

- Graphical user interface (GUI)
- Mission scripting language
- Control software running on the AUV

2.3.1 Graphical User Interface

The graphical user interface (GUI) was created using virtual instruments in LabVIEW 6i. The GUI affords the operator with a high level of control, from remote operation of the vehicle to setting low-level controller parameters. In addition, the GUI provides user-selectable sensor status for real-time monitoring. As a sample, fig. 12 shows the ROV control screen of the user interface. While in ROV mode, MACO can be controlled by a handheld joystick or by using the GUI pulse control, which is mapped to the arrow keys on the laptop.
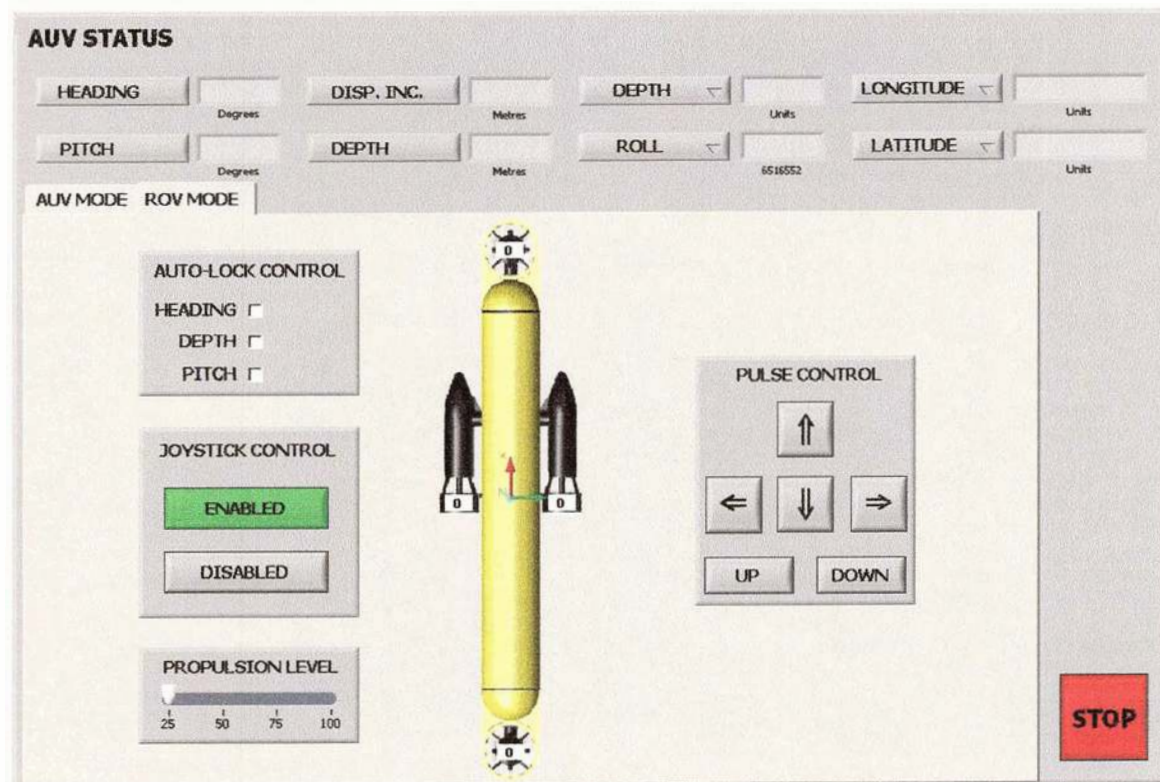
Fig. 12. The graphical user interface in ROV mode allows manual control of MACO.

The GUI has the following two main modes:

1. AUV Mode: This is used to upload and initiate mission and initialization script files.

2. ROV Mode: Using this, MACO can be controlled at depth while tethered or on the surface via wireless modem.

2.3.2 Scripting Language

The scripting language used for mission creation and control system initialization is called LUA 5.0.2. It allows a series of commands to be executed in a free-flowing sequence or with completion flag verification between commands. The use of a scripting language has several key benefits. One such advantage is the ability to compose complex missions that include program loops, sensor monitoring, and calculations that can be executed without recompiling system software written in C. This is invaluable from a system stability standpoint and, for an AUV, a system crash can mean losing the vehicle. LUA also enables high level commands with intuitive names to be created by grouping low level commands or even including program loops. For example, a saw tooth pattern (fig. 13) command could be generated that simply took tooth-pitch, depth 1, depth 2, and number of teeth as inputs.
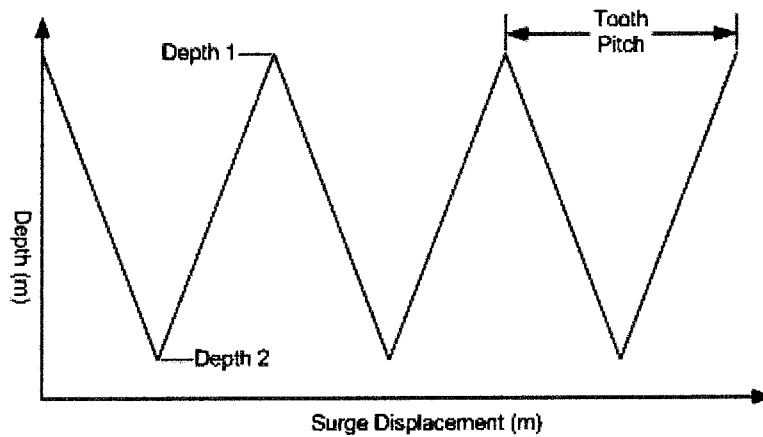
Fig. 13. Saw tooth pattern used in vertical profiling.

Within the command, controllers would be turning on and off, setpoints would be calculated and set, and sensor data could be recorded in a log file. The saw tooth pattern is a commonly used technique to extend vertical profiling of the water column to provide a planar resolution.

In addition to creating missions, scripts were also used for system initialization. Rather than hard coding system default parameters or entering them in manually using the GUI, a single initialization script was written that included all system and controller settings. The initialization script, or any mission script for that matter, can be modified using a standard text editor.

2.3.3 Control System Software

The AUV computer is running a QNX 6 real-time operating system. The control system software was written in the C programming language, which is transferable to any other platform. Fig. 14 illustrates the architecture of the control software developed for MACO.
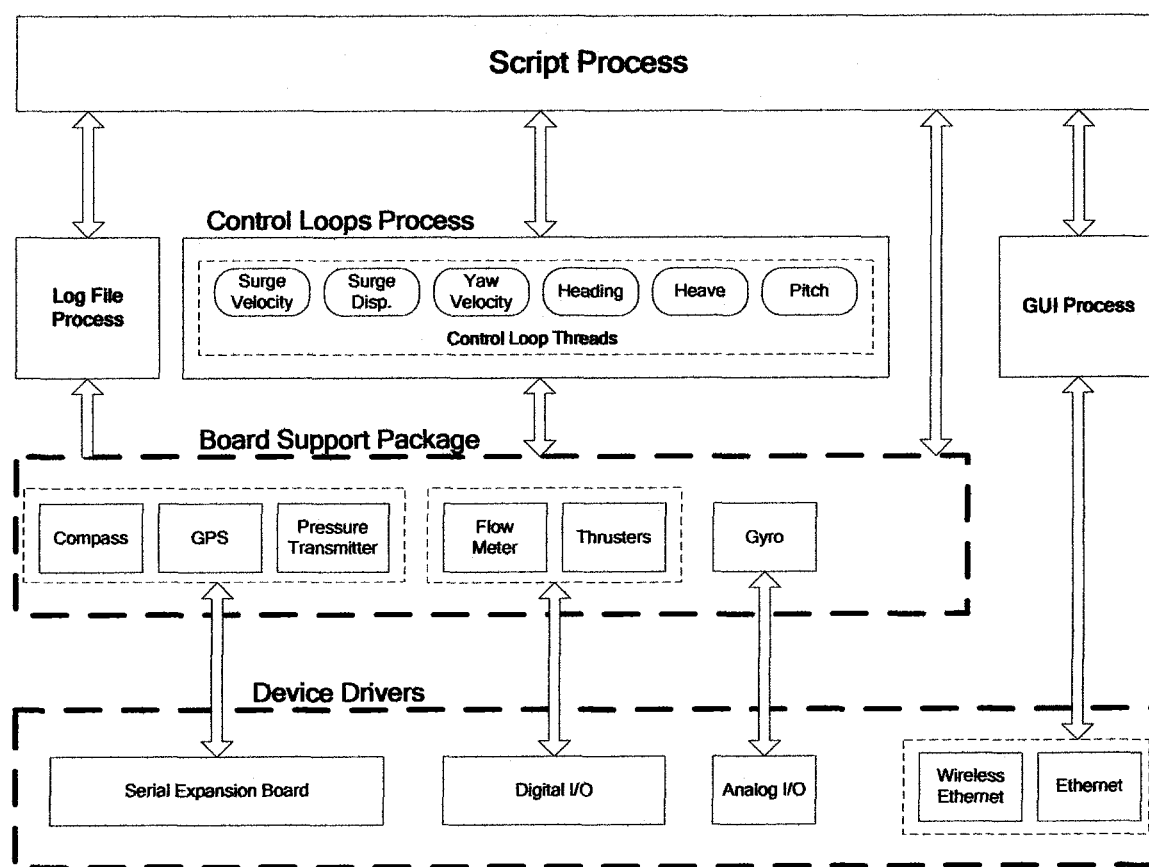
Fig. 14. Control system software architecture developed for MACO.

The software was written as a combination of processes running internal threads, with expandability as the design priority. Within the board support package, each sensor is written as a separate process with a standard communication interface. Creating a new

process for each sensor allows sensors to be added or removed without affecting the operation of existing sensors or of the controllers that access them. Because each process communications interface is the same, any controller can be seamlessly linked to any sensor without the issues of data protocol compatibility.

3 Experimentally Determined AUV Model Parameters

In addition to the information generated using CAD, very useful results can be obtained through water testing. Experimentation with the actual components accounts for all of the factors that are not included or correctly represented in a solid model.

To begin the testing process, the thrusters were characterized. This involved obtaining the steady-state input/output relationship and the step response characteristics of the thrusters. Next, the flow meter and pressure transmitter were calibrated to measure the motion of the AUV. Then the AUV was run through a series of open-loop, step-response trials for each DOF. The results of the open-loop trials were essential when validating the dynamics model.

3.1 Thruster Characterization

The thruster testing involved two steps. The first step involved determining the steady-state thrust output for a given input to the thruster drivers. The second step consisted of determining the transient response to a step input followed by a negative step input.

3.1.1 Thruster Steady-state Output

The objective of the steady-state output testing was to determine the thrust delivered by the thruster and thruster driver combination. This information was required to linearize the input output relationship and determine the maximum output in each configuration. A linear output simplifies controller design. The maximum output or saturation of an actuator is essential information to ensure that the controller is realistic and does not go outside of the controllable range.

To control the thrusters, the computer sends integers ranging from -100 to +100 to the digital input/output board. The board then outputs a series of pulses at 60 Hz with a pulse width ranging from 1 to 2 ms, which produces a +/- 12 V motor driver output. Centering the pulse width at 1.5 ms provides a no output. The steady state thrust output was measured at integer steps of 10% for the full range in both the positive and negative directions.
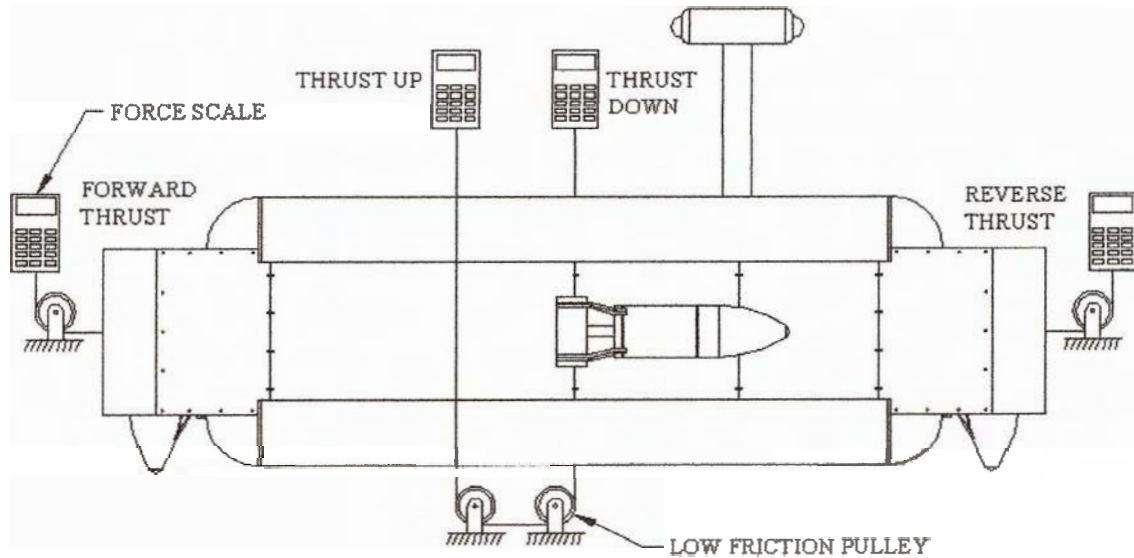
Fig. 15. Thrust measurement configurations.

The thrust was measured for the following four DOFs: positive surge, negative surge, positive heave, and negative heave (fig. 15). The moments generated for the rotational DOF, pitch and yaw, were determined using the measured thrust and the thruster spacing.

To measure the thrust accurately, an apparatus was constructed using a strain-gage-based force scale connected to the AUV with low friction pulleys and cord (fig. 16). The apparatus was secured to the poolside and the AUV was controlled in remote control mode using the tether and graphical user interface. It was particularly important to test the thrust using the entire vehicle. Early tests were conducted using an independent thruster in a tank attached to a force measurement device. Because the water flow through the thruster was not affected by the AUV hull, the thruster output was approximately 8% higher.
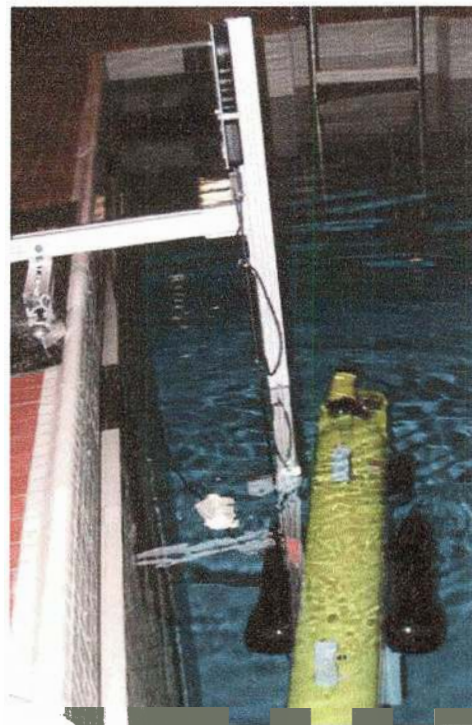
Fig. 16. Thrust measurement apparatus

Fig. 17 contains the results from the steady-state testing. The thrusters exhibit a dead zone, in which the propellers do not begin to turn until 15% and only begin to deliver a measurable thrust at 20%. This dead zone is primarily caused by the friction of the shaft seals. The remainder of the thruster response was then fit using a cubic polynomial.
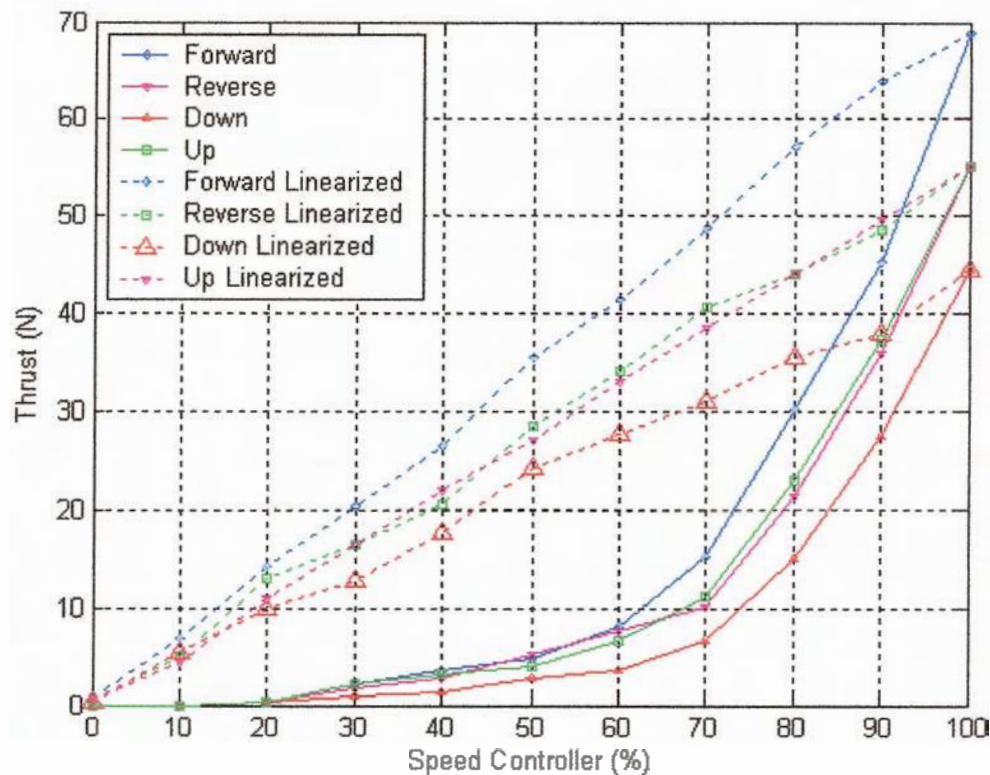
Fig. 17. Steady-state thruster output before and after linearization.

The offset between curves of the same DOF is a result of propeller bias. The propellers have 25% better performance in one direction. The negative effect the vertical thruster tunnels have on the output is also quite apparent (fig. 17). If not for this effect, the forward and reverse would have the same output as down and up respectively.

To achieve a linear response, the outputs were scaled such that the maximums were 100. Then the linear percent input was plotted with respect to the scaled output, and the resulting curve was then fit with a sixth order polynomial. By using the polynomial to precondition the linear input, a linear thrust output results, as shown by the dashed lines in fig. 17.

3.1.2 Thruster Transient Response

The objective of this test was to determine the transient response of the thrusters. As with any mechanical system, the thrusters suffer from a definite delayed response when actuated. Knowing that the thrusters do not respond instantaneously, and modelling them as such, improves the accuracy of the simulation.

The delay is most evident when full forward to full reverse is performed. To demonstrate this, a tachometer was fabricated to provide propeller velocity. The tachometer was comprised of a proximity sensor mounted to the propeller shroud and a shaft extension with a magnetic tip attached to the propeller shaft (fig. 18).

SHROUD —

PROXIMITY
SENSOR

PROPELLER —

MAGNET IN SHAFT
EXTENSION
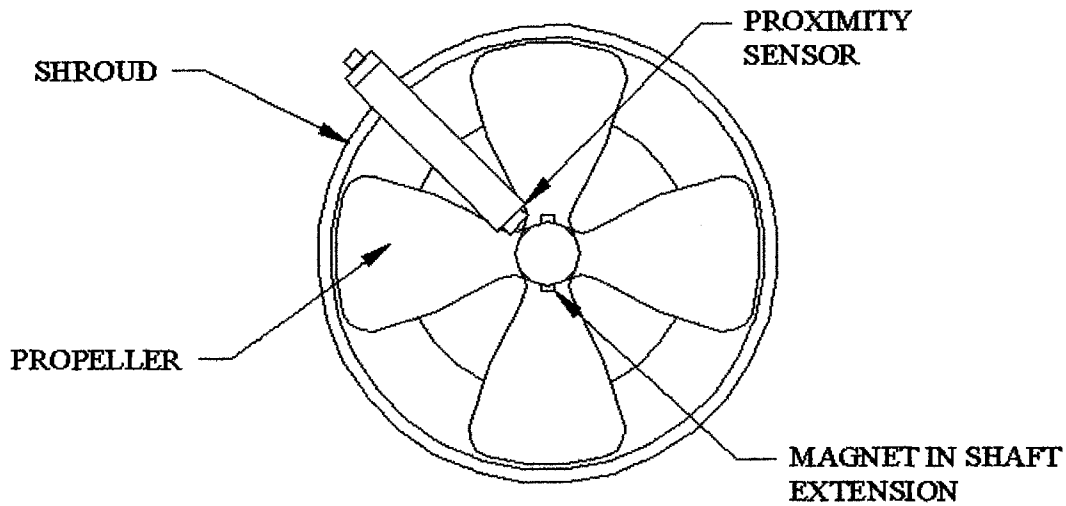
Fig. 18. Placement of the proximity sensor tachometer.

The tachometer provided two pulses per revolution, which were monitored using a data acquisition card. The thruster was given a maximum step input in the clockwise direction for two seconds (2 s) and then an equivalent step in the counterclockwise direction for the same period. The thruster response can be seen in fig. 19.
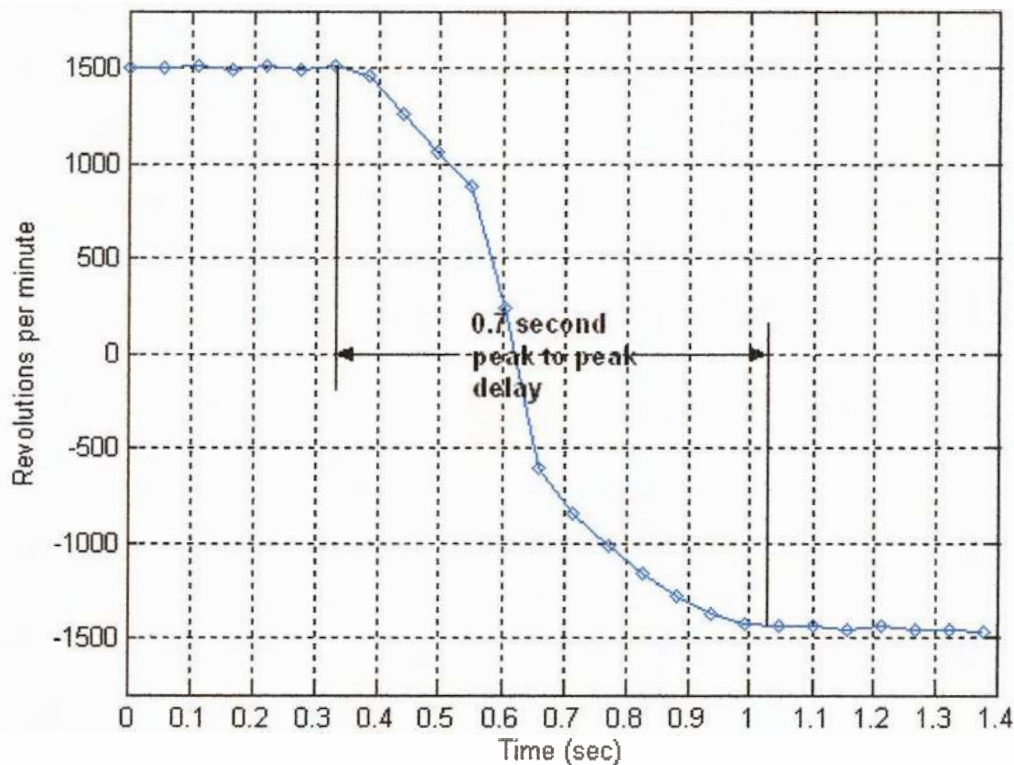
Fig. 19 Transient response of the thruster to a 100% positive to negative input swing.

Because thrust is produced during acceleration and deceleration regions, the transient response is best approximated as a rate limited slope as opposed to a pure delay. Maximum thrust occurs when the propeller is at maximum angular velocity. In view of that, the slope of the rate limiter for each DOF and sense can be calculated as shown in equation 1. The only exceptions are the pitch and yaw, where the maximum moments are used in place of maximum thrust.

$$T_{RATE} = \frac{T_{MAX}}{\omega_{MAX}} \times \alpha \qquad \qquad \textbf{Equation 1}$$

Where:

T_{RATE} = Rate of change of thrust
T_{MAX} = Maximum steady-state thrust
ω_{MAX} = Maximum angular velocity
α = Average angular acceleration as taken from fig. 19

3.2 Sensor Calibration

The flow meter and pressure transmitter are high-quality sensors, but the outputs are not in useful engineering units. The testing described in the following sections was carried out to find the required scaling and offset values for each sensor.

3.2.1 Flow meter

The flow meter is a turbine style with eight blades, four of which have an embedded magnet. The body of the flow meter contains a hall-effect sensor that emits a pulse each time a magnet passes. Therefore, a given flow rate of water produces a pulse train with a certain frequency output.

To determine the correlation between the forward velocity of the AUV and the frequency output of the flow meter, a number of constant-velocity tests were conducted. The horizontal thrusters were activated at six thrust levels ranging from 50% to 100%. Once the AUV reached constant velocity, the time was recorded for a displacement of 20 ms. At the same time, the AUV computer logged the frequency output of the flow meter. Fig. 20 contains the resulting data points as well as the calibration constant for the flow meter.
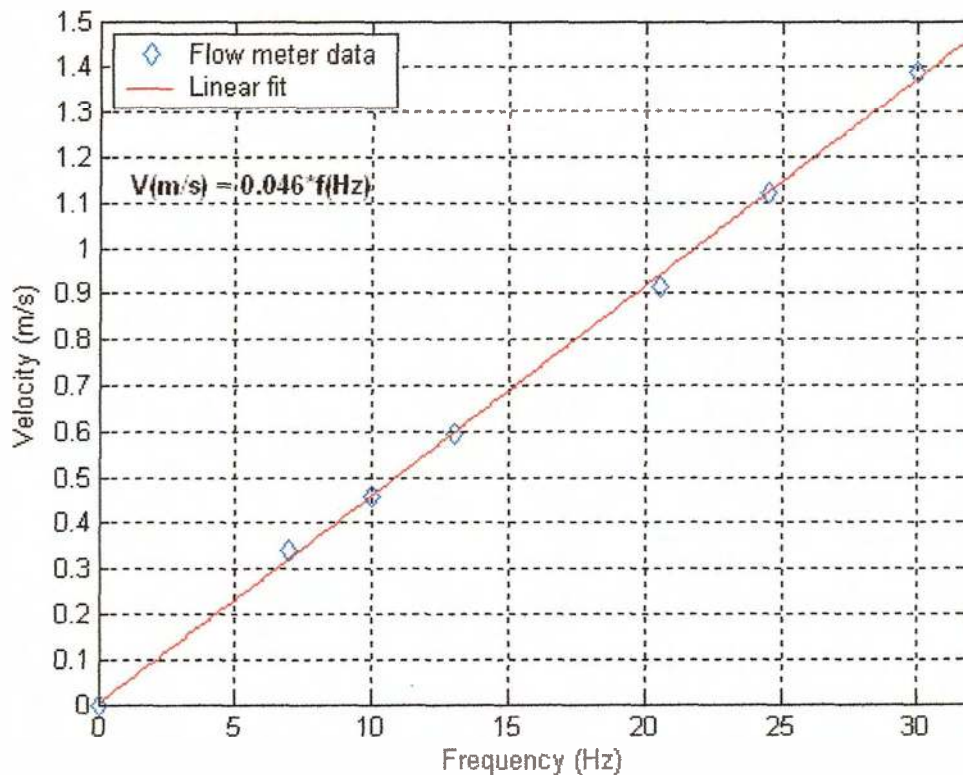
Fig. 20. Calibration data for the Seametrics flow meter.

3.2.2 Depth Sensor

A pressure transmitter is used to measure depth. It is a membrane-strain-based transducer with RS-232 serial output. However, the number representing pressure is of arbitrary scale and starting point; therefore, a scaling factor and constant offset were required. The sensor was calibrated by taking pressure measurements at five known depths. This was done by attaching a measuring tape to the AUV and then running the vehicle down to various depths in remote control mode. The AUV then kept tension on the tape measure while readings were taken from the GUI. Fig. 21 contains the resulting data points as well as the scale factor and offset for the depth sensor.
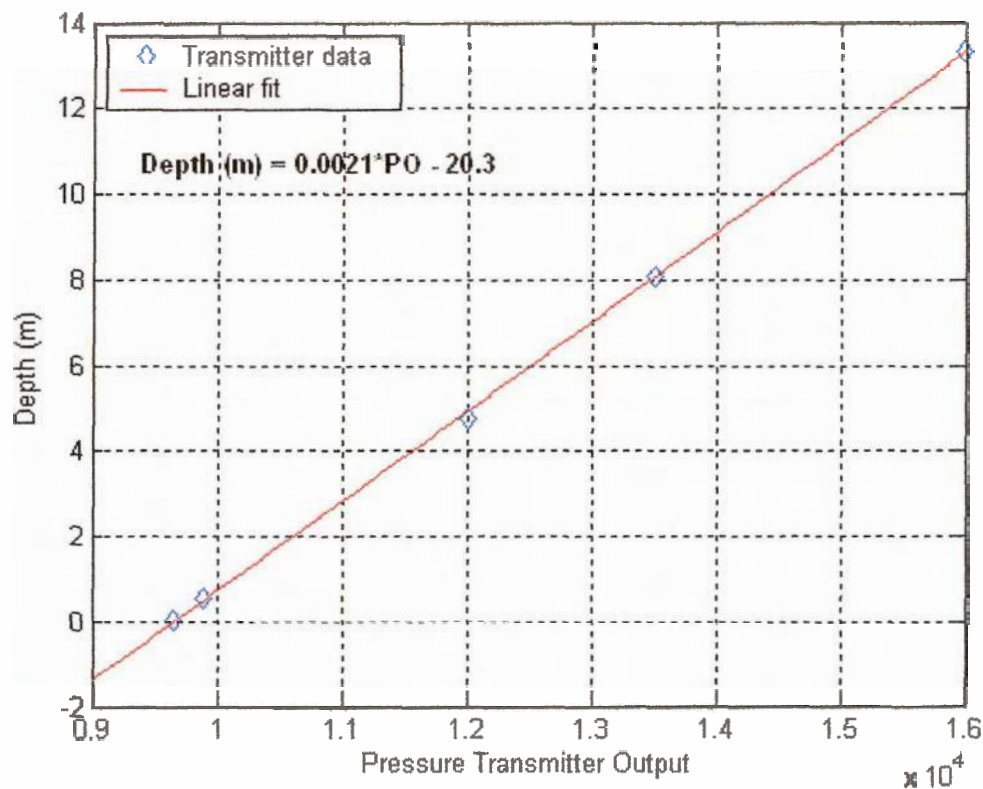
Fig. 21. Calibration data for the Wika D-10 pressure transmitter.

3.3 Vehicle Characterization: Drag, Inertia, and Righting Moment

Velocity step response data was collected for: surge, yaw, heave, and pitch. A test was also performed to determine the righting moment for pitch. The step response can provide crucial drag and inertial information for modelling a system.

The first objective of the step response tests was to obtain the maximum velocities for known thrusts. This is useful because the drag is equivalent to the thrust at that speed.

By plotting these data points, the drag at any velocity within the vehicle's range can be predicted. The drag coefficients were used both in modelling the AUV dynamics and feed forward controller design.

The second objective of the step response tests was to obtain the transient response curves, which were used for validating the models. Because the drag effects of the transient response can be isolated, the mass or inertial term in the model can be adjusted to bring the modelled responses in line with the experimental data.

The step responses for each DOF were collected at ten thrust levels ranging from 10% to 100%. The results were plotted and the drag and velocity information was assembled to form a second plot.

3.3.1 Surge

The steady-state velocity in surge was recorded for open-loop thrust levels ranging from 10% to 100%. The results are plotted as two sets of five data sets for clarity (fig. 22). The flow meter provides velocity data that is somewhat noisy. The steady-state velocity was also confirmed by taking the slope of the steady-state portion of the corresponding displacement plots.
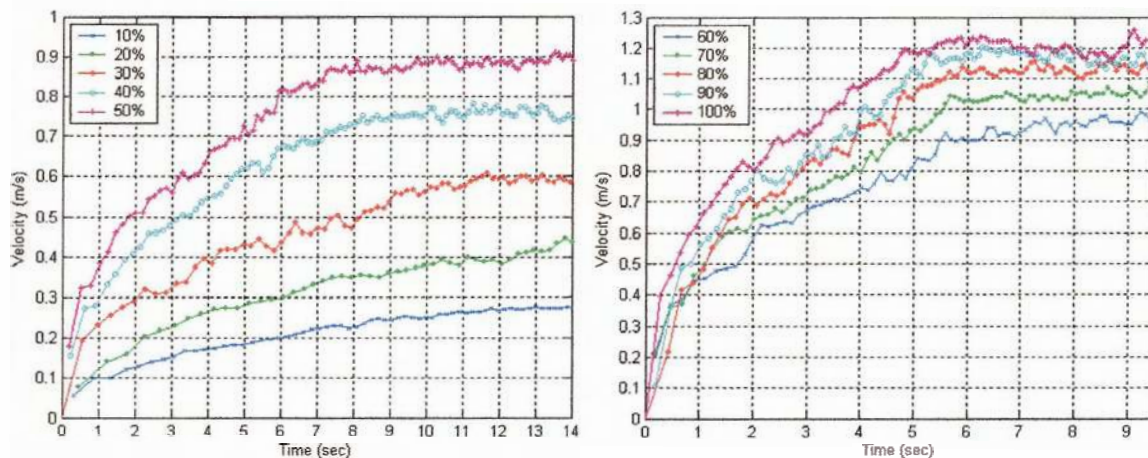
Fig. 22. Velocity step responses to 10 constant thrust levels.

Using the steady-state velocity data from fig. 22 and the corresponding open-loop thrust levels, a chart showing drag vs. velocity was generated (fig. 23).
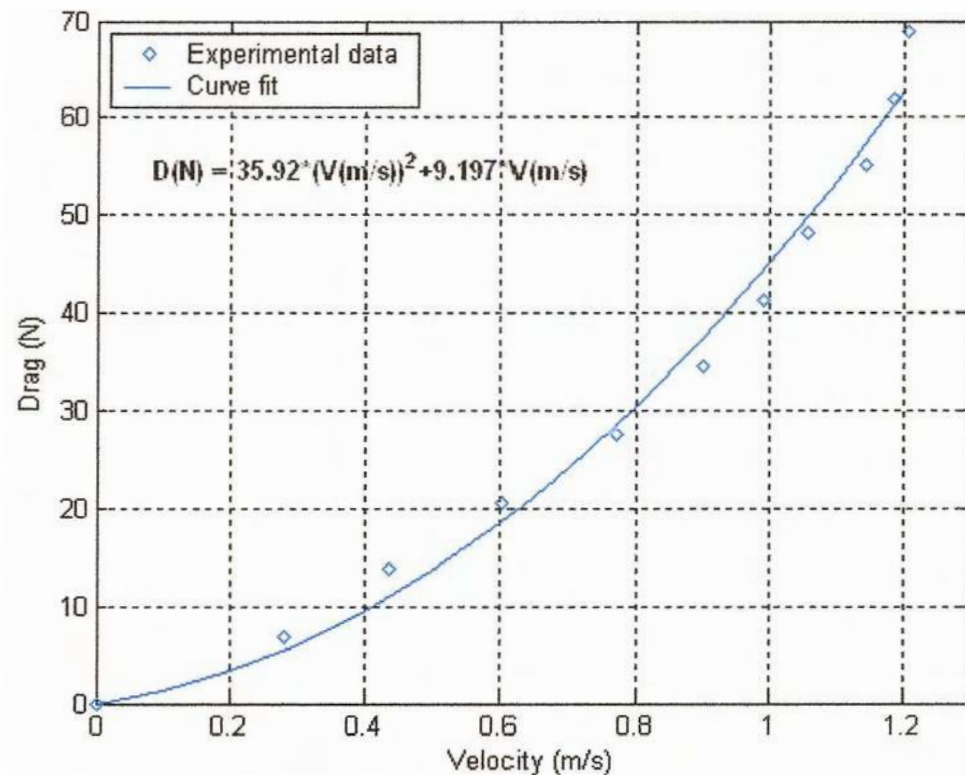
Fig. 23. The drag-velocity relationship in surge.

The fit is reasonably good and was used to model the drag characteristics for surge in the dynamics simulation.

3.3.2 Yaw

The steady-state angular velocities in yaw were recorded for open-loop torque levels ranging from 10% to 100% and are shown in fig. 24. The gyro measures rate in one axis only and provides stable readings when constrained to that axis. When the AUV is in free water, it suffers from a certain amount of roll. It is this oscillatory rolling that is projected onto the rate data shown in fig. 24. As was done with the surge data, the steady-state velocity was also confirmed by taking the slope of the steady-state portion of the corresponding displacement plots. The displacement plots were generated by two means: i) by integrating the gyro data and ii) by taking information directly from the compass, which is roll compensated.
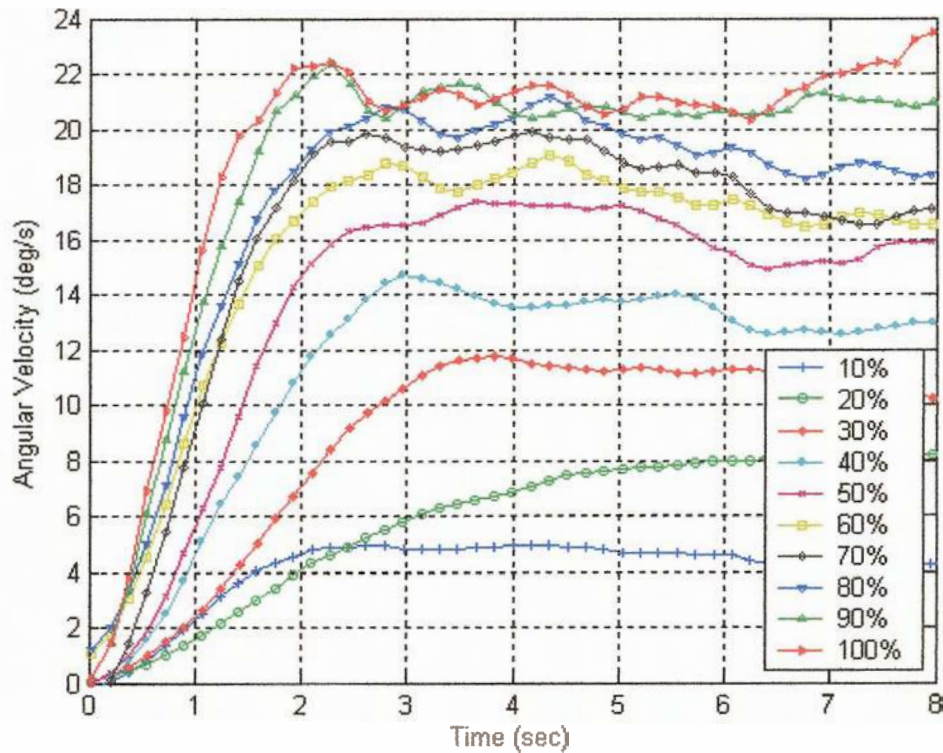
Fig. 24. Angular velocity step responses to 10 constant torque levels.

Using the steady-state velocity data from fig. 24 and the corresponding open-loop torque levels, a chart showing drag vs. velocity was generated (fig. 25).

$$D(Nm) = 0.0149 * (V(deg/s))^2 + 0.0857 * V(deg/s)$$
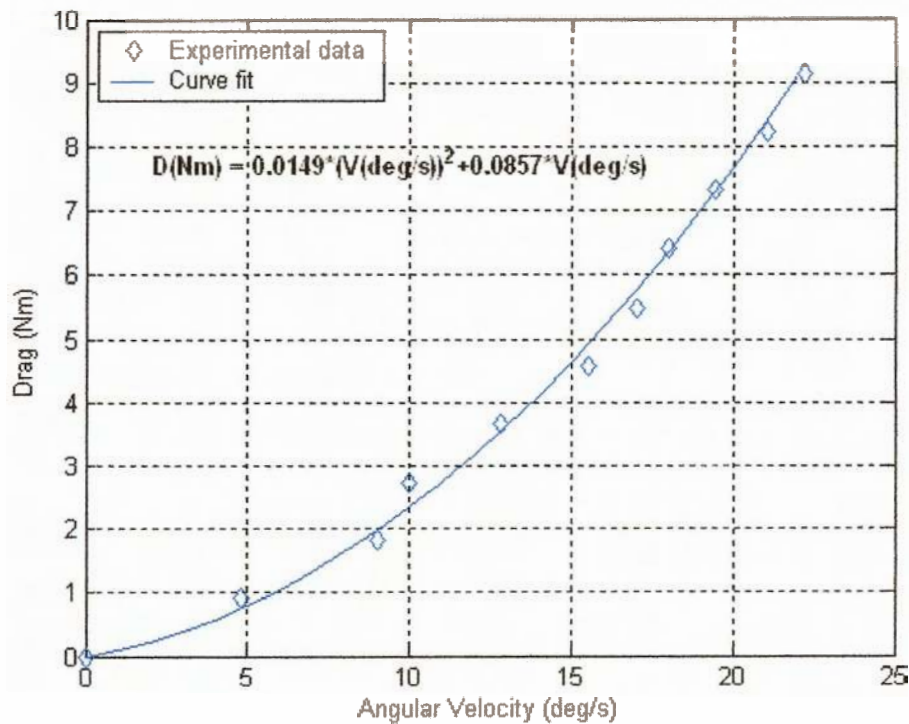
Fig. 25. The relationship between drag and angular velocity in yaw.

The reasonably good fit provided a suitable basis for modelling the drag characteristics for yaw in the dynamics simulation.

3.3.3 Heave

The AUV is not equipped with a velocity sensor in the heave direction. As a result, the position (depth) response was recorded for open-loop thrust levels ranging from 10% to 100%. The slope of the steady-state segment of each data set was taken as the steady-state velocity. The position response data sets for all ten open-loop runs are shown in fig. 26.
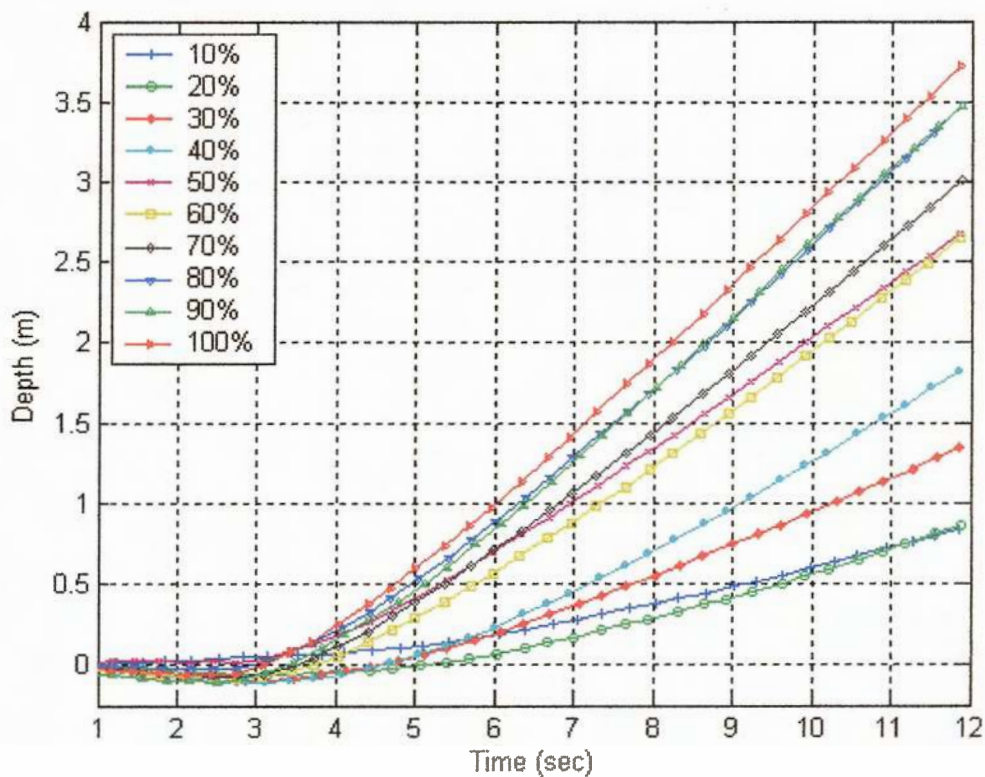
Fig. 26. Depth responses to 10 constant thrust levels.

Using the steady-state velocity data extracted from fig. 26 and the corresponding open-loop thrust levels, a chart showing drag vs. velocity was generated (fig. 27).
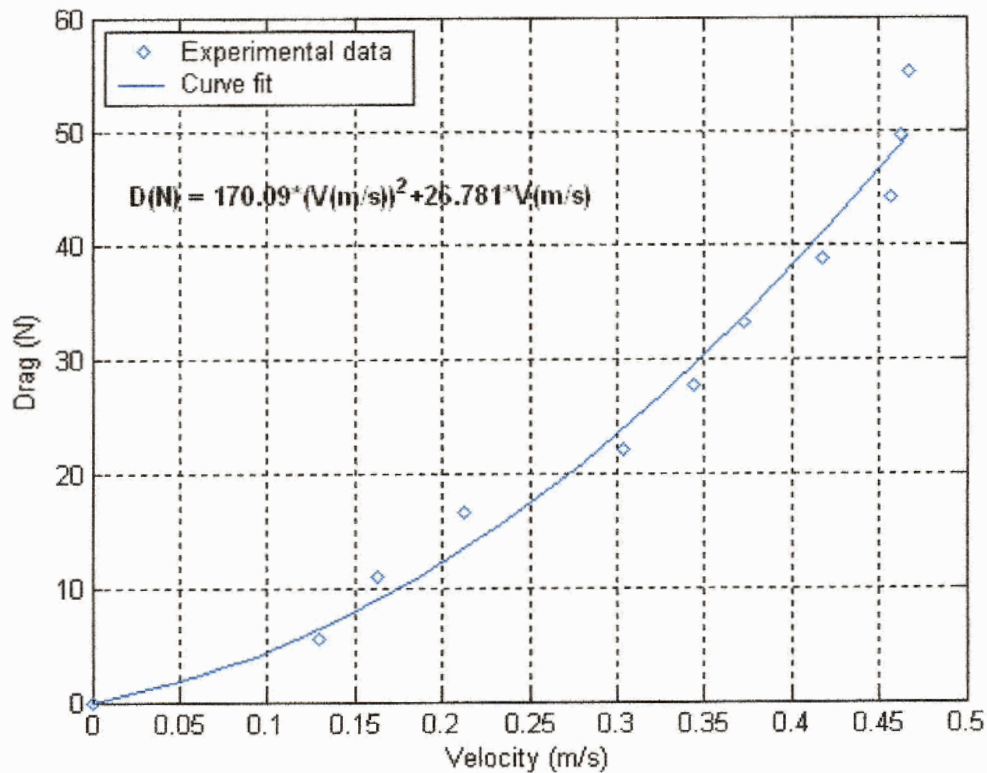
Fig. 27. The relationship between drag and velocity in heave.

The fit is reasonably good and was used to model the drag characteristics for heave in the simulation.

3.3.4 Pitch

As with heave, the AUV is not equipped with a sensor to measure angular velocity in pitch. As a result, the angular position response was recorded for open-loop thrust levels ranging from 10% to 80%. The slope of the steady-state segment of each data set was taken as the steady-state velocity. The complete data set is shown in fig. 28.
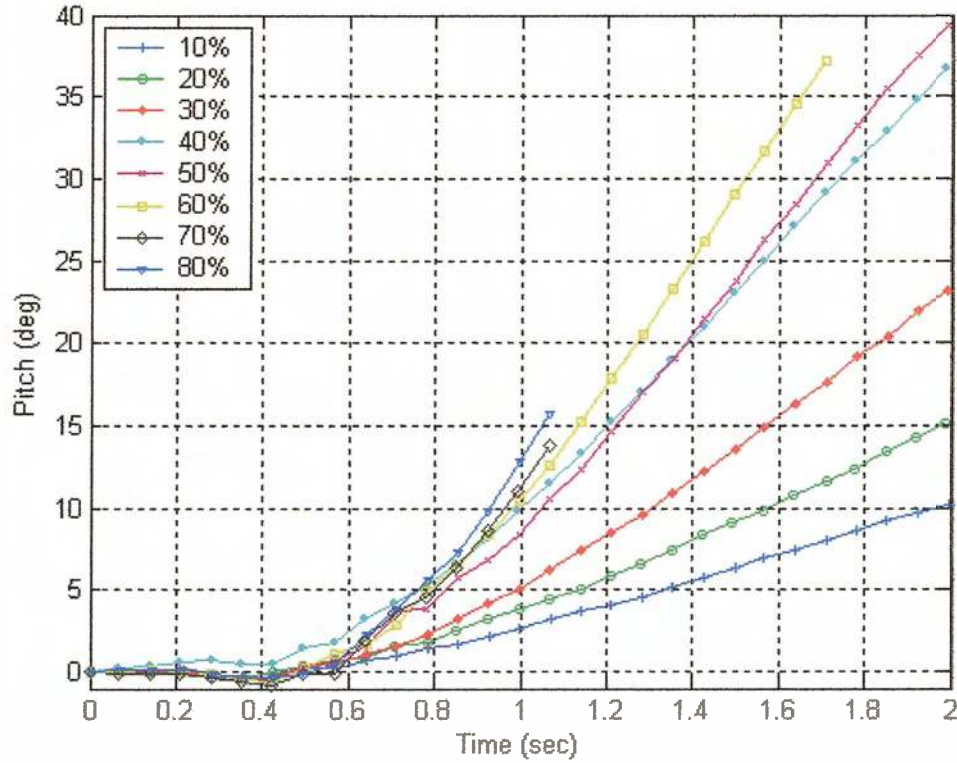
Fig. 28. Position step responses to 10 constant torque levels.

Using the steady-state velocity data extracted from fig. 28 and the corresponding open-loop thrust levels, a chart showing drag vs. velocity was generated (fig. 29).

$$D(Nm) = 0.0072 \cdot (V(deg/s))^2 + 0.3486 \cdot V(deg/s)$$
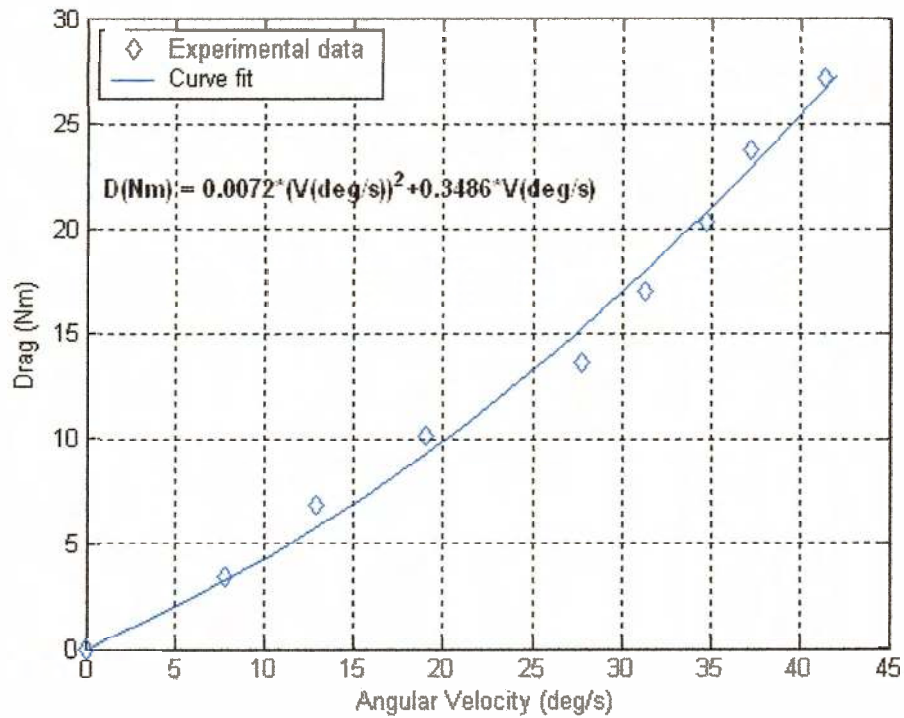
Fig. 29. The relationship between drag and angular velocity in pitch.

Unlike the other DOFs, the pitch axis also has a restoring moment that acts to oppose an increasing pitching angle. As a result, the velocity does not actually reach steady state. The drag relationship in fig. 29 provides an approximation of the actual AUV drag characteristics. However the linear term dominates the function, which suggests a strong influence from the restoring moment. The restoring or righting moment is caused by the opposing forces of the centre of buoyancy and centre of gravity acting on a component of their separation. The component length or moment arm is a function of the separation and the sine of the pitch angle.

To determine the righting moment, the steady-state pitch angle was measured for six open-loop thrust levels ranging from 10% to 60%. Fig. 30 illustrates the steady-state pitch levels and corresponding thrust levels.
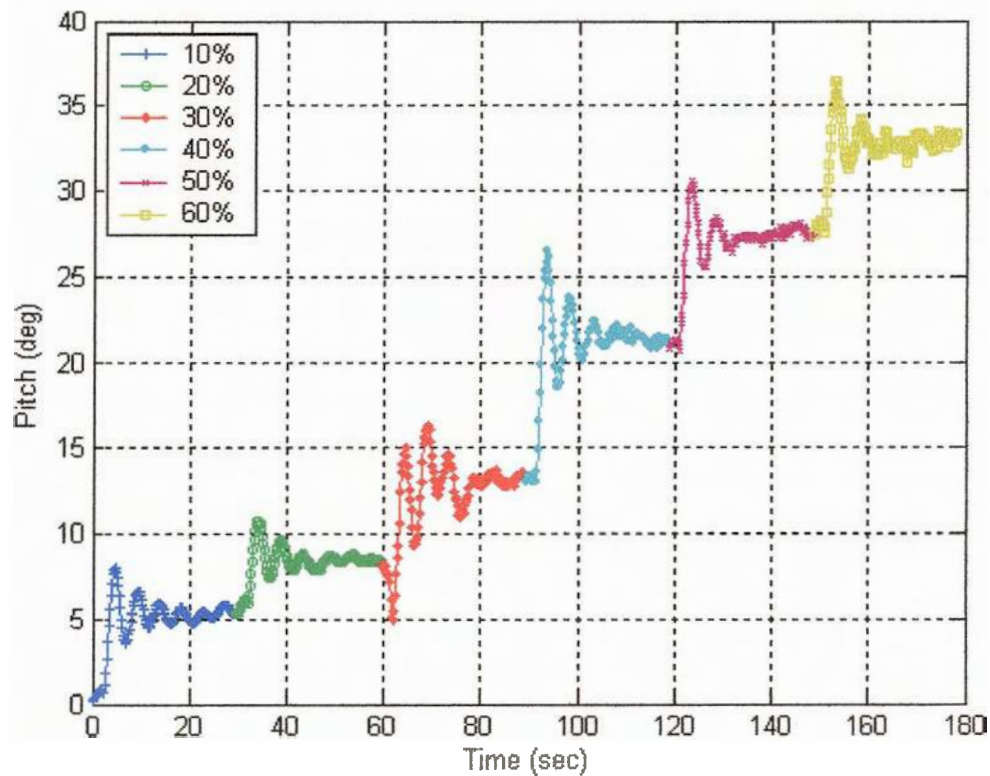
Fig. 30. Steady-state pitch angle at six constant input torque levels.

Over the small pitch angles that the AUV experiences, the righting moment can be approximated as linearly proportional to the pitch angle. Fig. 31 illustrates the relationship between the righting moment and pitch angle.
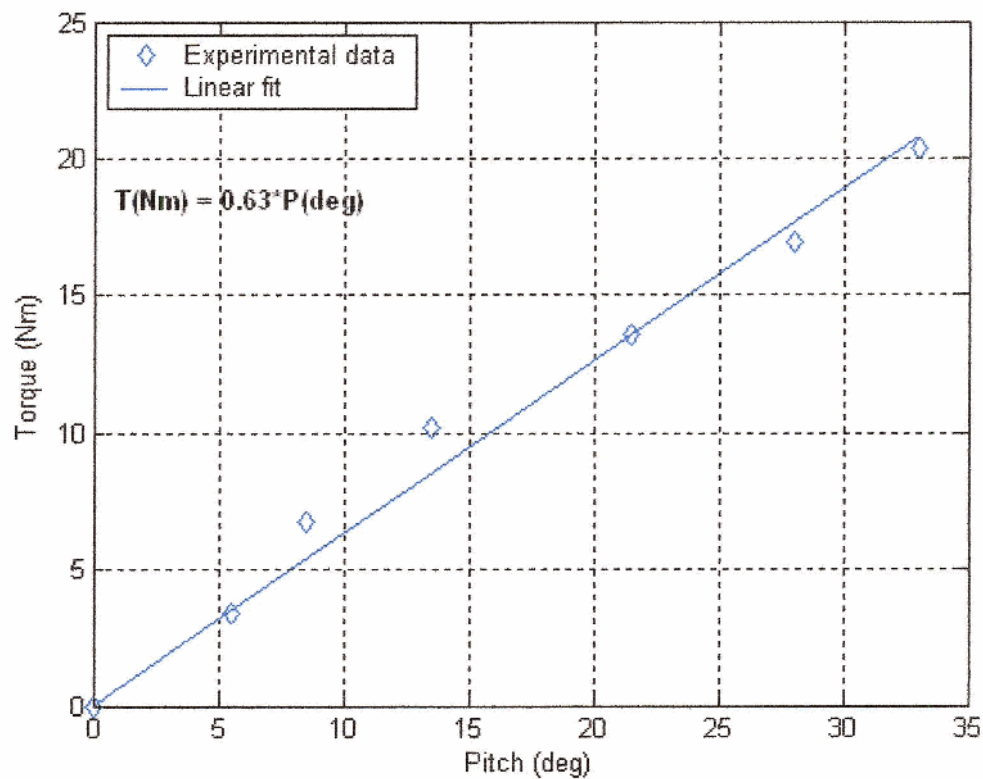
Fig. 31. The righting moment as a function of the AUV pitch angle.

This linear relationship is added to the AUV model and its effects are summed with the thruster input and drag torque.

4 Modelling of AUV System

Simulink is used to model the continuous AUV dynamics and the discrete thrusters, computer, and sensors. The models are comprised of graphical blocks that represent mathematical functions. Appendix A contains brief descriptions of each of the blocks used to model the AUV system.

4.1 Continuous AUV Dynamics

This AUV has four controlled DOF: surge, yaw, heave, and pitch. In the sections to follow, the dynamics of each DOF is described and the Simulink models are presented. In order to verify that the models are accurate representations of the actual AUV dynamics, the simulated step responses of each are compared at the end of each section.

For each comparison, a sample of the step response data collected during open-loop pool and lake testing (chapter 3) is plotted with a simulated response to an equivalent thrust input. The magnitude of the steady-state velocity and the shape of the transient region are good indications of an accurate drag coefficient and inertial term respectively. By adjusting these terms, the model can be fine-tuned to agree with the experimental data, allowing for accurate predictions during controller design. In addition to drag and inertia, the righting moment must also be adjusted for the pitch model.

4.1.1 Surge

The dynamics of the AUV's forward motion consists of a balance of forces along the X-axis as shown in equation 2. The contributing force vector directions are illustrated in fig. 32.

$$mx'' = F_T - B_1(x')^2 - B_2(x')$$ Equation 2

Where:

m	= Mass of the AUV and the water trapped within the wet hull
x''	= AUV forward acceleration
F_T	= Thrust force of both horizontal thrusters
B_1	= Quadratic damping (drag) coefficient
B_2	= Linear damping (drag) coefficient
x'	= AUV forward velocity

Fig. 32. Free body diagram of the AUV for forward motion control.

The forward motion dynamics described by equation 2 are shown in block diagram representation in fig. 33. The motion of the system is continuous but non-linear and is represented by the input thrust acting against the drag function on the mass of the vehicle.
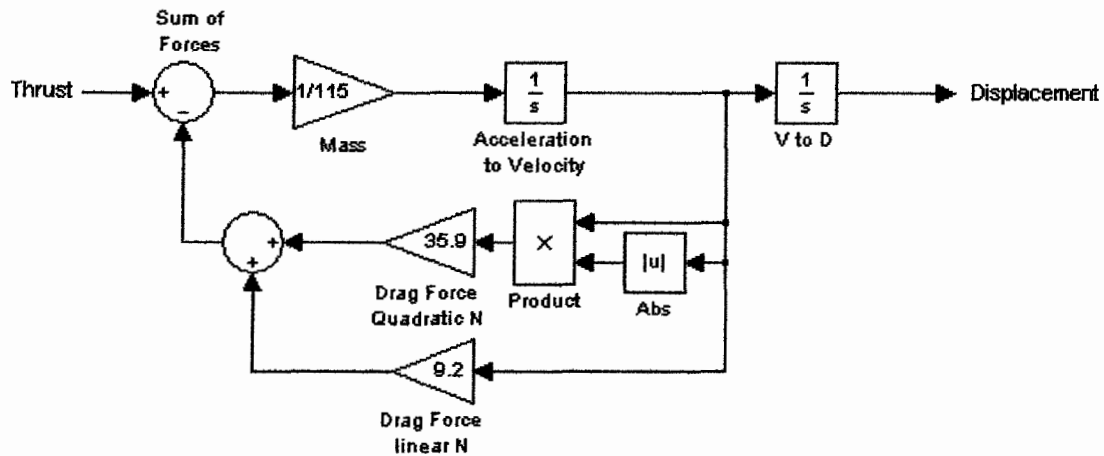
Fig. 33. Block representation of AUV forward motion.

Fig. 34 provides a direct comparison of the simulated response of the model with the experimental data. Two thrust step inputs of 40% and 80% were given to the system and the results were recorded. The model is in good agreement with the experimental result during the initial stage of the transient response and in steady state. However, the sharper corner of the velocity responses suggests that the inertial term may be underestimated.
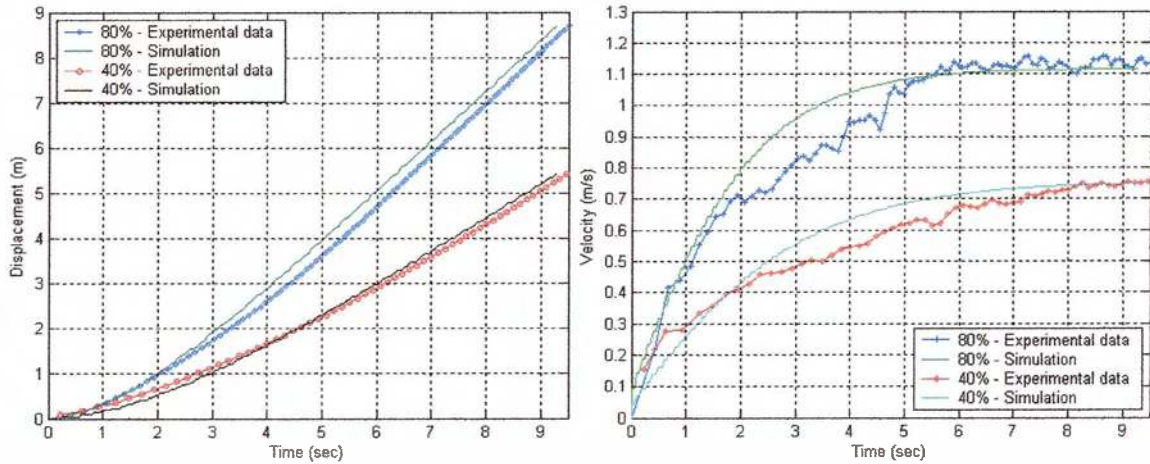
Fig. 34. Experimental and simulated open-loop a) displacement and b) velocity responses to 40% and 80% thrust levels in surge.

4.1.2 Yaw

The dynamics of the AUV's angular motion about the Z-axis, referred to as yaw, consists of a balance of moments as shown in equation 3. Vector directions are illustrated in fig. 35.

$$J\theta'' = T_T - B_1(\theta')^2 - B_2(\theta')$$

Equation 3

Where:

J	= Mass moment of inertia of the AUV and the water trapped within the wet hull
θ''	= AUV angular acceleration
T_T	= Thrust torque of both horizontal thrusters
B_1	= Quadratic damping (drag) coefficient
B_2	= Linear damping (drag) coefficient
θ'	= AUV angular velocity
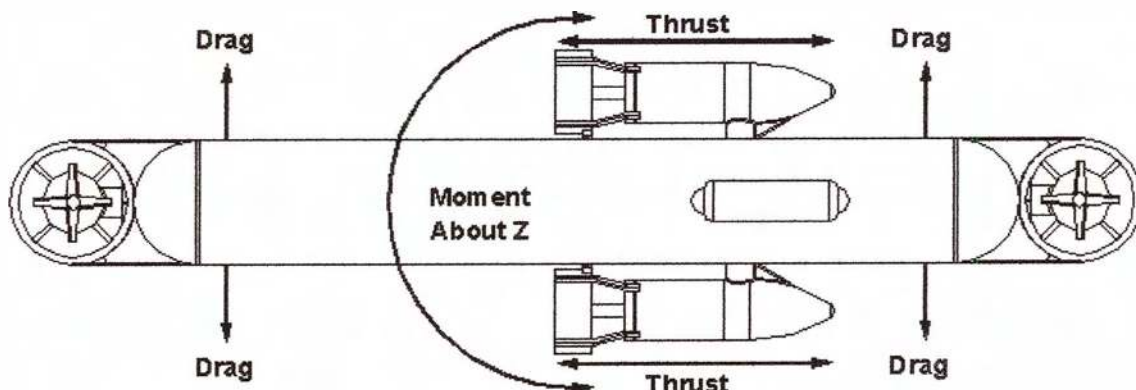
Fig. 35. Free body diagram of the AUV for yaw control.

The yaw dynamics described by equation 3 are shown in block diagram representation in fig. 36. The motion of the system is continuous, but non-linear. It is represented by the input torque acting against the drag function on the moment of inertia of the vehicle.
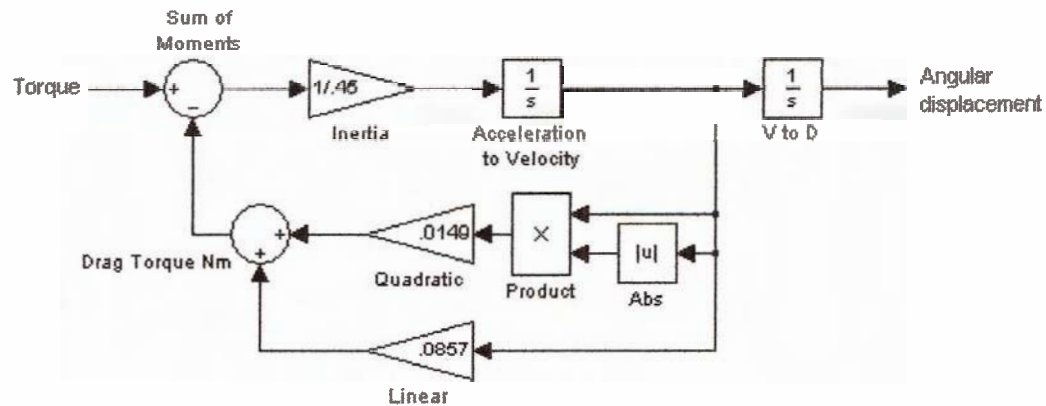
Fig. 36. Block representation of AUV angular motion about the Z-axis.

Fig. 37 provides a direct comparison of the simulated angular displacement and angular velocity responses of the model with the experimental data. Two torque step inputs of 40% and 90% were given to the system and the results were recorded. The model is in good agreement with the general shape of the experimental results. The slopes of the displacement response curves are very close, which confirms the proper representation of drag. The displacement offset is due to the oscillatory data, which looks very similar to typical overshoot of a closed-loop system. An open-loop velocity response should reach the maximum value at steady state with no overshoot. As mentioned in chapter four, these oscillations are due the rolling of the AUV. As the AUV rolls, the plane of the gyro changes orientation and begins reading a component of the pitch and the roll velocities.
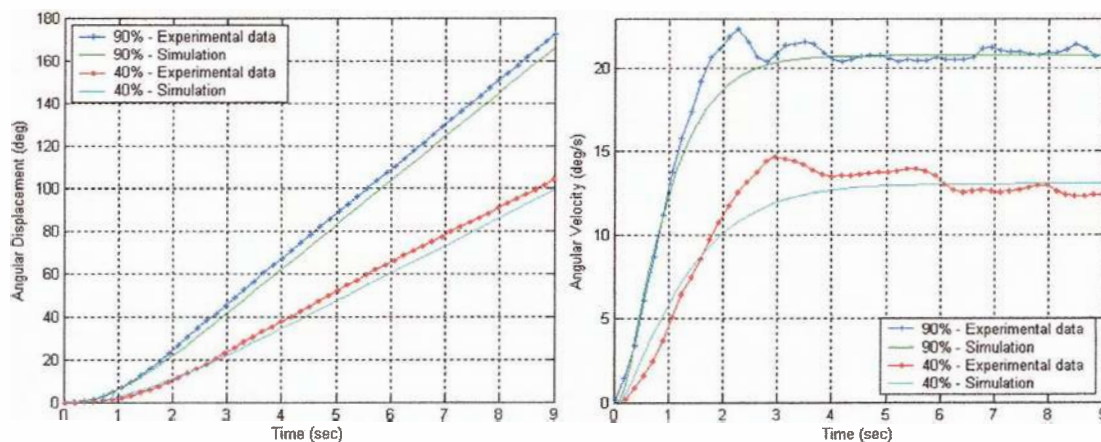
Fig. 37. Experimental and simulated open-loop a) displacement and b) velocity responses to 40% and 90% torque levels in yaw.

4.1.3 Heave

The dynamics of the AUV's vertical motion consist of a balance of forces along the Z-axis as shown in equation 4. Vector directions are illustrated in fig. 38.

$$mz'' = F_T - B_1(z')^2 - B_2(z') + C_B \qquad \text{Equation 4}$$

Where:

m	= Mass of the AUV and the water trapped within the wet hull
z''	= AUV vertical acceleration
F_T	= Thrust force of both vertical thrusters
B_1	= Quadratic damping (drag) coefficient
B_2	= Linear damping (drag) coefficient
z'	= AUV forward velocity
C_B	= Buoyancy constant (net +/-ve buoyancy)
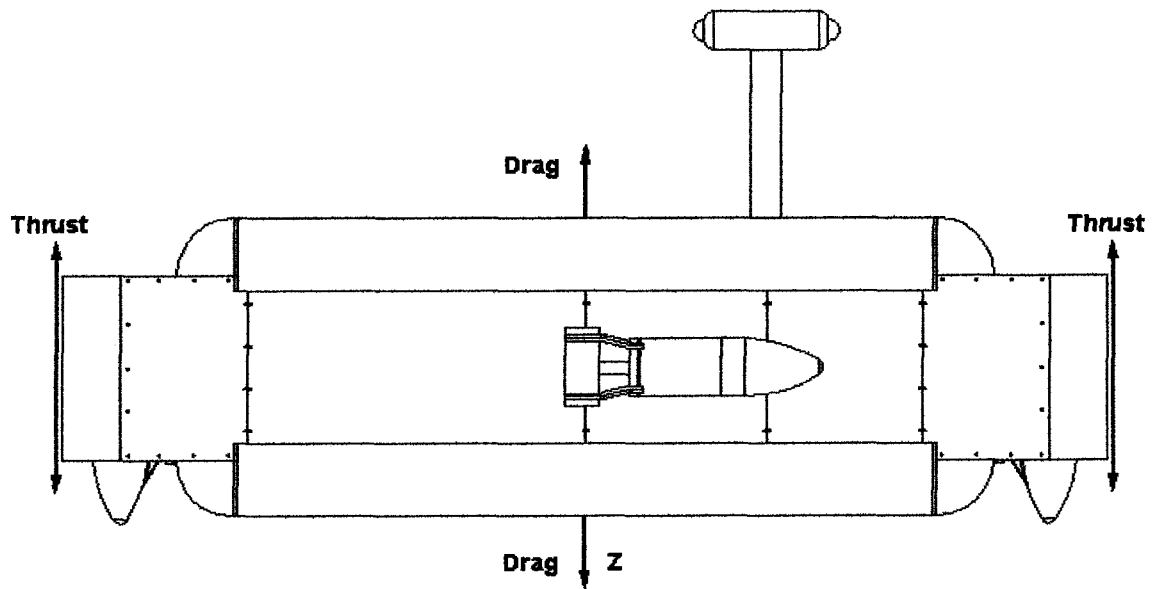
Fig. 38. Free body diagram of the AUV for depth control.

The AUV's motion dynamics described by equation 4 are shown in block diagram representation in fig. 39. The motion of the system is continuous, but non-linear with the input.
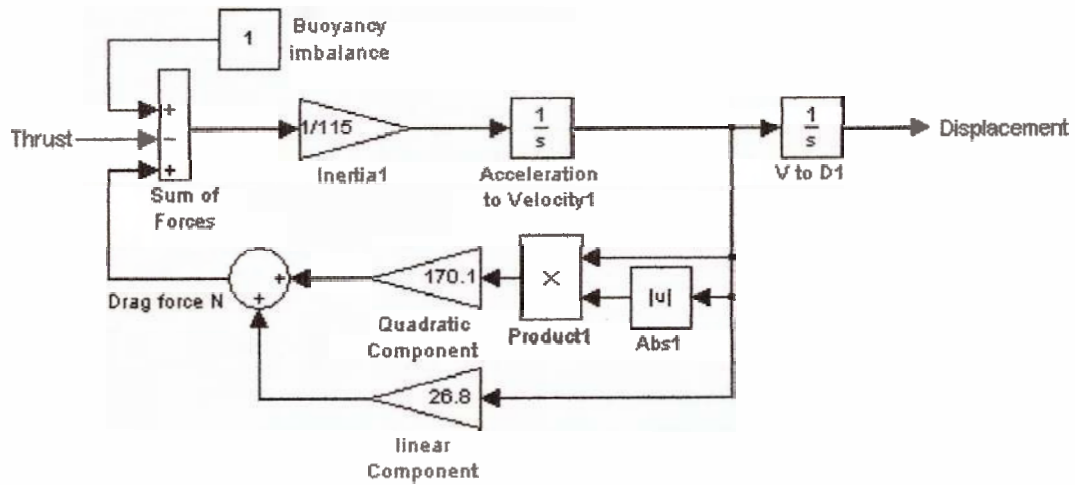
Fig. 39 - Block representation of AUV vertical motion.

Fig. 40 provides a direct comparison of the simulated response of the model and the experimental data. Two thrust step inputs of 50% and 80% were given to the system and the results were recorded. The model provided a very close estimate of the actual AUV dynamics.
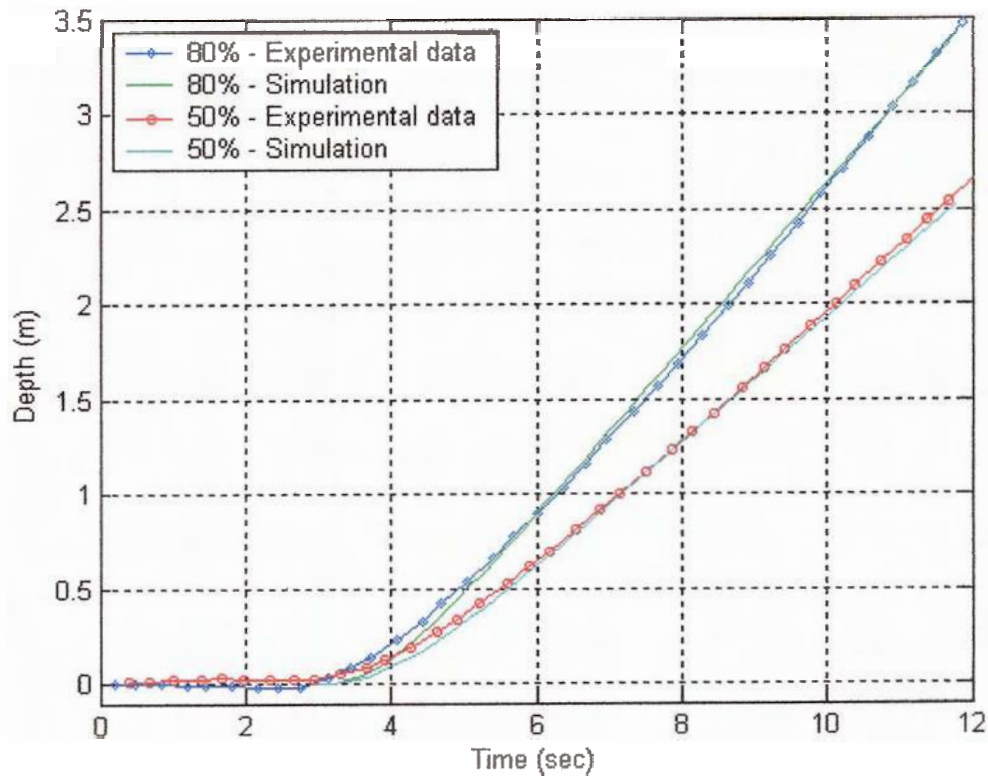
Fig. 40. Experimental and simulated open-loop displacement responses to 50% and 80% thrust levels in yaw.

4.1.4 Pitch

The dynamics of the AUV's angular motion about the Y-axis, referred to as pitch, consists of a balance of moments as shown in equation 5. Vector directions are illustrated in fig. 41.

$$J\theta_y'' = T_T - B_1(\theta_y')^2 - B_2(\theta_y') + C_F(x')^2 - C_R \sin(\theta_y)$$ **Equation 5**

Where:

J	=	Mass moment of inertia of the AUV and the water trapped within the wet hull
θ_y''	=	AUV angular acceleration about the Y-axis
T_T	=	Thrust torque of both vertical thrusters
B_1	=	Quadratic damping (drag) coefficient
B_2	=	Linear damping (drag) coefficient
θ_y'	=	AUV angular velocity about the Y-axis
C_F	=	Drag moment constant due to forward velocity
x'	=	Forward velocity
C_R	=	Righting moment constant (product of the buoyant force and distance between centre of buoyancy and centre of gravity)
θ_y	=	Angular position about the Y-axis (pitch)

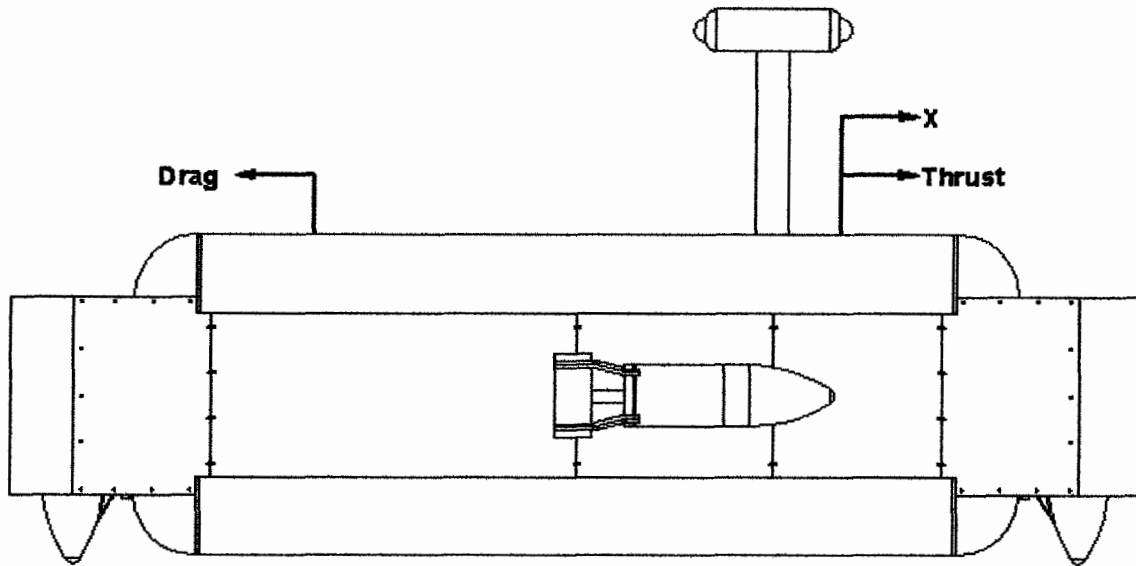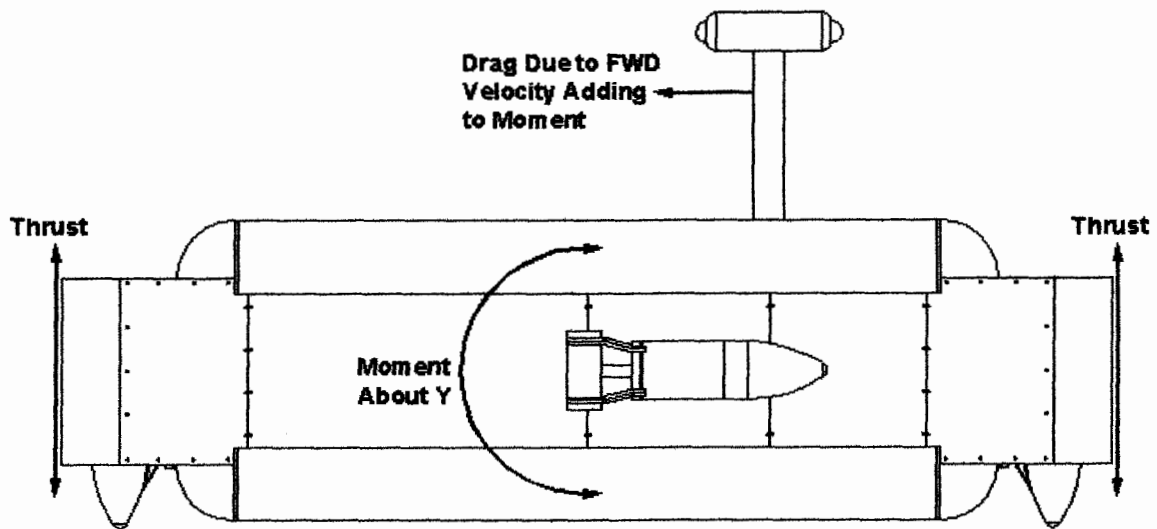**Fig. 41. Free body diagram of the AUV for pitch control.**

The pitch dynamics described by equation 5 are shown in block diagram representation in fig. 42. As in the yaw dynamics, the motion of the system is continuous, but non-linear. The motion is represented by summing the torque contributions from the input, asymmetric drag caused by forward velocity, restoring moment, and the drag function acting on the moment of inertia of the vehicle.
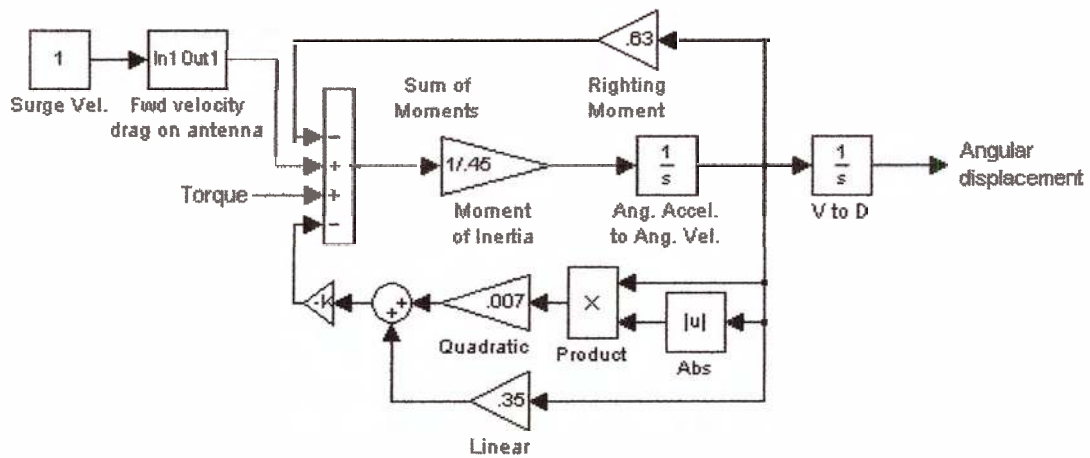
Fig. 42. Block representation of AUV angular motion about the Y-axis.

Fig. 43 provides a direct comparison of the simulated response of the model and the experimental data. Two torque step inputs of 30% and 80% were given to the system, and the results were recorded. The slopes of the assumed steady-state velocities predicted by the model are not exactly the same as the experimental results. The simulated velocities of the 80% and 30% trials greater and lesser respectively than the experimental data. This suggests that the shape, and not just the scale, of the modelled drag curve needs to be adjusted.
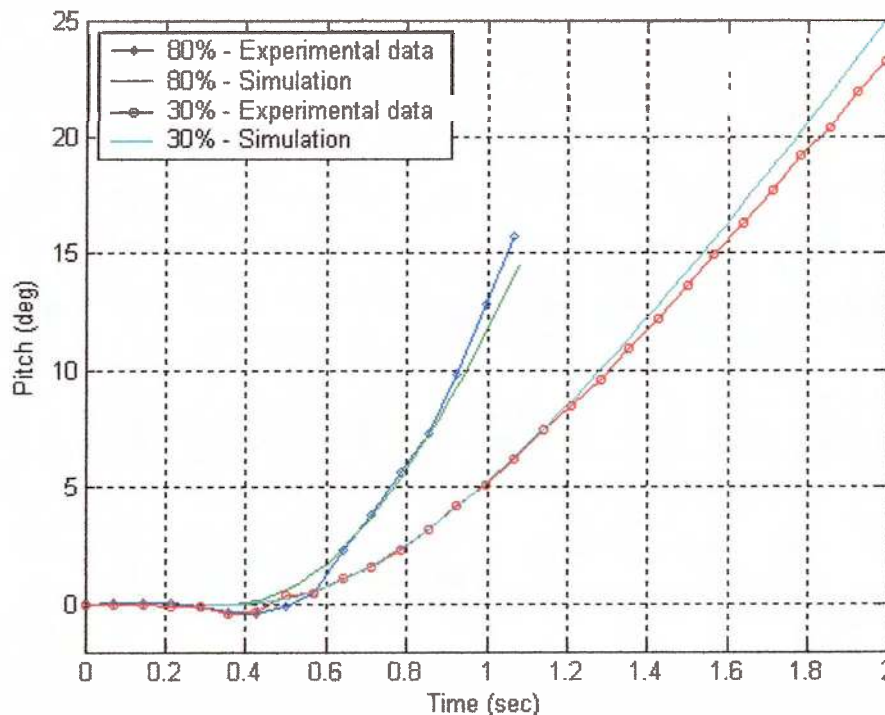
Fig. 43. Experimental and simulated open-loop displacement responses to 30% and 80% torque levels in pitch.

4.2 Discrete Components

The motion of the AUV is continuous, but the thrusters used to actuate it and the sensors used to measure its motion are discrete. Therefore the sampling period, quantization, acquisition and communication delay, and noise associated with these discrete components must be taken into account. Delay has the largest impact, and if it is not accounted for, the model will appear to be much more stable than the actual system. As a result, the controller design will yield unrealistic predictions. This is clearly demonstrated in chapter 5.

4.2.1 Thruster Drivers

The thruster drivers accept a pulse width modulated signal from the computer and output a proportional voltage between +12 volts and –12 volts. These devices operate at 60 Hz and incorporate a zero order hold (ZOH) between outputs, which are also quantized to 32 discrete values in positive and negative. The speed controller is presented in block form in fig. 44.
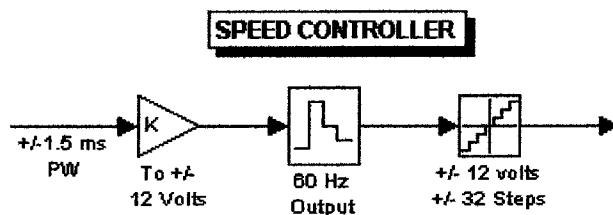
Fig. 44. Block representation of the speed controller.

4.2.2 Thrusters

The thruster accepts a +/- 12 volt input and outputs a thrust force. Strictly speaking, the thruster is a continuous device, but the response can be approximated as a ramp as shown in chapter 3. In addition to the ramped response, there is a delay of approximately 100 milliseconds between computer request and the requested thrust out. This delay is caused by a combination of things such as computing, digital i/o, and the motor driver and is lumped in with the computer. The thrusters are simply represented in fig. 45 by a gain and rate limiter.
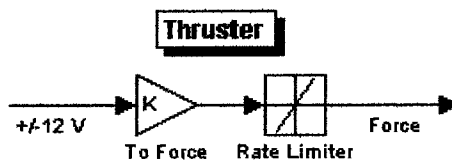
Fig. 45. Block representation of a thruster.

4.3 Computer

The computer represents the software computations, digital and analog i/o, inner stack communications, and many other factors. To represent these characteristics accurately would be very challenging and not particularly beneficial. Therefore the computer and associated hardware is simply symbolized as transport delay as shown in fig. 46. The value of this delay will be the final value to be tuned once the control loop is closed in chapter 5.
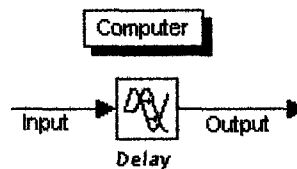
Fig. 46. Block representation of the computer.

4.4 Sensors

The following sections describe the sensors used in the feedback loops of each controlled state of the AUV's motion. The technique used to model the sensor output is discussed and the Simulink block representation is given.

4.4.1 Flow Meter: Surge Velocity

The forward velocity is measured using a turbine flow meter, which generates four pulses per revolution of the turbine wheel. The frequency of the pulse train is proportional to water velocity passing through the sensor. One difficulty with this device is that the sampling time is a function of velocity; so high and low speeds produce fast and slow sampling frequencies respectively. In addition, the flow meter is not directional so a reed valve is used to block reverse flow. As a result, the controller is not aware of any reverse velocity.

To model the flow meter, a variable transport delay as a function of velocity was used to model the delay, a zero order hold with a fixed mean sampling rate was used to approximate the hold period, and a saturation represented the reed valve. This combination including the delay function with limiter is shown in fig. 47.
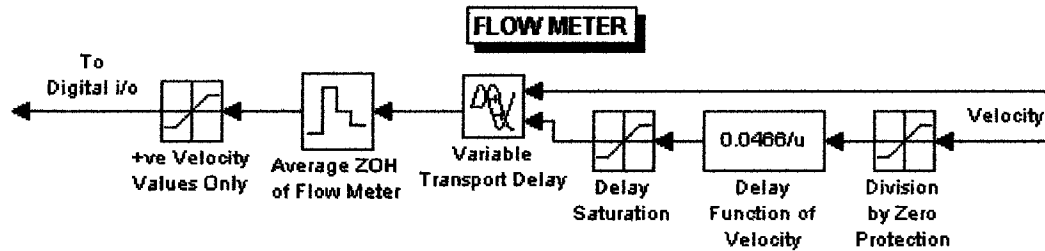
Fig. 47. Block representation of flow meter used to measure velocity.

4.4.2 Flow Meter: Surge Displacement

The forward displacement is also measured using the flow meter. However, instead of measuring the time between pulses, each pulse is counted. Each pulse represents a known distance so modelling is a simple matter of quantizing the system displacement into finite steps, as shown in fig. 48.
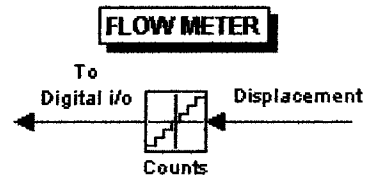
Fig. 48. Block representation of flow meter used to measure displacement.

4.4.3 Gyro: Yaw Angular Velocity

The angular velocity is measured using a solid state MEMS gyro, which generates a 67Hz pulse width modulated output. A running average of five outputs is then taken to smooth the signal. The resolution of the gyro is 0.95 deg/s. However, the averaging has the effect of artificially increasing this resolution by five times.

The gyro was modelled using a zero order hold, a transport delay, and quantization (fig. 49). The zero order hold with a 15 ms sampling period was used to simulate the operating frequency. The transport delay of 45 ms (5/2 samples) and the quantization of 0.19 (0.95/5) deg/s was used to approximate the effects of the averaging filter.
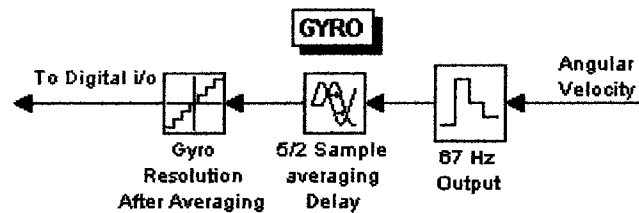
Fig. 49. Block representation of gyro used to measure angular velocity in yaw.

4.4.4 Compass: Heading

The heading is measured using a flux gate compass, which has an output frequency of 13.7 Hz across an RS-232 serial link. The resolution of the compass is 0.1 deg and it has internal filtering options, which at the current settings induce a delay of 2.5 sampling periods.

The compass was modelled using a zero order hold, a transport delay, and quantization (fig. 50). The zero order hold with a 73 ms sampling period was used to simulate the operating frequency. The transport delay of 182 ms (5/2 samples) represents the delay of the internal filter. The quantization of 0.1 corresponds to the resolution of the device.
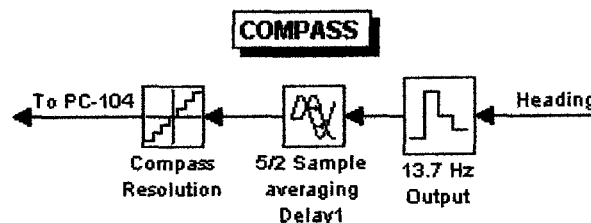
Fig. 50. Block representation of the compass used to measure heading.

4.4.5 Pressure Transmitter: Depth

The depth is measured using a pressure transmitter. This is a special type of pressure transducer, which outputs directly, using RS-232 serial protocol. The data is provided at 20 Hz with a resolution of 50,000 over the 100-m depth range.

The pressure transmitter was modelled using a zero order hold with a 50 ms sampling period to reflect the operating frequency and quantization of 2 mm steps to reflect the resolution (fig. 51).
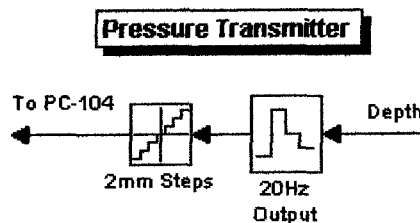
Fig. 51. Block representation of the pressure transmitter used to measure depth.

4.4.6 Liquid Tilt Sensor: Pitch

The pitch is measured using a liquid tilt sensor, which is part of the fluxgate compass package. As with the heading, the value of pitch is output at 13.7 Hz, using RS-232

serial protocol. There is an internal filter that uses a running average of three samples to smooth the output. The resolution of the level sensor is 0.1 deg.

The level sensor was modelled using a zero order hold, a transport delay, and quantization (fig. 52). The zero order hold with a 73 ms sampling period was used to simulate the operating frequency. The transport delay of 109 ms (3/2 samples) represents the delay of the internal filter. The quantization of 0.1 corresponds to the resolution of the device.
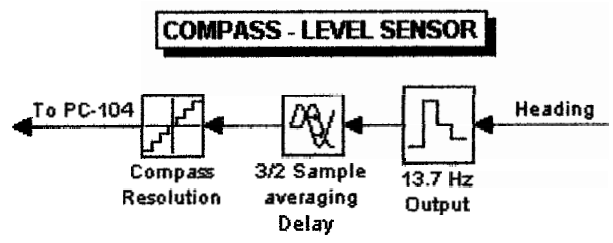
Fig. 52. Block representation of the compass level sensor used to measure pitch.

5 Controller Design and Simulation

The objectives of this chapter are to show the design of closed-loop controllers for modelled systems using Simulink and to demonstrate the importance of discrete modelling. Simulink allows the user to quickly recognize response trends as the gains are varied. This results in a much quicker convergence on a suitable controller. In contrast, tuning an actual system in the field can be very time consuming and often requires elaborate measurement. The controller design and simulations for each DOF were developed in the following way:

1. A general controller type was selected.

2. The individually modelled components were assembled to form a closed-loop system.

3. The controllers were tuned graphically through an iterative approach by observing the setpoint responses to a series of gain levels.

The importance of accurately modelling discrete components becomes most evident in a closed-loop system. When the loop is closed, the discrete nature of the system components can have a detrimental effect on a controller's stability. The delays, quantization, and discrete sampling (zero order holds) introduced by the computer and sensors can destabilize a controller that would otherwise be very effective in a purely continuous system. The delayed and quantized thruster output will also have an effect here. To emphasize the importance of accounting for the discrete nature of system elements, several predicted responses of continuous systems have been included for comparison. For reference, fig. 53 depicts the main elements of a simple closed-loop control system.
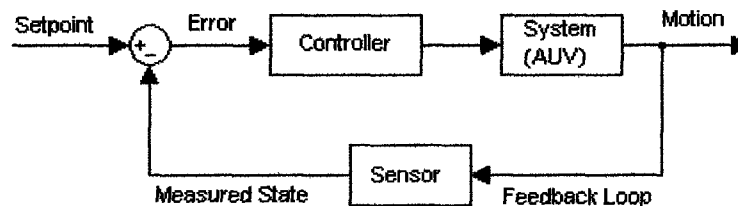
Fig. 53. Simplified closed-loop control system.

5.1 General Controller Description

There are three types of controllers used in the AUV system: the proportional-integral-derivative (PID) controller, the velocity feedback controller, and the feed forward controller. The specific requirements of each DOF are satisfied using a combination, or pared down version, of the three controller types. The following sections provide descriptions of these controller types and justification for their selection.

5.1.1 PID Controller

The PID controller is a widely used industrial controller with mathematically intuitive terms, as described by equation 6. This made it an appealing choice as the base controller for the AUV system.

$$O_{CPID} = K_p e + K_i \int e + K_d \frac{de}{dt}$$
Equation 6

Where:

O_{CPID} = Controller output to system

K_p = Proportional gain

K_i = Integral gain

K_d = Derivative gain

e = Error between the setpoint and the measured state

$\int e$ = Running summation of the error

$\frac{de}{dt}$ = Rate of change of the error

Kp has a large influence when the error is large and will move the system closer to the setpoint, but it has little effect on steady-state error unless very large.

Ki is mainly used to reduce steady-state error caused by a constant or slowly changing imbalance or disturbance. It accomplishes this by allowing the steady-state error to accumulate over time, to create the required request for actuation to eliminate the error.

Kd is used to dampen the system. It has the effect of opposing changes in the measured state. It allows Kp and Ki to be larger and to have more control over the system without suffering from overshoot and oscillations. It does this by reducing the rate of change of the state.

In some cases not all three terms are necessary to meet the control requirements of each DOF and to set the gain values to zero. Fig. 54 illustrates basic closed-loop position control using the PID controller.
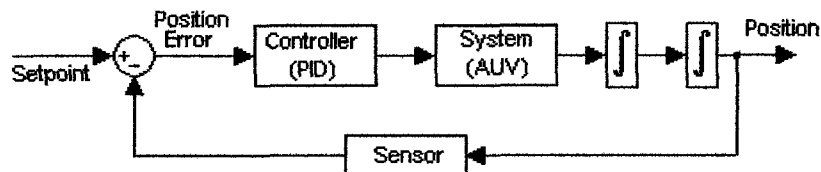
Fig. 54. The base PID controller used for position control.

5.1.2 Feed Forward Controller

A feed forward controller is an open-loop controller. This means that this type of controller receives no information on what the system is actually doing. The output is strictly a function of the setpoint or reference as shown in equation 7.

$$O_{CFFwd} = K_{FFwd} GR$$

Equation 7

Where:

O_{CFFwd} = Controller output to system

K_{FFwd} = Feed forward gain

G = Function describing the system's open-loop characteristics

R = Setpoint or reference

To be effective, it requires a function that can accurately describe the steady state of the system resulting from any available level of actuation. In the case of the AUV, the quadratic drag versus velocity relationships are used. The feed forward can be inserted in parallel with a PID controller to control velocity, as shown in fig. 55.
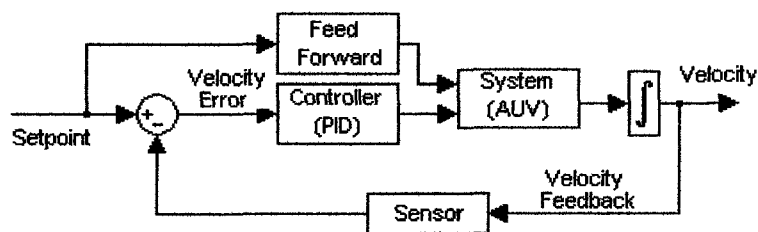
Fig. 55. The addition of the feed forward controller.

5.1.3 Velocity Feedback Controller

Velocity feedback is a technique used to improve the performance of position controller. Both the velocity signal and the positional signal are fed back to the input to produce the actuating error signal (fig. 56).
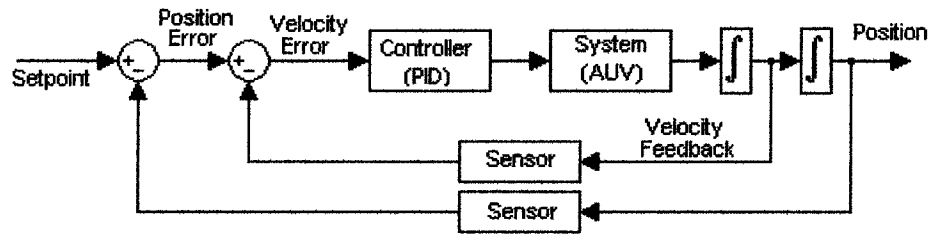
Fig. 56. Position controller with a nested velocity loop.

A basic position controller relies on the damping or drag of the system for deceleration, while a nested velocity loop allows for a controlled approach to the setpoint. If the AUV is approaching the setpoint too rapidly, a negative velocity error is produced and the thrusters will actually reverse direction if required, to maintain the prescribed deceleration.

5.2 Surge Motion

Surge motion is controlled on two levels: velocity and displacement. Because the feedback sensor used to measure these is unidirectional, only the forward or positive sense is considered. In the sections to follow, the controller types used, block diagram representations, and setpoint response curves are presented for surge velocity and displacement.

5.2.1 Surge Velocity

Forward velocity control is accomplished by using a flow meter as the sensor to measure the state and a PD controller with feed forward to achieve and hold the setpoint. The block diagram representation of the entire forward velocity model for the discrete and continuous system is included in appendix B.

5.2.1.1 Controller: Proportional and Derivative with Feed Forward

The AUV is expected to achieve the reference velocity quickly and then maintain that velocity for long periods. It must also be able to stop quickly with zero overshoot (reverse velocity). Because the AUV cannot sense reverse velocity, in the case of an overshoot, the controller would consider the zero crossing to be a full stop. As a result, the AUV would continue to drift backwards (fig. 58).

To meet these requirements, the forward velocity controller is a PD type with feed forward. Because the drag characteristics are known, and the AUV will travel for long

periods at a constant velocity, an open-loop feed forward is used to provide the required thrust to achieve the reference velocity. The feed forward provides a relatively fast response and the system is very stable, but the feed forward offers no stopping assistance so, with feed forward alone, the AUV would drift to a stop (fig. 58).

To improve the acceleration and provide some stopping power, a strong proportional controller is added. The derivative term is used to ensure a slow approach to zero velocity. The Simulink representation of the controller is shown in fig. 57.
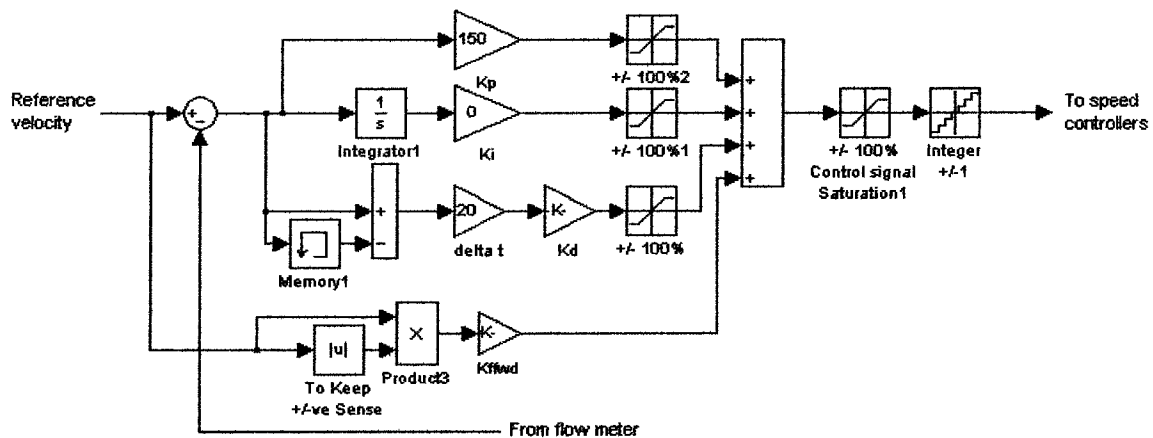
Fig. 57. Block representation of forward velocity controller.

5.2.1.2   Setpoint Response Curves

To show how the controllers could reach the reference and then come back to a stop, the response curves to a step, followed by delayed, negative step of the same magnitude, are shown in fig. 58.

The key points to notice from each plot in fig. 58 are as follows:

1. This controller has a fast response with no overshoot.

2. This is a faster controller, but suffers from overshoot. Note that the response has a negative velocity overshoot when stopping. The AUV cannot sense this so it continues drifting backwards slowly to a stop.

3. This is the feed forward controller only. It is clear that the feed forward controller has no part in stopping the AUV.

4. This represents the continuous response with the same Kp as plot 1.

5. Here the continuous model has a completely unrealistic response with a Kp of 1000. Still, there is no instability.
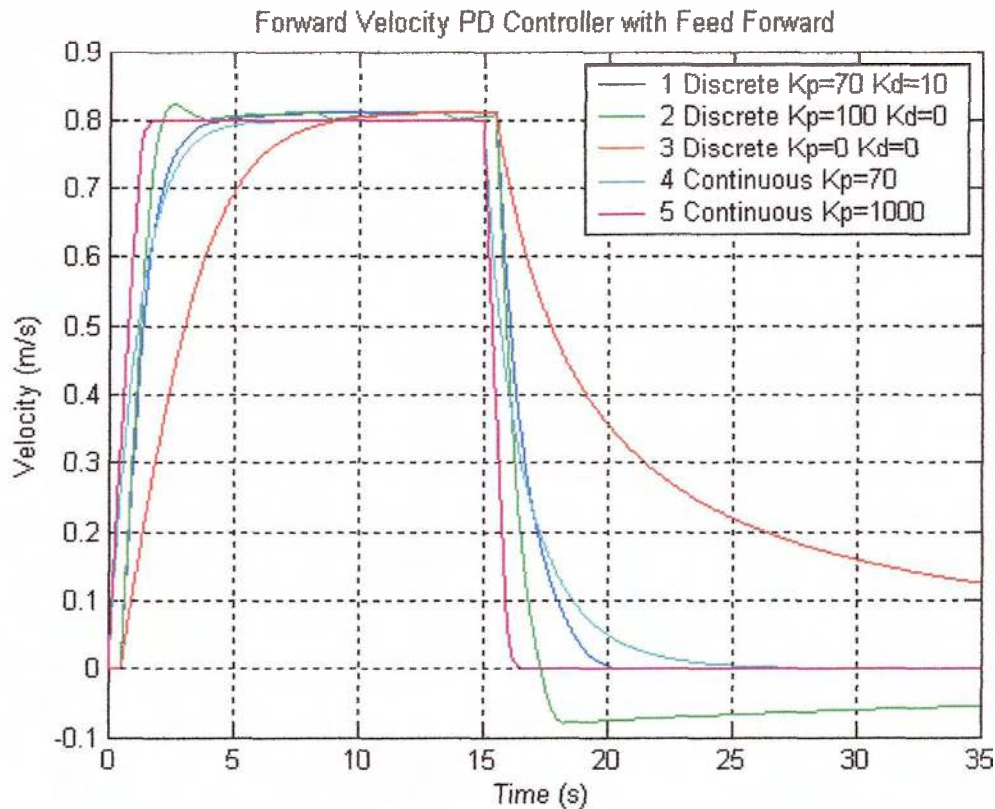
Fig. 58. Step response curves of several forward velocity controllers.

5.2.2 Surge Displacement

Forward displacement control is accomplished using a flow meter as the sensor to measure the state and a P controller with nested velocity feedback to achieve and hold the setpoint. The block diagram representation of the entire forward displacement discrete model is included in appendix C.

5.2.2.1 Controller: Proportional with Velocity Feedback

The AUV is expected to accelerate to cruising velocity, hold that velocity for the required amount of time, and then decelerate to a stop. This is a standard trapezoid motion control profile. As mentioned in the previous section, there must be no overshoot so the approach to stop must not be too aggressive.

To meet these requirements, the forward displacement controller is a P type with velocity feedback and velocity ceiling. This is accomplished by first multiplying the error of the position loop with the proportional gain. The product is then used as the reference signal to the forward velocity controller described in the previous section. The acceleration and

deceleration slopes are controlled by the proportional gain, and the cruising velocity is set using saturation on the reference velocity. The Simulink representation of the controller is shown in fig. 59.
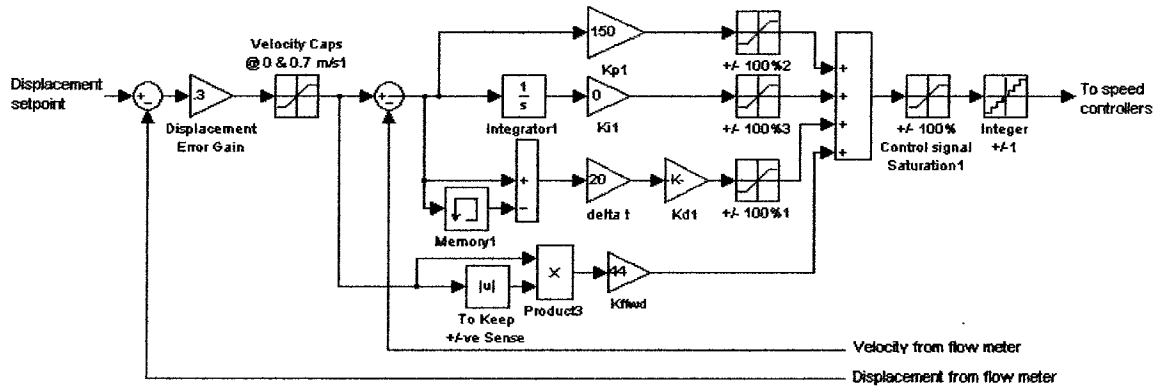
Fig. 59. Block representation of forward displacement controller.

5.2.2.2 Setpoint Response Curves

The performance of the forward displacement controller is observed with a step input of 8 ms. The key points to notice from each plot in fig. 60 are:

1. The high error gain causes overshoot, and the velocity limiter at 0.4 m/s gives a very slow response.

2. The overshoot is still present with an error gain of 0.4, but the response is much faster, with a high cruising velocity of 0.7 m/s.

3. An error gain of 0.2 eliminates the overshoot.

4. A very fast response can be achieved by allowing the maximum AUV velocity, but this type of motion would consume the AUV batteries much too quickly.

Fig. 60. Setpoint response curves of several forward displacement controllers.

The plots in fig. 61 are the velocity profiles that correspond to the displacement profiles in fig. 60. The notable points from each plot in fig. 61 are as follows:

1. The velocity is limited very early to 0.4 m/s, causing the slow displacement response. Notice the aggressive deceleration caused by the error gain. With a slope this sharp, the AUV waits too long before starting to stop, making an overshoot unavoidable.

2. The effect the error gain has on deceleration is most obvious when comparing this plot with plot 3.

3. See comment 2.

4. Here the maximum velocity set is not reached during the 8 m displacement.
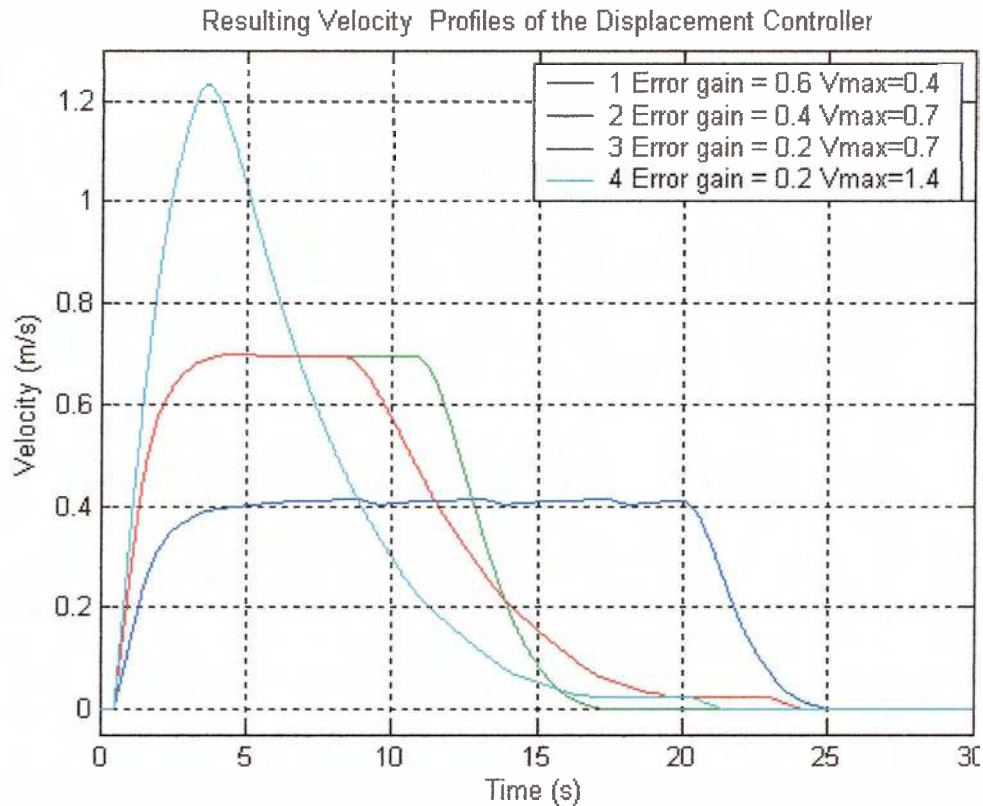
Fig. 61. Trapezoidal velocity profiles of the AUV under displacement control.

5.3 *Yaw Motion*

As with surge, yaw motion is also controlled on two levels: velocity and displacement. However, the motion in yaw is measured and controlled in the positive and negative directions. In the sections that follow, the controller types used, block diagram representations, and setpoint response curves are presented for yaw velocity and displacement.

5.3.1 Angular Velocity Control

Angular velocity control is accomplished using a gyro as the sensor to measure the state and a PD controller with feed forward to achieve and hold the setpoint. The block diagram representation of the entire angular velocity model for the discrete and continuous system is included in appendix D.

5.3.1.1 Controller: Proportional and Derivative With Feed Forward

Aside from test operations, the AUV would not be required to maintain a constant angular velocity for extended periods. The AUV is required to achieve and then sustain

the reference velocity quickly and then follow a changing setpoint. A small amount of overshoot is acceptable, provided that any oscillations are damped out rapidly.

To meet these requirements, the angular velocity controller is a PD type with feed forward. As with the forward velocity, the drag characteristics are known and therefore an open-loop feed forward is used to provide the required thrust to achieve the reference angular velocity. The proportional controller improves the acceleration and provides the stopping power, and the derivative term is used to dampen oscillations. The Simulink representation of the controller is shown in fig. 62.
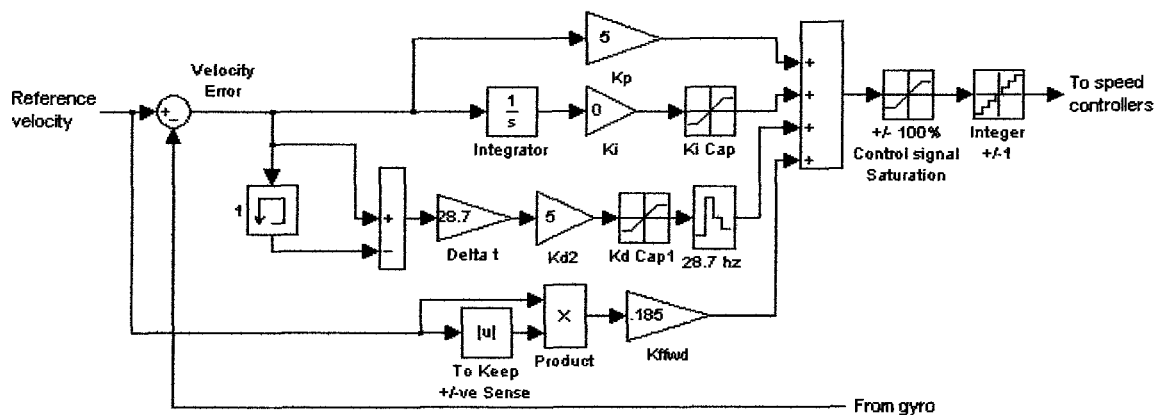
Fig. 62. Block representation of yaw angular velocity controller.

5.3.1.2 Setpoint Response Curves

To show how the controllers could reach the reference and then come back to a stop, the response curves to a step, followed by delayed, negative step of the same magnitude, are shown in fig. 63.

Note the key points from each plot in fig. 63, :

1. This controller has a fast response with very little overshoot.

2. This is the same controller as plot 1, but without the damping provided by the derivative term.

3. This discrete controller causes sustained oscillations at a Kp of only 30.

4. This continuous controller has the same parameters as plot 2, but has no signs of overshoot.

5. Plot 5 exemplifies the limitations of the continuous approximation of a discrete system. A Kp of 1000 produces an ideal profile with no signs of instability, while the discrete model in plot 3 is clearly unstable at a Kp of 30.

Angular Velocity PD Controller with Feed forward
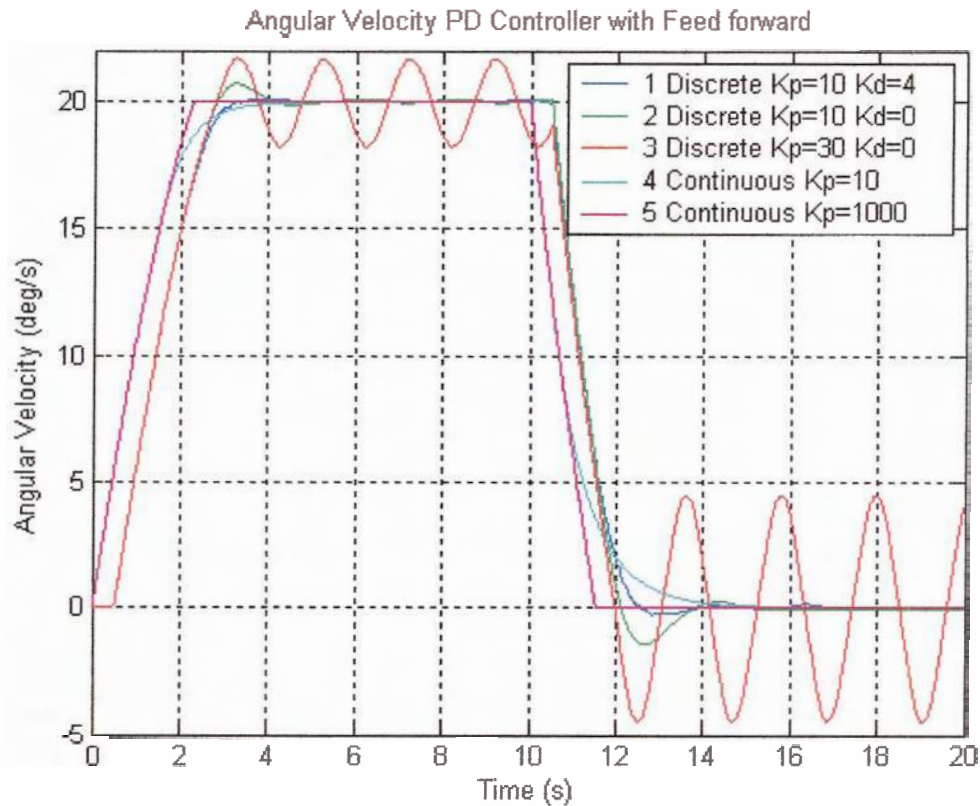
Fig. 63. Setpoint response curves of several angular velocity controllers.

5.3.2 Heading

Heading control is accomplished using a compass as the sensor to measure the state and a P controller with nested velocity feedback to achieve and hold the setpoint. The block diagram representation of the entire discrete heading control model is included in appendix E.

5.3.2.1 Controller: Proportional With Velocity Feedback

As changes in heading make up a very minute percentage of the AUV mission time, the heading controller is not required to be particularly fast. It is more important that this controller be stable with minimal oscillations.

Again, a P-type controller with velocity feedback and velocity ceiling is used to control the angular displacement. As described in section 5.1.3, this type of controller feeds the position error through the proportional gain and then limits this value to the maximum desired angular velocity. This signal is used as the reference signal to the angular

velocity controller. The acceleration and deceleration are controlled by the proportional gain, and the cruising velocity is set using saturation on the reference velocity. The Simulink representation of the controller is shown in fig. 64.


Fig. 64. Block representation of the heading controller.

5.3.2.2   Setpoint Response Curves

The response of the heading controller is examined with a setpoint change of 90 deg. It can be seen, from the two distinct groups of plots in fig. 65, that it is the velocity limiter that determines the general slope of the displacement response. It is also clear that deceleration rate controlled by the error gain is responsible for the level of overshoot.

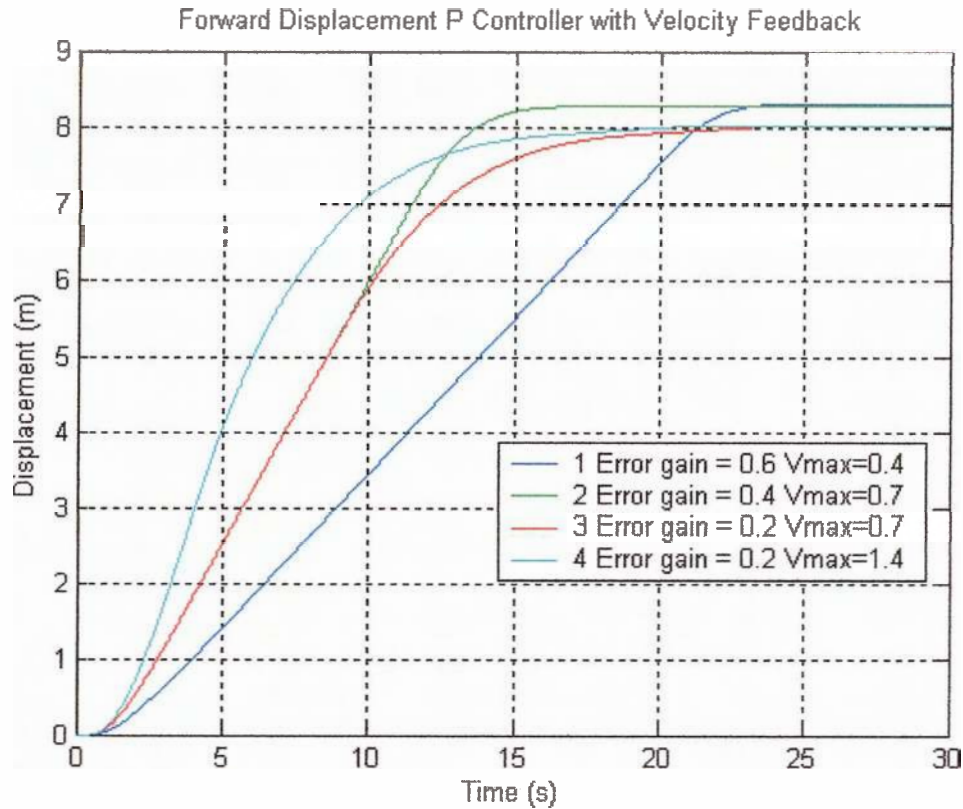**Fig. 65. Setpoint response curves of several controllers.**

The plots in fig. 66 are the velocity profiles corresponding to the angular displacement profiles in fig. 65.
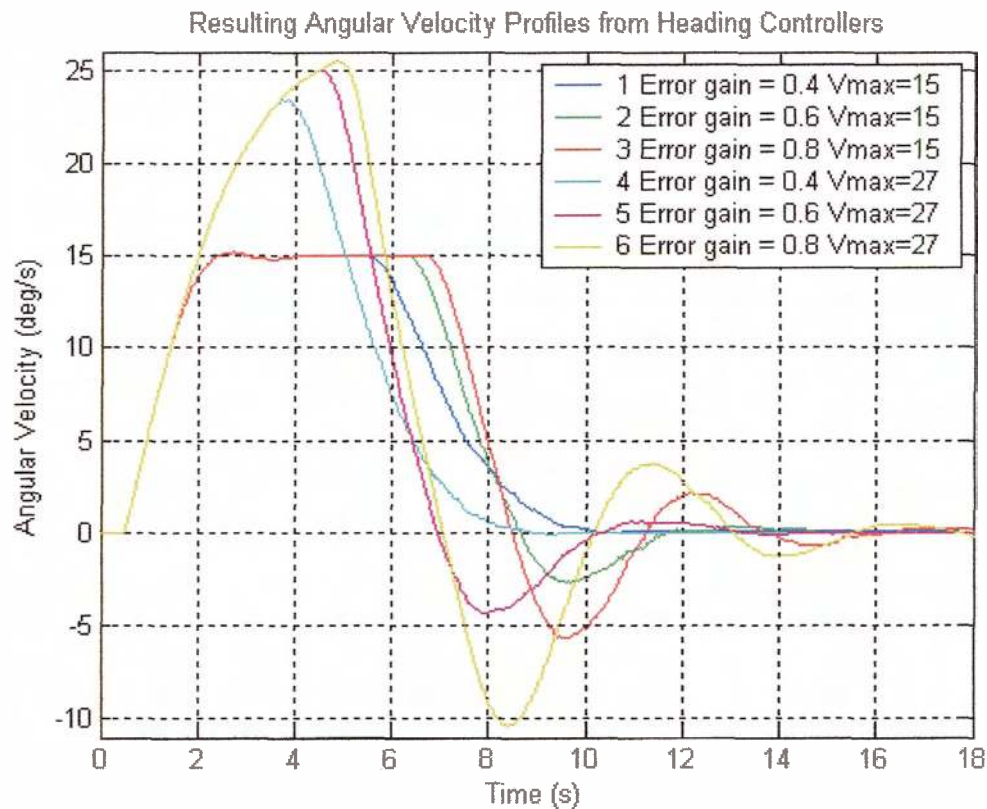
Fig. 66. Setpoint response curves of several controllers.

5.4 Depth

Depth control is accomplished using a pressure sensor to measure the state and a proportional-integral-derivative controller to achieve and hold the setpoint. The complete block diagram representation of the discrete depth control model is included in appendix F.

5.4.1 Controller: Proportional, Integral and Derivative

The AUV should move to the required depth and hold that depth. Because there is no velocity feedback and position errors will initially be quite large, the AUV will reach full vertical velocity and overshoot the setpoint. This is acceptable, provided the AUV does not oscillate and quickly locks on to the requested depth. In some cases, an additional payload such as a sensor or a camera may be added to the AUV. This may cause the vehicle to be positively or negatively buoyant.

To meet these requirements, the depth controller is a PID controller with a strong derivative term to reduce the overshoot and oscillations and an integrator to eliminate steady-state error caused by buoyancy imbalances. The Simulink representation of the controller is shown in fig. 67.
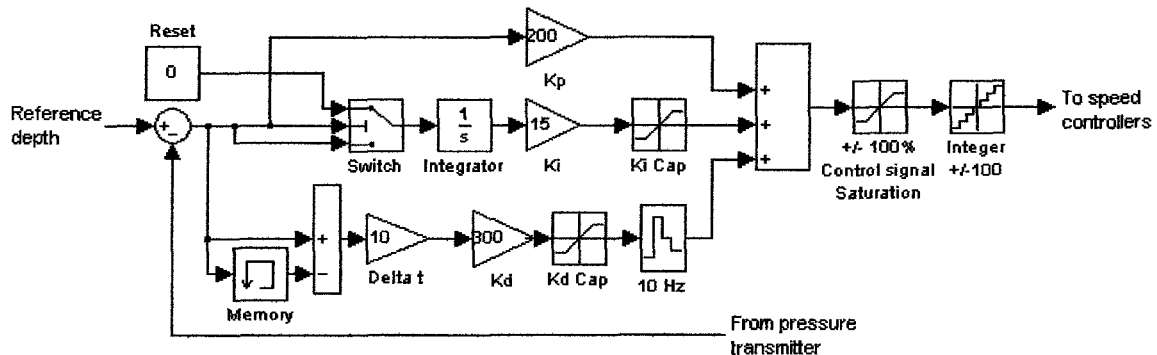
Fig. 67. Block representation of the depth controller.

5.4.2 Setpoint Response Curves

Fig. 68 illustrates the graphical tuning progression of the PID depth controller. The following comments describe each plot step through the process:

1. Plot 1 suffers from low-frequency oscillations and is very slow.

2. Here Kp is increased to improve the response time.

3. Kp is increased again, but with less notable results, so the proportional constant is left at 50.

4. To dampen out the oscillations, a derivative term is added to the controller with excellent results.

5. The system is improved further by doubling the derivative to 100.

6. The Kp is then set to 120, but the difference is only slight.
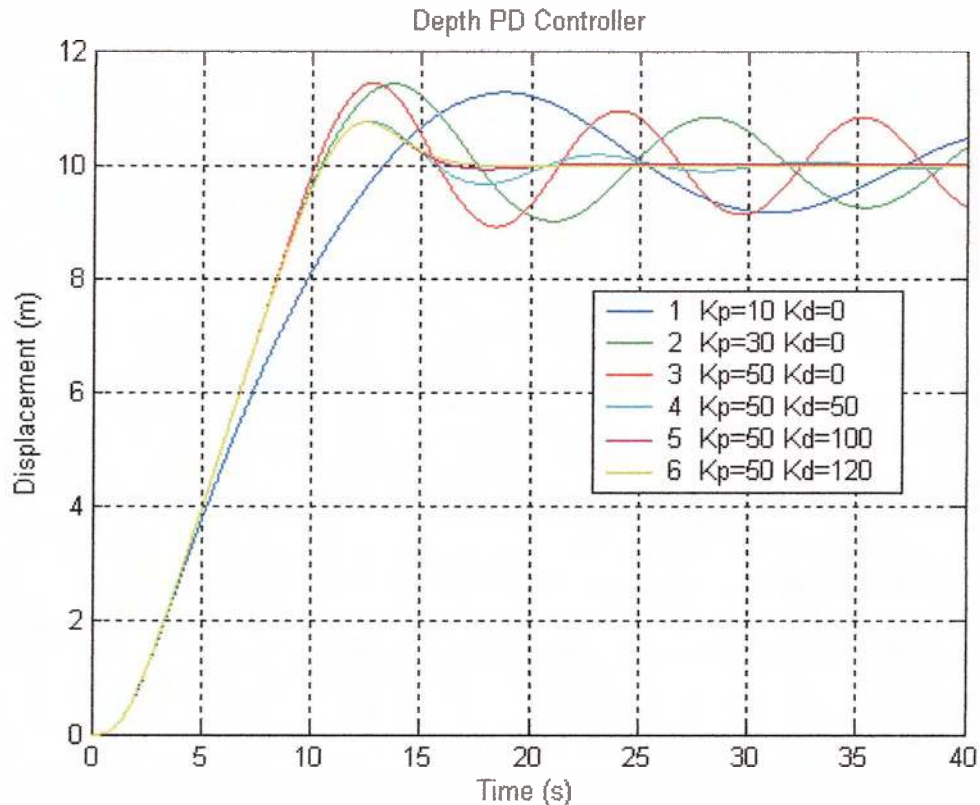
Fig. 68. Setpoint response curves of several controllers.

5.5 *Pitch*

Pitch is controlled using a level sensor to measure the state and a derivative controller with feed forward to stabilize the setpoint. The block diagram representation of the entire discrete depth control model is included in appendix G.

5.5.1 Controller: Derivative with Feed Forward

The AUV is expected to maintain a stable pitch of zero degrees throughout the mission. Oscillations in pitch can adversely affect the accuracy of the heading reading from the compass.

To meet these requirements, the pitch controller is a derivative controller with feed forward. The inherent righting moment of the AUV is a function of pitch angle and removes the need for a proportional term. The feed forward gain is actually multiplied with the square of the surge velocity, not the angular velocity about the Y-axis. The feed forward is tuned to cancel the effects of hydrodynamic imbalances such as that caused by

the GPS/wireless Ethernet antenna tower (fig. 41) or other payload. The Simulink representation of the controller is shown in fig. 69.

Fig. 69. Block representation of pitch controller.

5.5.2 Setpoint Response Curves

Motion about the Y-axis is unique, as mentioned above, because of the righting moment inherent in the AUV. Although it is not a direct substitute for a proportional controller, fig. 70 clearly demonstrates that addition of even a small proportional term causes instability in the pitch control.

A Kp of 2 causes the amplitude of the oscillations to increase. A Kp of 1 causes oscillations that do attenuate, but very slowly. The system is most stable in the absence of a proportional term in the controller.

Fig. 70. Destabilizing effect of a proportional term in the pitch controller.

Clearly a damping controller is required to cancel the periodic motion. For comparison with controllers that incorporate damping, plot 1 of fig. 70 is repeated in fig. 71. Plot 2, with a Kd of 2 is very effective at stabilizing the AUV. However, if Kd is increased beyond 2, the derivative controller also begins to cause oscillations.
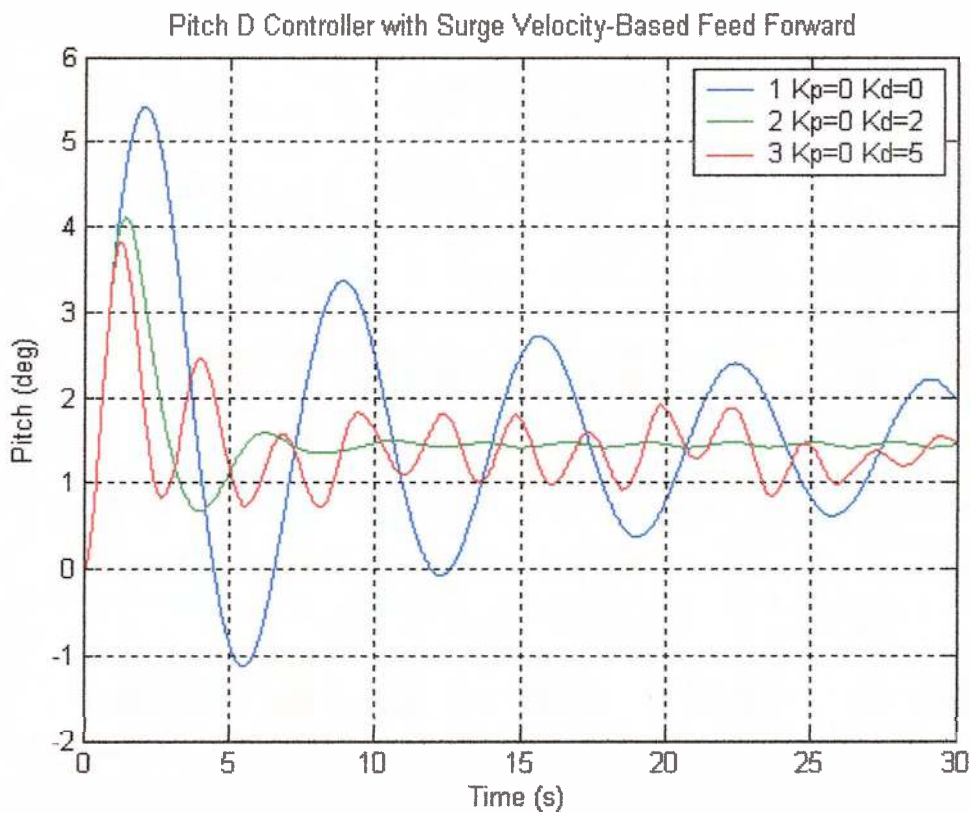
Fig. 71. Damping effect of the derivative term on the pitch controller.

Due to the geometry of the AUV (fig. 41), the vertical thrusters can create a large amount of torque. Because pitch control only requires a very small range of the available torque, the quantization is noticeable.

As described above, the feed forward used in the pitch controller is based on the surge velocity. Fig. 72 shows that, for a very small change of 0.01 m/s in forward velocity, the thruster output must jump to the next discrete step if it is on the threshold. A forward velocity of 1.05 m/s results in the same response as plot 2. This is by no means detrimental to the pitch controller, but it is interesting to note where discontinuities such as quantization have the greatest effect on the system.
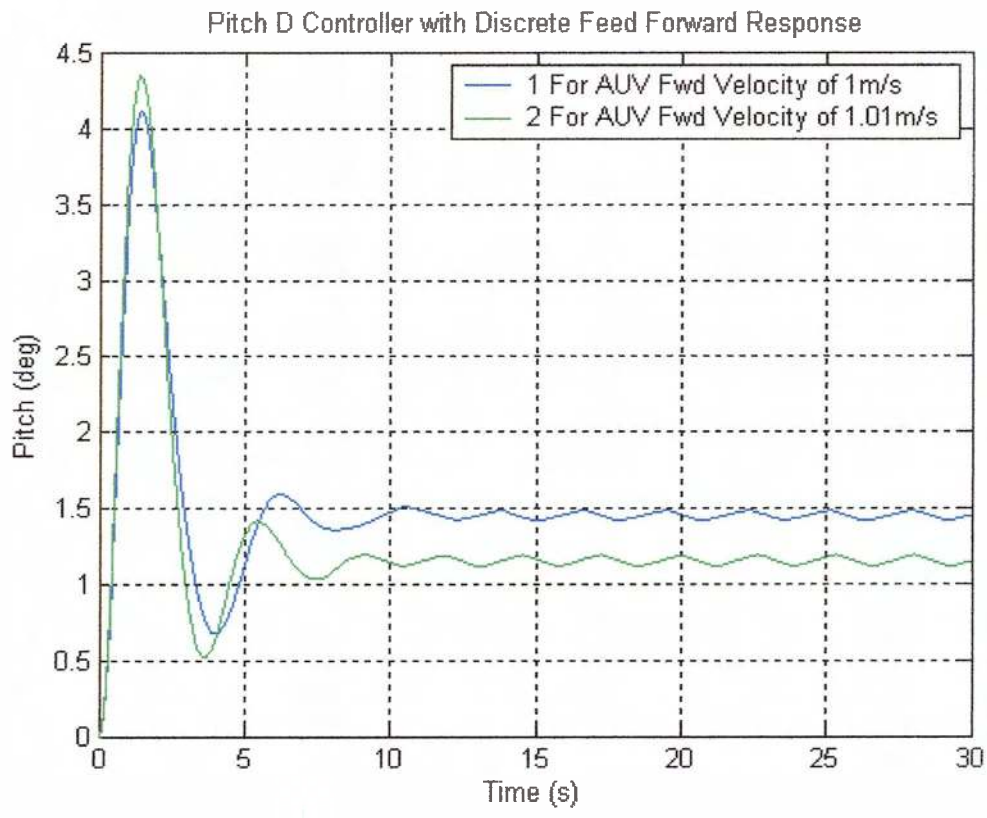
Fig. 72. Quantized levels of pitch due to quantized thruster output.

6 AUV Evaluation

The performance of the AUV was evaluated from two perspectives: (i) the closed-loop performance of each closed-loop DOF, and (ii) the AUV's performance in following a predefined mission path. In the previous chapters, control system parameters were experimentally determined, models were developed and evaluated, and controllers were designed based on the optimum model performance. In this chapter, the predicted closed-loop responses of the simulations are compared with the actual motion of the AUV. This confirms the accuracy of the models and allows evaluation of the controllers' performance.

With individual DOF optimally controlled, the navigation of the AUV during a mission was observed. The performance evaluation is based on how well the AUV follows a mission path during lake and sea trials. During these trials, the AUV mission path was compared with Global Positioning System (GPS) data that served as an absolute reference to monitor the error accumulation.

6.1 *Controller/Simulation Evaluation*

The objective of this work was to directly compare the modelled and experimental closed-loop responses for each DOF of the AUV. A strong correlation between the response curves verifies that the system of individually modelled subcomponents accurately represents the AUV under closed-loop control. To obtain the experimental response data, the controllers designed in Simulink were implemented in the actual AUV control software. Then the AUV and the model were both given the same setpoint and the dynamic responses of each were recorded. The following subsections contain plots of the experimental and simulated dynamic response curves for direct comparison. Table 4 provides a list of the dynamic responses that are presented for each degree of freedom in the sections to follow.

Table 4. The dynamic response comparisons presented throughout chapter 7.

Degree of Freedom	Dynamic Response Presented
Surge	Velocity - Achieve and maintain a reference forward velocity and then stop with no overshoot.
	Displacement - Traverse prescribed displacement and then stop.

Yaw	Angular velocity - Achieve and maintain a reference angular velocity and then stop and maintain zero angular velocity.
	Angular displacement - Reach and hold a reference heading.
Heave	Displacement - Reach and hold a reference depth.
Pitch	Displacement - Dampen angular position oscillations.

6.1.1 Surge velocity

For this test, the AUV was required to achieve a surge velocity of 1 m/s, maintain this speed, and then stop with zero negative overshoot. The actual and predicted response curves are in good agreement (fig. 73). The AUV reached the 1 m/s setpoint, but then held at approximately 0.95 m/s. This may have been caused by the feed forward function or the battery charge level. A low-gain integrator could be added if it became necessary to reduce all steady-state error. The output of the flow meter is slightly erratic during acceleration from rest, however it provides a smooth deceleration output that agrees closely with the model.

Fig. 73. The experimental and simulated closed-loop responses of the surge velocity controller.

6.1.2 Surge displacement

For this test, the AUV was required to travel a distance of 10 m at a cruising velocity of 0.7 m/s with no overshoot. The actual and predicted displacement response curves are in good agreement, as shown in fig. 74a. Fig. 74b shows the actual and predicted responses of the nested velocity controller to the setpoint requests made by the displacement controller. Again, the experimental velocity is slightly lower than the 0.7 m/s cruising velocity that was specified. However, the transient portions of the curves are in very good agreement and the controller provides a strong deceleration with no negative overshoot.
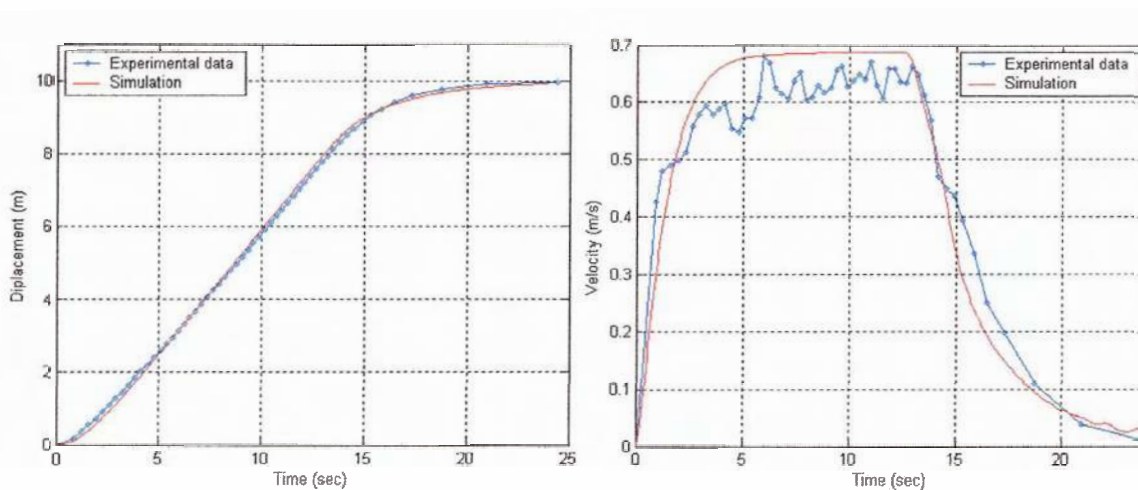
Fig. 74. a) The experimental and simulated closed-loop displacement responses. b) The nested velocity controller response to setpoint changes made by the displacement controller.

6.1.3 Yaw velocity

For this test, the AUV was required to achieve an angular velocity of 15 deg/s, maintain this velocity, and then stop and hold at 0 deg/s. The actual and predicted response curves are in good agreement, as shown in fig. 75. The AUV undershot the setpoint angular velocity by approximately 1 deg/s, again most likely because of the feed forward function or a low battery charge level. It is notable that the model is predicting the start of small oscillations as the AUV completes its deceleration. The oscillations are present in the experimental results. The controller is providing very strong control with approximately 3 s rise and fall times, accompanied by a small amount of steady-state oscillations.
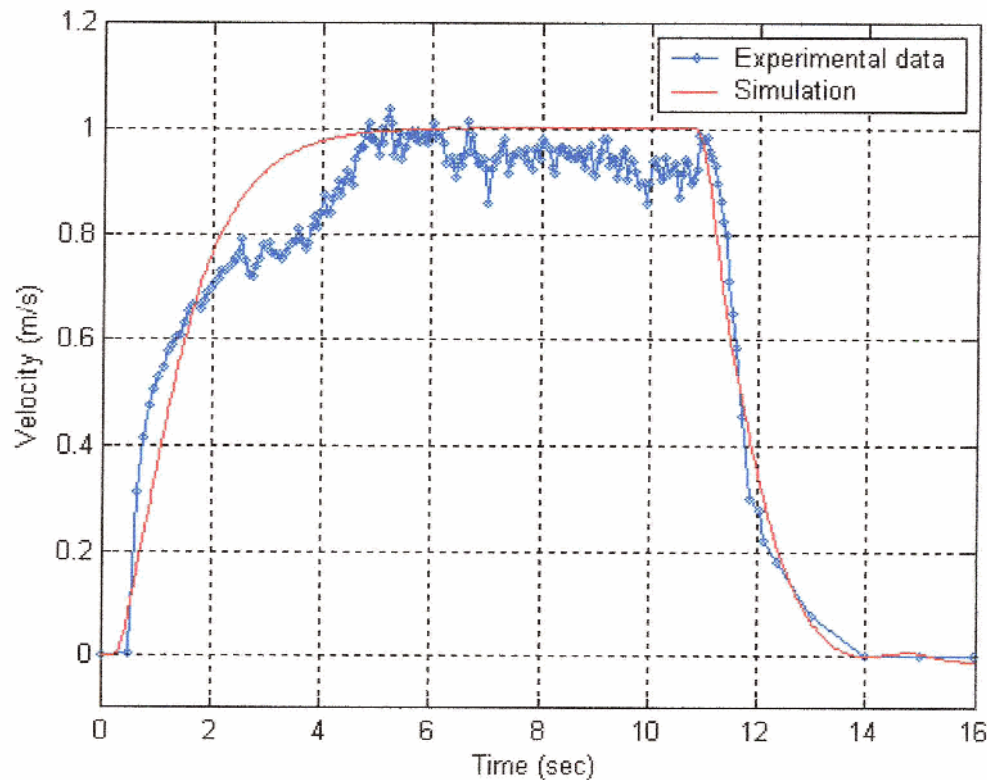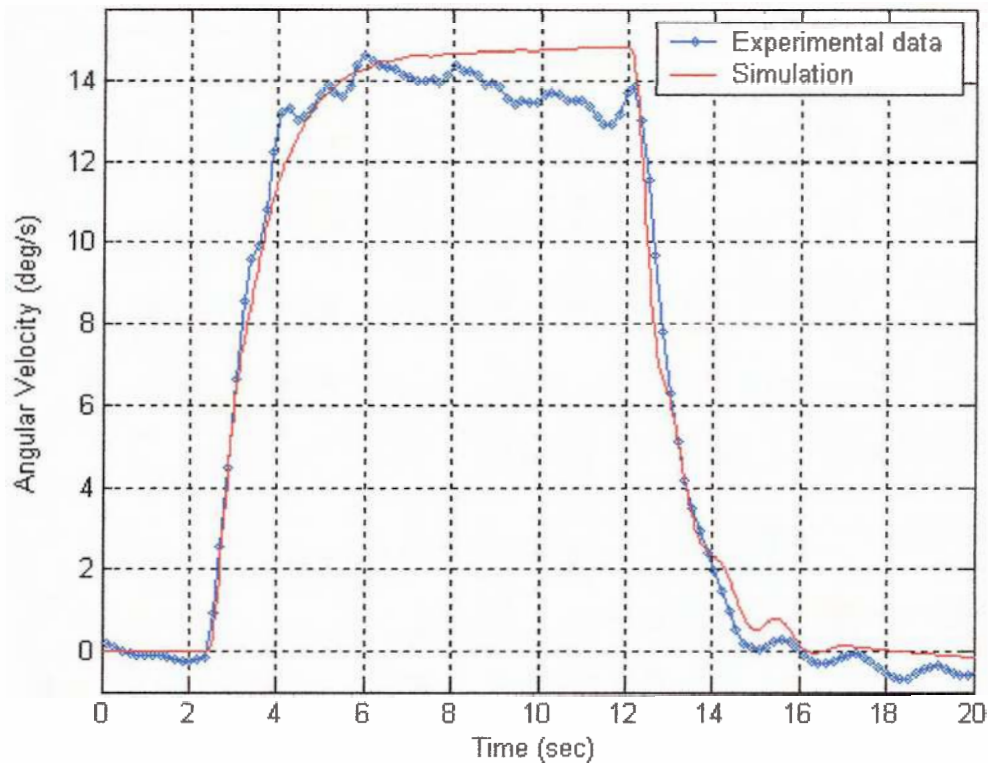
Fig. 75. The experimental and simulated closed-loop responses of the yaw velocity controller.

6.1.4 Heading

For this test, the AUV was required to hold at 0 deg, and then turn to 90 deg and hold with little or no oscillations. The actual and predicted heading response curves are in good agreement, as shown in fig. 76a. Fig. 76b shows the actual and predicted responses of the nested angular velocity controller to the setpoint requests made by the heading controller. The three sections of the velocity profile: acceleration, constant rate at 9 deg/s, and deceleration are very closely predicted by the model. The heading controller is tuned very conservatively and could provide much faster rise times. The gain is close to optimal, but the constant velocity could be safely doubled.
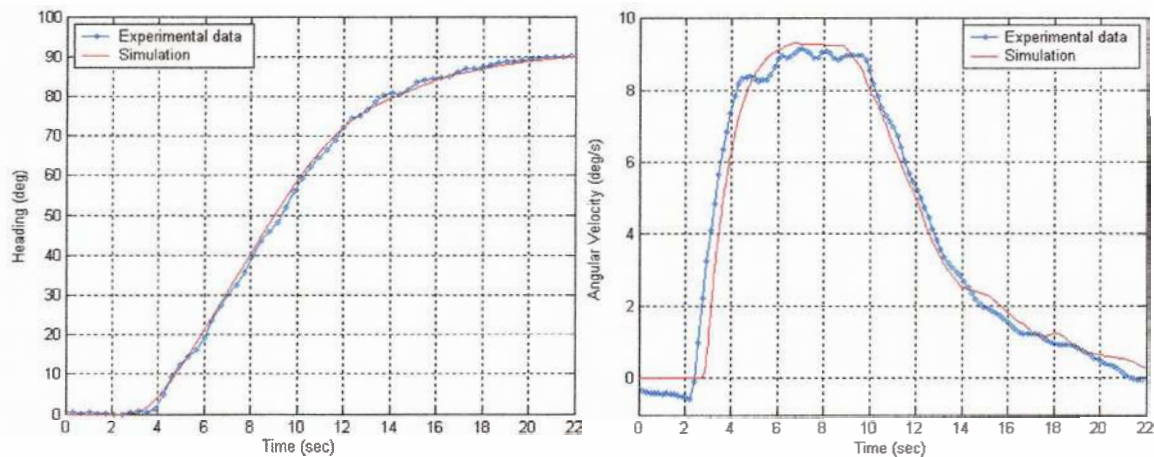
Fig. 76. a) The experimental and simulated closed-loop heading responses. b) The nested angular velocity controller response to setpoint changes made by the heading controller.

6.1.5 Depth

For this test, the AUV was required to begin at the surface, then dive to a depth of 5 m and maintain this depth with minimal oscillations. The actual and predicted depth response curves are in good agreement, as shown in fig. 77. The model is predicting a slightly stronger deceleration, but the setpoint is achieved at the same time. The controller provides a stable response with no oscillations and a constant diving velocity of approximately 0.5 m/s.
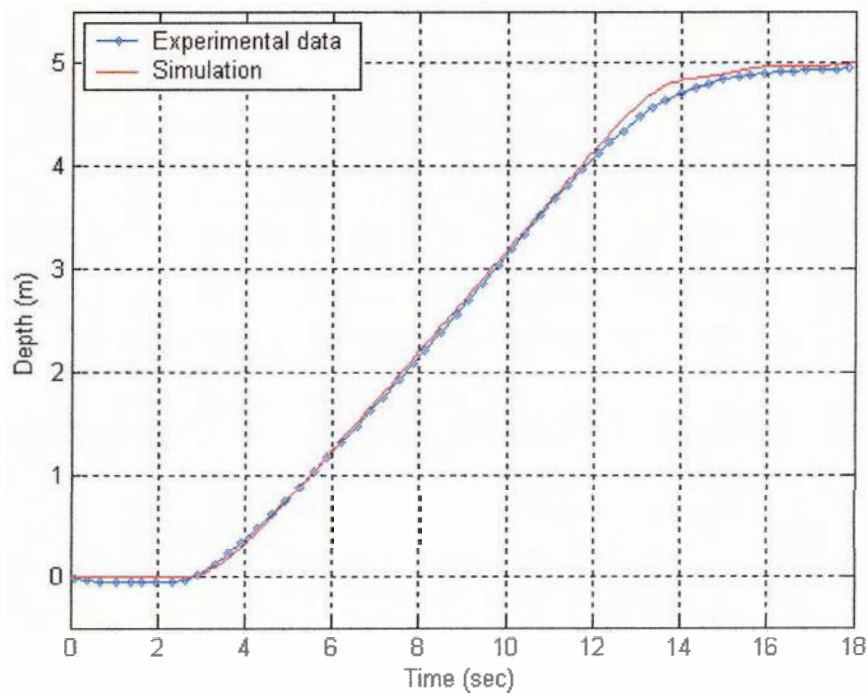
Fig. 77. The experimental and simulated closed-loop responses of the depth controller.

6.1.6 Pitch Damping

For this test, the AUV was held at a pitch angle of 20 deg using open-loop thruster control, and then released. Immediately after the release the differential controller was turned on to dampen the oscillations. The controller then dampened the oscillations to within 4% in 7 seconds. The actual and predicted response curves are in good agreement with respect to the amplitude of the oscillations (fig. 78). The model predicted a slightly lower frequency of oscillation, which means the drag and inertia terms are too high with respect to the righting moment torque.
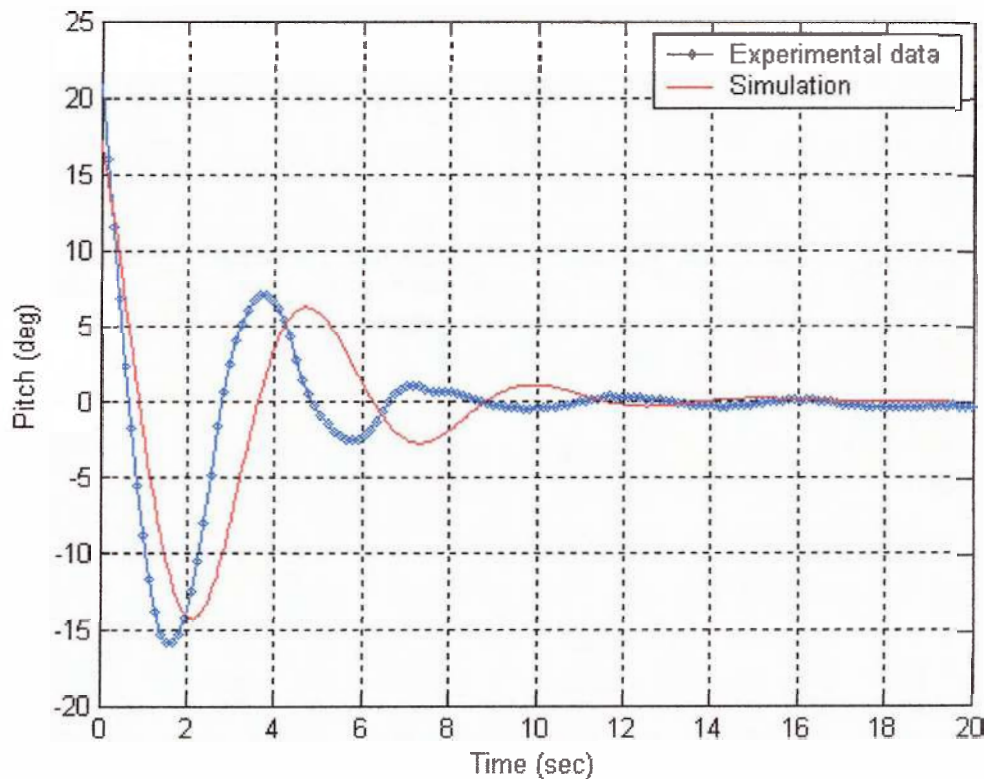
Fig. 78. The experimental and simulated closed-loop responses of the pitch controller.

The pitch controller is essential to the operation of MACO because an oscillating system can cause liquid level sensor readings to become erratic and also makes for a poor science platform, particularly for video imaging. Fig. 79 illustrates the vast improvement the differential controller made when compared with the natural damping of the system with no controller. The settling time was reduced from more than 40 s to less than 10 s.
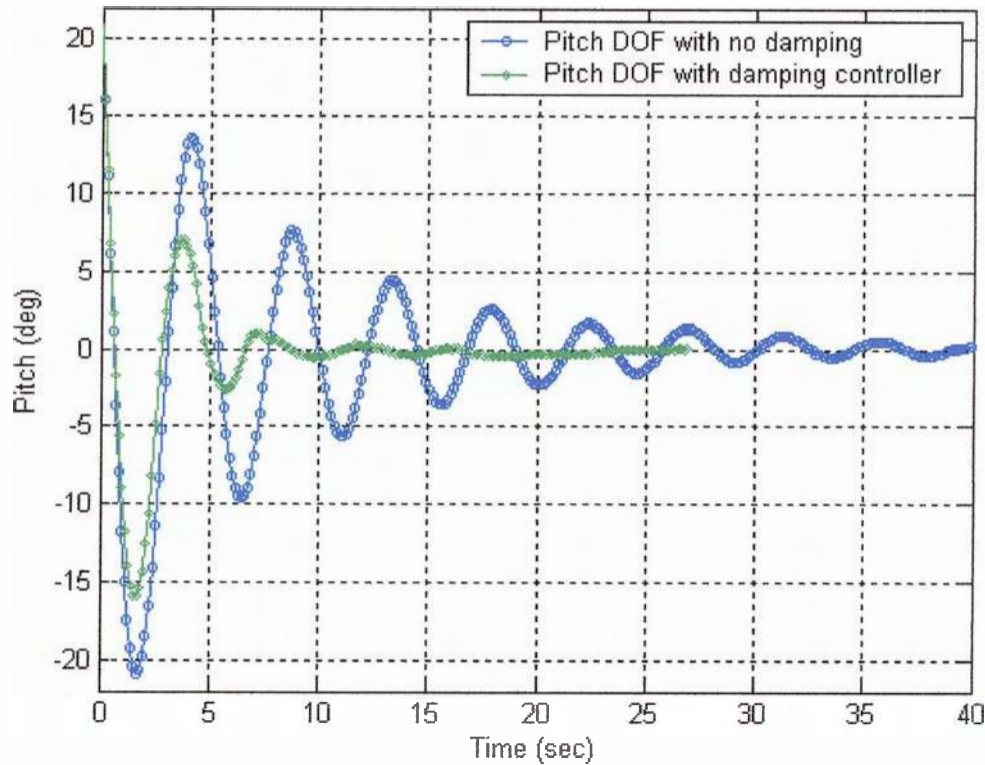
Fig. 79. Experimental data showing i) the natural oscillations of the undamped AUV and ii) the reduced settling time with the differential controller implemented.

6.2 AUV Performance Evaluation

The definitive testing of the AUV came during the mission trials. During these trials the entire system came into play. The complete missions were defined by script files (appendices H, I, and J), which were uploaded to the AUV from the deployment vessel via wireless link. Once the mission was initiated, all of the controllers were operating simultaneously. The objective of this section is to examine how accurately the AUV followed a prescribed path. In order to meet the accuracy requirements of DRDC, it was essential that the AUV maintain a depth within 0.5 m of the reference depth and under ideal conditions (i.e., absence of wind and water current), not deviating from the prescribed path by more than 5% of the mission length at any point along the mission.

As examples of overall AUV performance, three missions are presented: (i) Elk Lake surface trial, (ii) Elk Lake trial at a depth of 5 m, and (iii) Halifax sea trials for DRDC. During both missions at depth, the AUV was programmed to surface periodically,

reacquire a GPS link, and calculate its current position. This position data was stored in a log file and was subsequently compared with the intended mission path.

6.2.1 Elk Lake Surface Trial

A surface mission was preformed to ensure the AUV systems were operating properly and to verify that the script file was correct. As a precaution, floats were attached to the AUV during the mission. The floats were large enough to overcome maximum downward thrust of the AUV. The drag of the floats and the pitching and rolling caused by the surface conditions were undesirable, but had no significant effect on the performance. The wind, however, caused a net drift of 0.55 m/min at 262 deg (fig. 80a). With this drift vector removed, the isolated navigational error can be observed (fig. 80b). Fig. 80 shows the paths followed for the actual mission, the planned mission, and the actual mission with the drift vector removed.

Fig. 80. Surface mission GPS data: a) uncompensated b) current/wind compensated.

The maximum position error during the mission with and without drift was 28 m or 3.3% mission length and 12 m or 1.4% mission length respectively. Both the raw and the compensated position error with respect to elapsed mission time are shown in fig. 81. The script file of the Elk Lake surface trial is in appendix H.
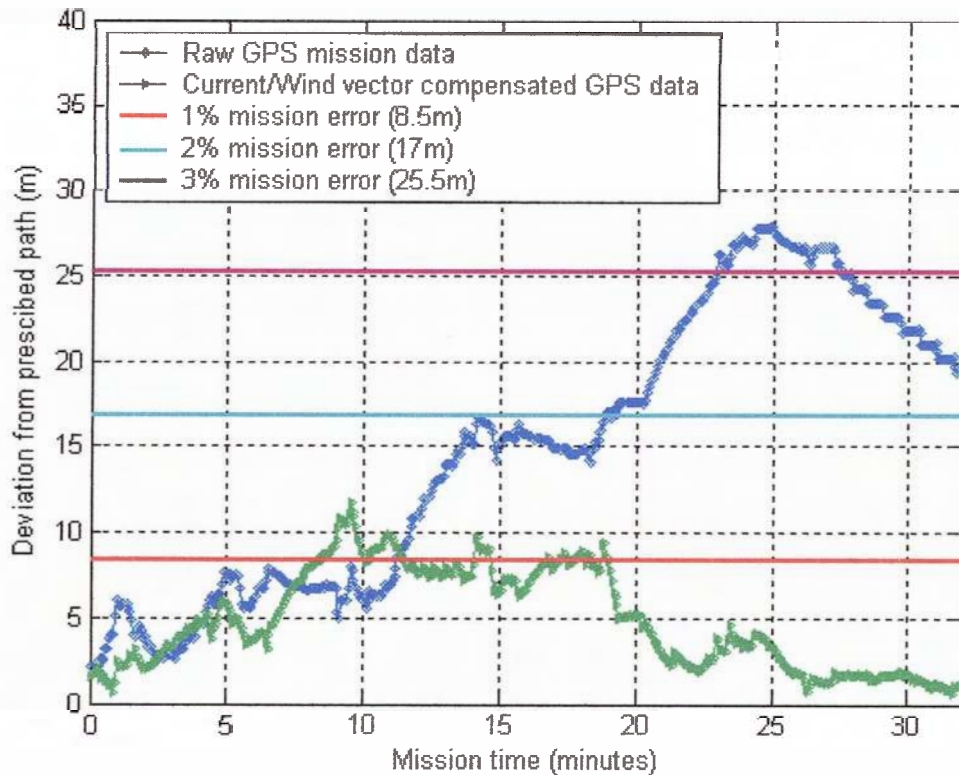
Fig. 81. Position error magnitude for the raw and the current/wind compensated GPS data during the mission.

6.2.2 Elk Lake Five-Metre Trial

With the reliable operation of the AUV confirmed, a subsurface mission was performed to observe the performance of the AUV in the absence of surface effects. Elk Lake has a maximum depth of approximately 15 m; therefore a safe operating depth of 5 m was selected. Aside from the depth change and corner point surfacing for GPS, the mission path was the same as the surface trial. Unfortunately, the GPS wasn't able to reacquire during the 20 s it spent at each surfacing point, and therefore the AUV only logged the starting and finishing positions. The actual and planned mission paths are shown in fig. 82.
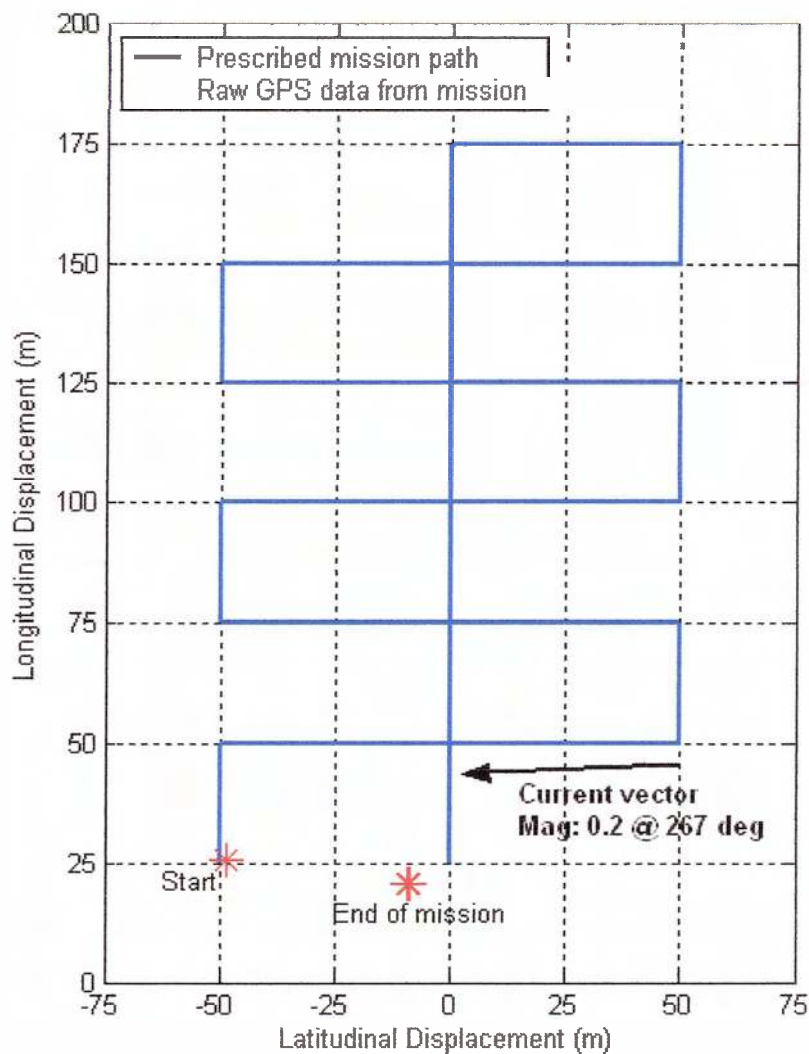
Fig. 82. Five-metre mission start and finish positions with respect to the prescribed mission.

The overall position error during the mission was 8.8 m or approximately 1% of the total mission length. Based on the final position of the AUV, it was determined that there was a very small current vector of 0.2 m/min at 267 deg. The script file of the Elk Lake five-metre trial is in appendix I.

6.2.3 DRDC Mission in Halifax

The DRDC sea trial represented the ultimate test for the AUV. The mission was not more challenging than the rehearsal trials, but the following aspects added to the critical nature of the mission:

The mission path was unknown prior to arrival on the Quest.

- The operations were to be performed in open-ocean conditions, where the AUV would be unrecoverable in the case of a malfunction.

- The client had sophisticated equipment deployed on the seafloor awaiting calibration by the AUV.

Following a successful deployment of their acoustic array, DRDC provided the longitudes and latitudes of the array element localization mission. Using these coordinates and correcting for local declination of 19.6 deg, the mission path, consisting of depths, headings, and leg lengths, was generated. The total mission length was 1.42 km, consisting of a rectangle followed by a corner-to-corner diagonal.

Because the AUV uses a form of dead-reckoning navigation, in which only the surge component of velocity with respect to water is measured, vehicle drift caused by water current goes undetected. To minimize the effect of the current, the mission was to proceed during slack tide. Even so, the small current that was present caused a net drift of 2.4m/min at 332 deg, as shown in fig. 83a. This drift vector was removed and the isolated navigational error can be observed in fig. 83b. It should be noted that the raw data set was shifted for coincident starting points. The data was also rotated by -6 deg to account for a hard-iron calibration problem with the compass at the time of this mission.
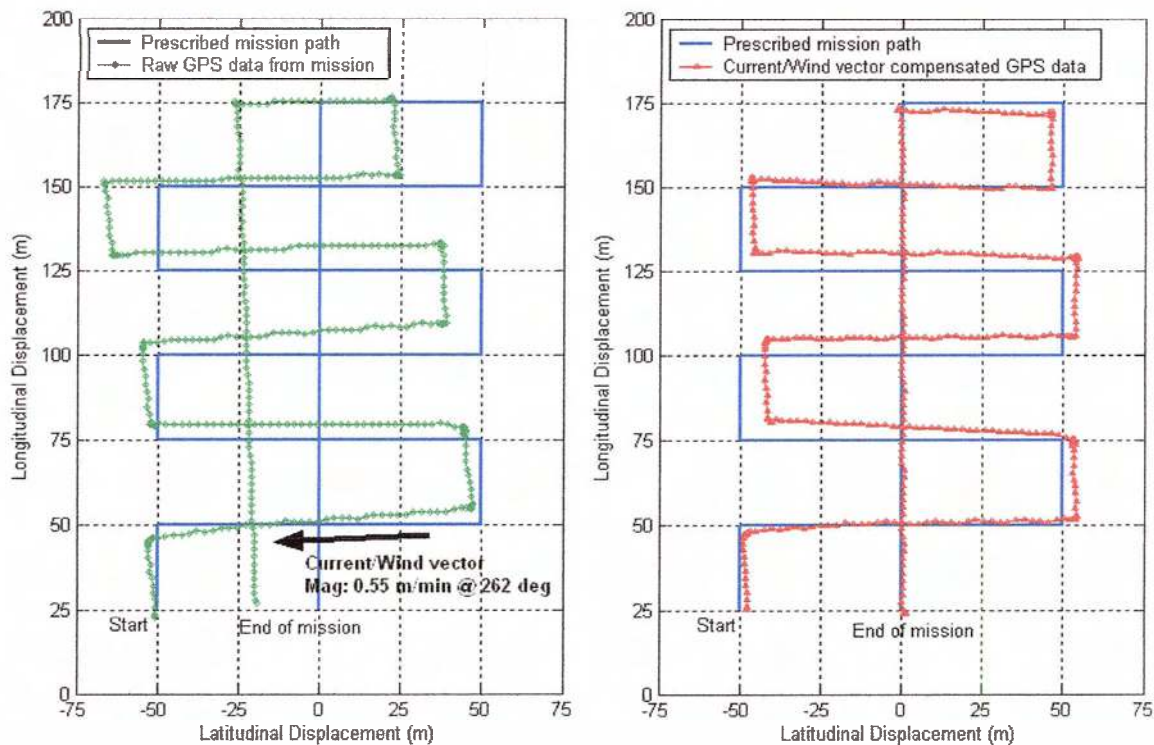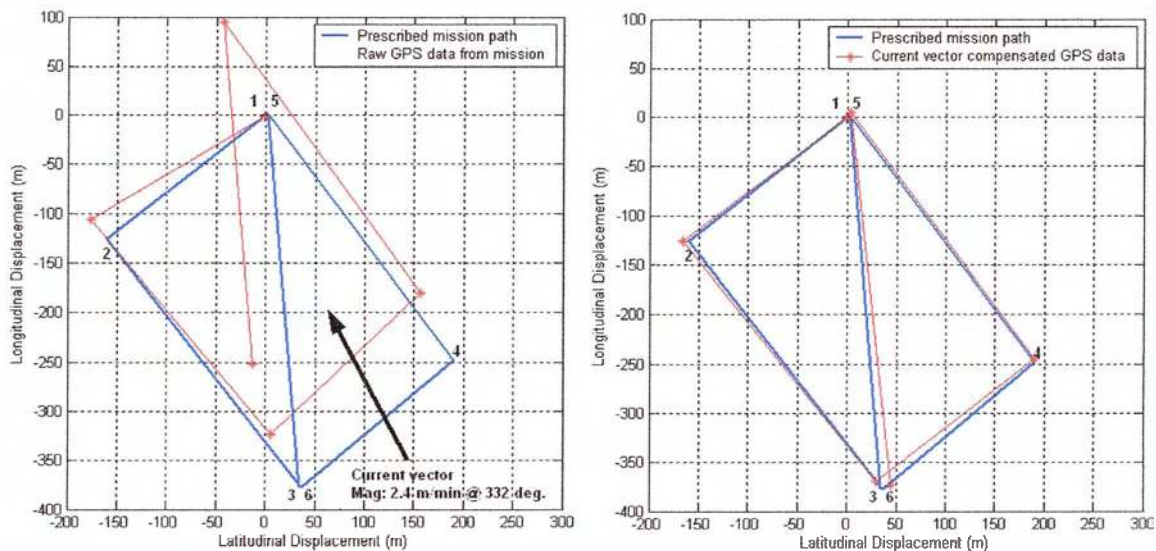

Fig. 83. Halifax mission GPS data: a) uncompensated b) Current vector compensated.

The maximum position error during the mission, with and without drift, was 134 m or 9.5% mission length and 11 m or 0.8% mission length respectively. Both the raw and the compensated position error with respect to elapsed mission time are shown in fig. 84. It

is interesting to note that the slope of the accumulating error of the raw data is very close to the magnitude of the current vector removed. The script file of the Halifax sea trial is in appendix J.
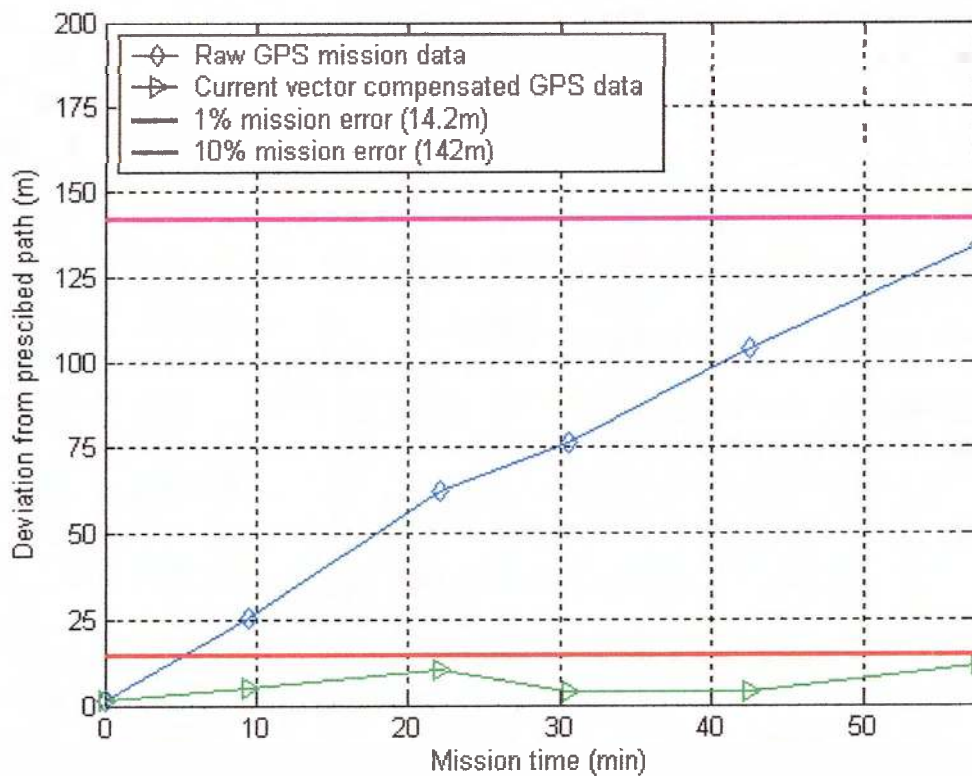
Fig. 84. Position error magnitude for the raw and the current compensated GPS data during the Halifax mission.

7 Conclusions and Recommendations

7.1 Conclusions

The overall development of the AUV MACO went very well. The engineering methodology used to create the design specifications from the client's requirements produced a concise vehicle description. This description provided direction during the subsequent development of the software and the mechanical and electrical systems. Following are the key conclusions drawn during the modelling and controller design processes.

The experimental parameter acquiring methods proved to be a very effective means to generate the quadratic drag curves used in modelling and the feed forward controllers. However, all of the open-loop trials were based on speed controller values that correlate to thrust levels. This relationship between speed controller values and thrust was validated using measurement apparatus, but is based on the current battery charge state. A battery charge state different than that at the time of characterization will result in scaled thrust levels. The effects were noticeable, but not detrimental and the open-loop data was very useful on creating models for each degree of freedom (DOF).

Simulink was an extremely useful tool for graphically representing the AUV system dynamics. This became particularly evident when modelling the discrete characteristics of the computer and feedback sensors such as the sampling rate, quantization, zero-order-hold, and transport delay.

The importance of correctly representing the discrete nature of components of a closed-loop control system was clearly illustrated by the response plots in Chapter 5. It was shown that when MACO was represented as an entirely continuous system, it remained stable even when subjected to oversaturated actuation. In contrast, when MACO was represented as discrete it began to destabilize in a similar fashion to the actual system. Based on the work done here, a delay in the system had the most significant affect on the stability. As a result, care must be taken when averaging sensor data. Although it is sometimes required when using a differentiator, averaging will produce an additional delay over and above the inherent sensor delay.

The decoupled approach to AUV modelling and controller design is well suited to hybrid AUVs. It simplifies the problem greatly and the evaluations in Chapter 6 validate the effectiveness of this method. Of course, MACO is not a truly decoupled system. Thrusters are shared by separate DOF, which can lower the individual actuation saturation points if the other DOF is placing demands of the thruster. The asymmetric hydrodynamics caused by the antenna tower and the slung payload caused a pitching moment as a function of forward velocity. This function caused a coupling of the pitch and surge DOF, but was controlled with the addition of a cross-DOF feed forward function.

Notwithstanding the uncompensated drift error, MACO perform flawlessly during the sea trials in Halifax. MACO's small size makes it an ideal candidate for integration with a rapid deployment array element localisation system. The use of AUV technology definitely enhances operations such as those conducted by DRDC and its low cost makes MACO an attractive asset.
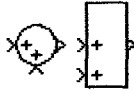
7.2 Recommendations for Future Work

Based on the development process of MACO and the operations during the lake and sea trials, the following modifications would greatly improve the modelling process and navigational accuracy:

- thrust prediction using velocity feedback on thrusters.
- amalgamation of the open-loop characterization scripts into a single script file followed by first-pass automated data processing.
- incorporation of a second gyro to measure pitch rate.
- in both pitch and yaw, the gyro rate output should be integrated to give pitch and heading and be reset periodically with the absolute sensors (tilt and compass).
- incorporation of linear accelerometers aligned with surge and heave to aid in modelling.
- include a quadratic and a linear term in all feed forward functions.
- develop and implement navigation algorithms using GPS correction and global drift estimation.

8 Appendices

8.1 Simulink Block Descriptions

Block	Name	Description
	Sum	This block combines the magnitudes of the input signals.
Integrator	Integrator	This block provides a running summation of the input.
du/dt Derivative	Derivative	This block provides the rate of change of the input.
Gain	Gain	This block multiplies the input by the specified value and returns the product as the output.
Saturation	Saturation	This block will only allow signals that are above a minimum and below a maximum to pass.
Quantizer	Quantization	This block will only allow discrete values of amplitude to be output. It will hold the current value until the next higher or lower discrete value has been reached.
Zero-Order Hold	Zero-order hold	This block samples the signal and will hold that value for a predetermined sample period, then resample and repeat.
Transport Delay	Transport delay	This block shifts the output forward in time by a predetermined amount of time on a continuous basis.
Variable Transport Delay	Variable transport delay	This block shifts the output forward in time by a variable amount of time on a continuous basis.

8.2 Surge Velocity Block Diagram
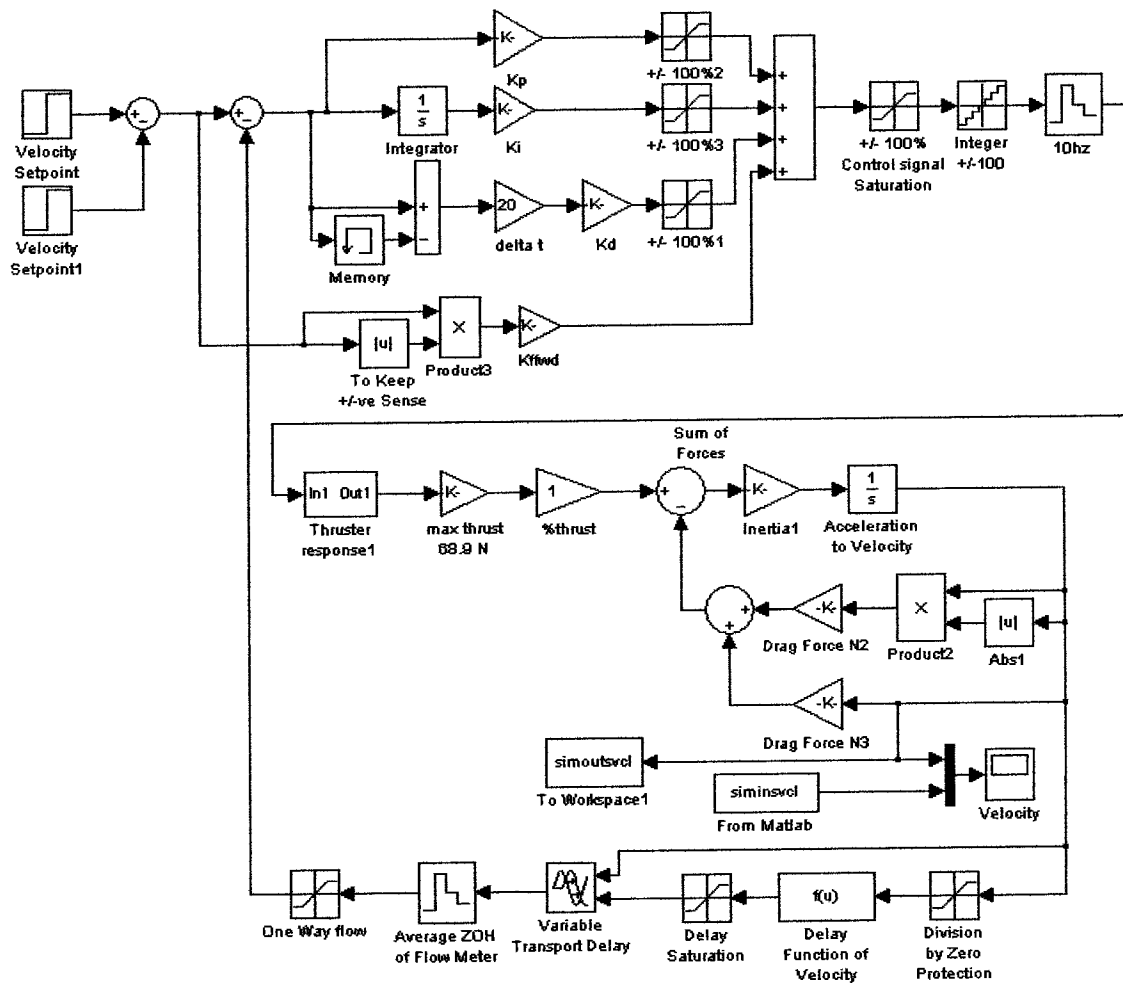
8.3 Surge Displacement Block Diagram
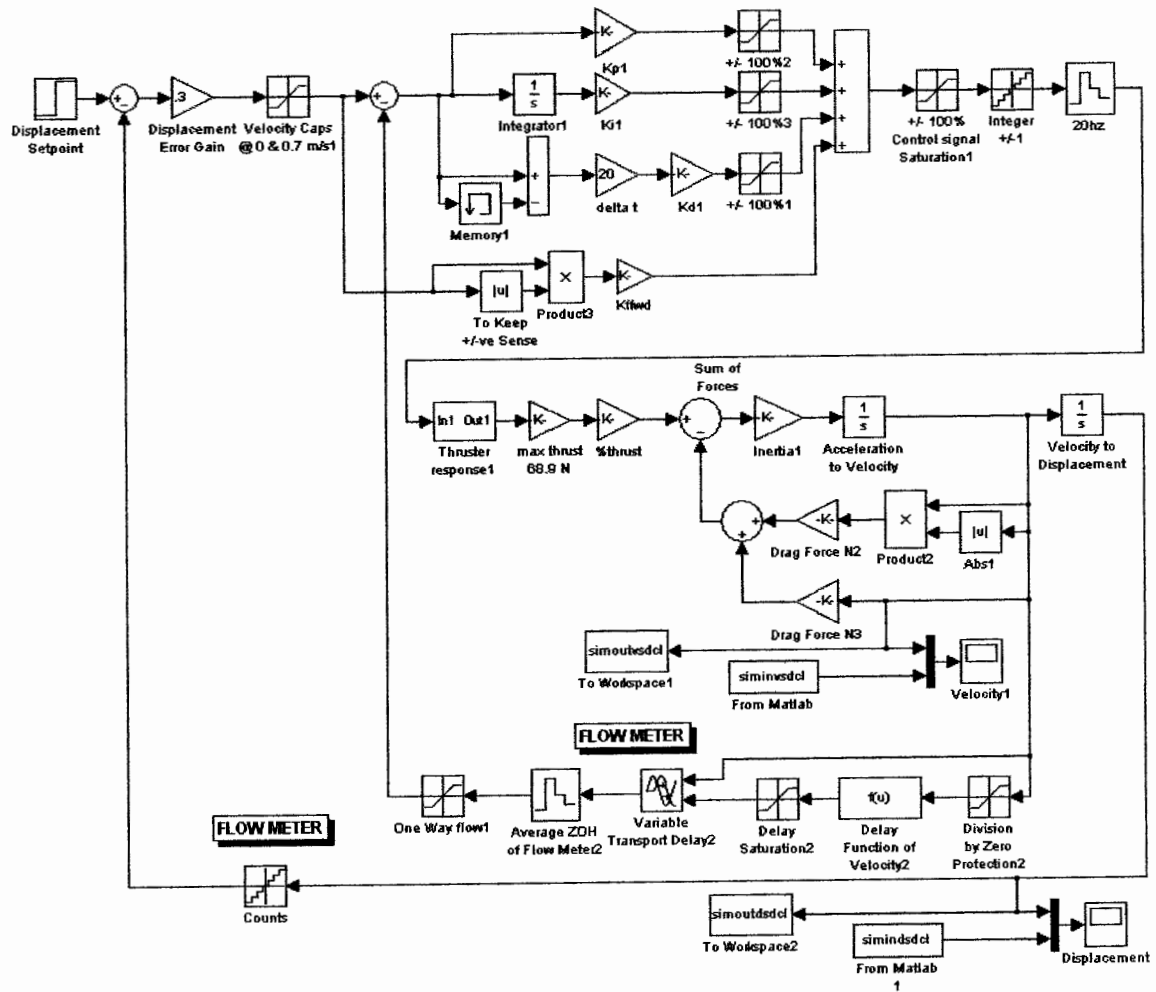
8.4 Yaw Velocity Block Diagram
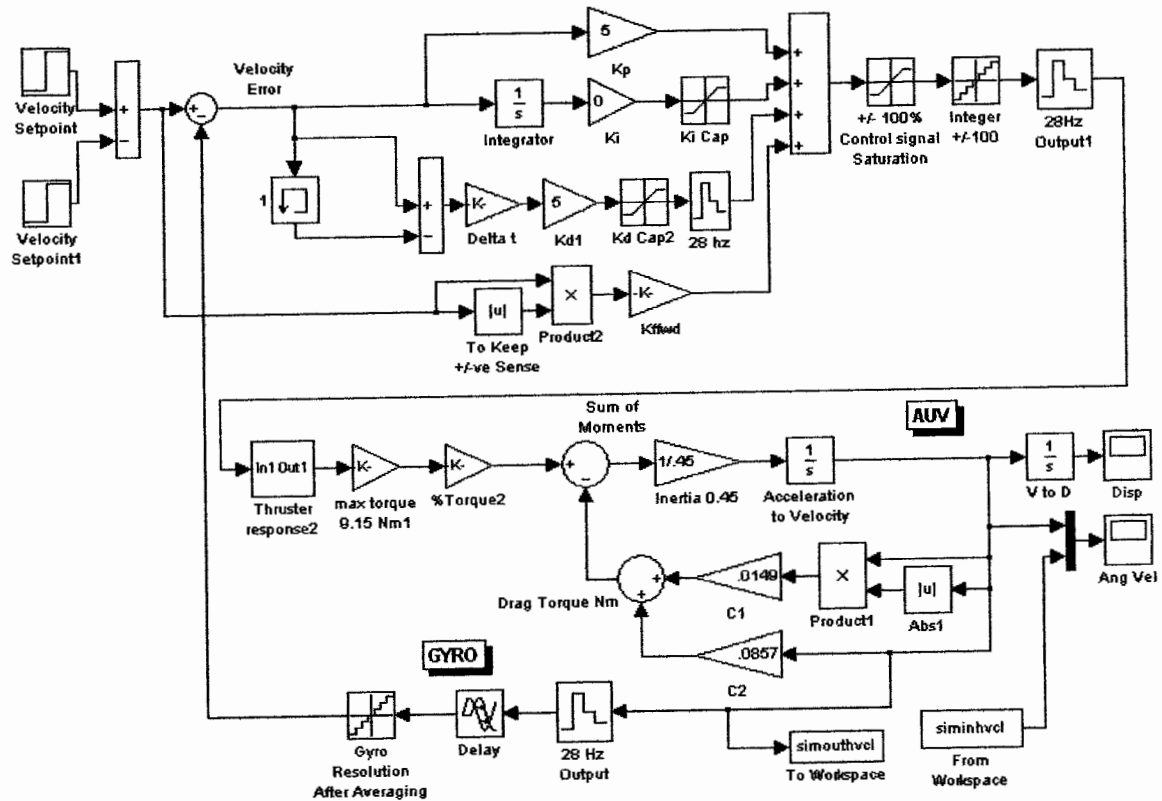
8.5 Heading Block Diagram
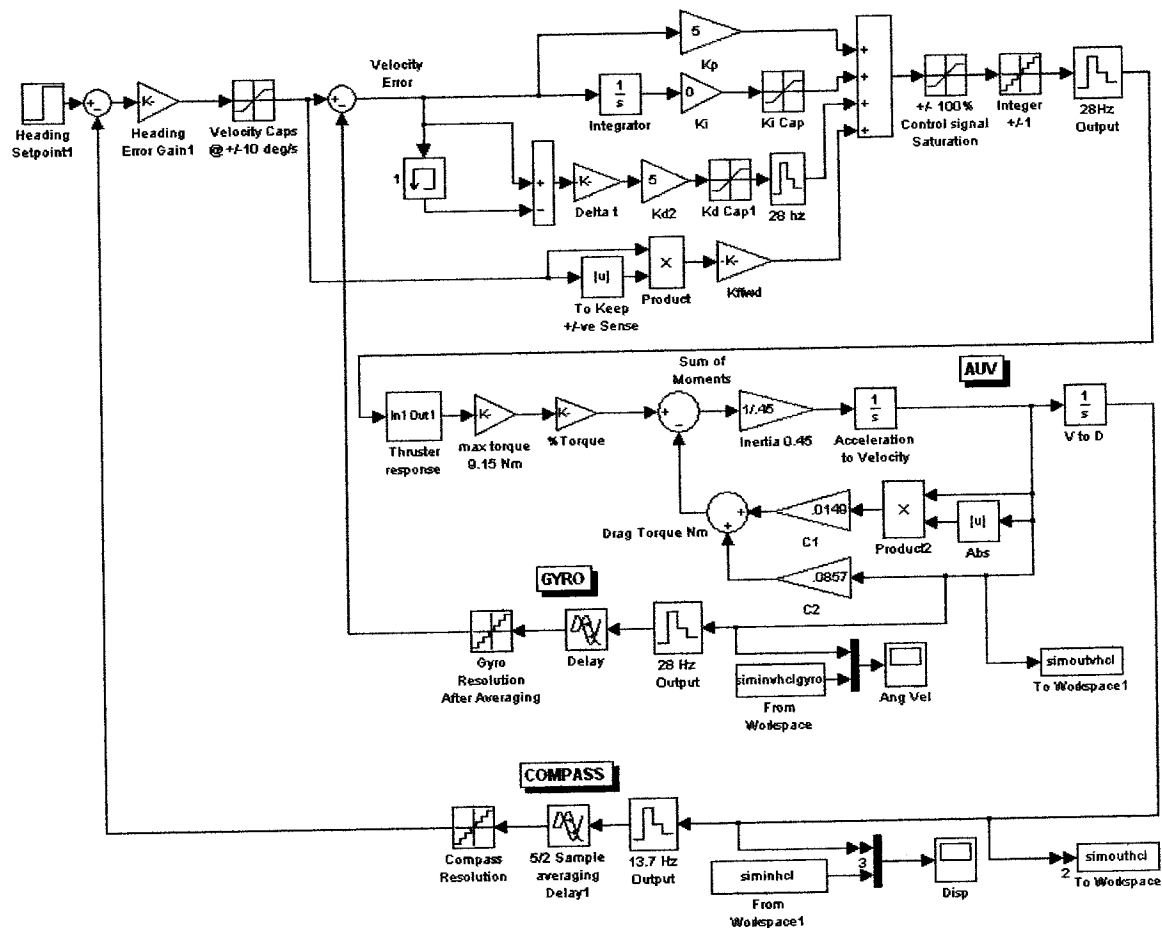
8.6 Depth Block Diagram
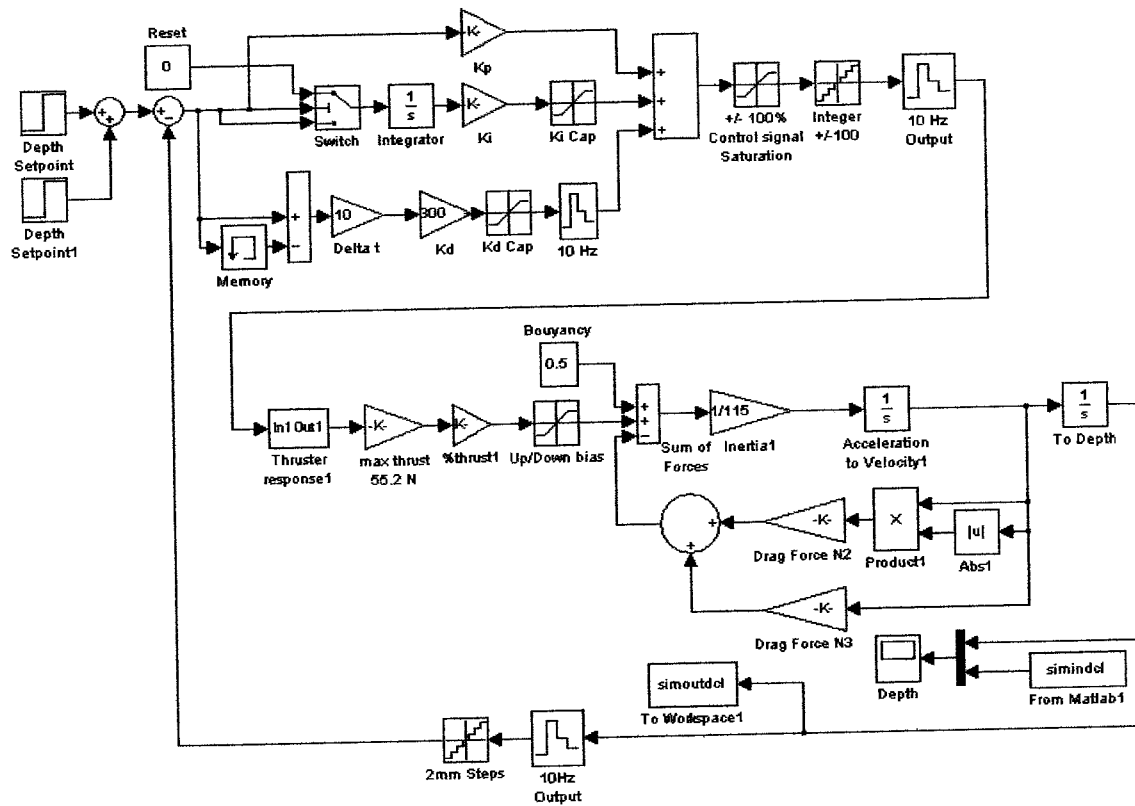
8.7 Pitch Block Diagram
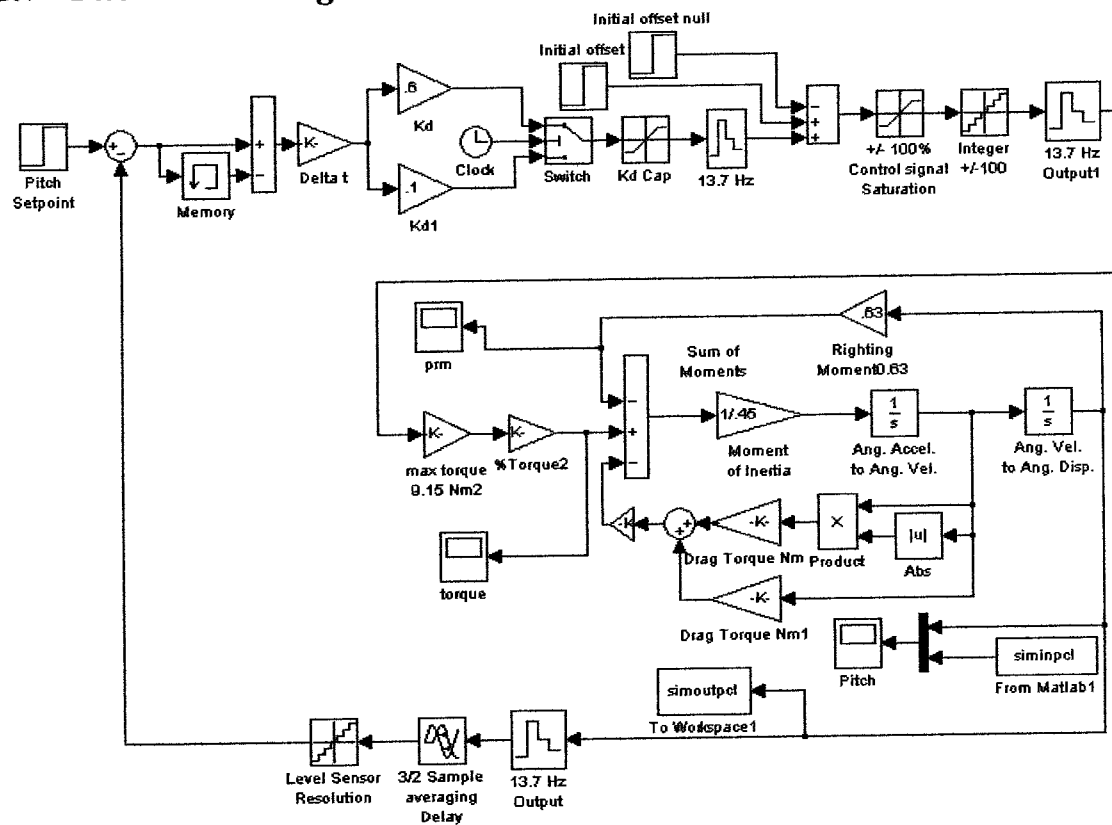
8.8 Elk Lake Surface Mission Script File

```
-- Surface mission on Elk Lake logging
GPS

headingDatum = 180

function headingInc(heading)
    if (heading > 180) or (heading < -180)
then
        error("too big")
    end

    if headingDatum > 360 then
        error("bad datum")
    elseif headingDatum < 0 then
        error("bad datum")
    end

    headingDatum = headingDatum +
heading
    if headingDatum > 360 then
        headingDatum = headingDatum - 360;
    elseif headingDatum < 0 then
        headingDatum = headingDatum +
360;
    end
    headingAbs(headingDatum)
end

function surfaceNow()
    depthAbs(0.35)
    pitchAbs(0)
    twiddleThumbs(20)
end

startLogFile("lakeSurface.log", 6)

surfaceNow()
twiddleThumbs(30)

--section 1
depthAbs(0.4)
headingAbs(90)
surgeDispInc(25)
```

```
--section 2
depthAbs(0.4)
headingAbs(0)
surgeDispInc(100)

--section 3
depthAbs(0.4)
headingAbs(90)
surgeDispInc(25)
surfaceNow()

--section 4
depthAbs(0.4)
headingAbs(180)
surgeDispInc(200)

--section 5
depthAbs(0.4)
headingAbs(90)
surgeDispInc(25)
surfaceNow()

--section 6
depthAbs(0.4)
headingAbs(0)
surgeDispInc(200)

--section 7
depthAbs(0.4)
headingAbs(90)
surgeDispInc(25)
surfaceNow()

--section 8
depthAbs(0.4)
headingAbs(180)
surgeDispInc(200)

--section 9
depthAbs(0.4)
headingAbs(90)
surgeDispInc(25)
surfaceNow()
```

```
--section 10
depthAbs(0.4)
headingAbs(0)
surgeDispInc(200)

--section 11
depthAbs(0.4)
headingAbs(90)
surgeDispInc(25)
surfaceNow()

--section 12
depthAbs(0.4)
headingAbs(180)
surgeDispInc(200)

--section 13
depthAbs(0.4)
headingAbs(90)
surgeDispInc(25)
surfaceNow()

--section 14
depthAbs(0.4)
headingAbs(0)
surgeDispInc(100)
surfaceNow()

--section 15
depthAbs(0.4)
headingAbs(270)
surgeDispInc(175)
surfaceNow()

headingLoopOff()
surgeDispLoopOff()

stopLogFile("lakeSurface.log")

twiddleThumbs(300)
twiddleThumbs(300)
twiddleThumbs(300)
twiddleThumbs(300)
```

8.9 Elk Lake Five-Metre Mission Script File

-- 5m mission on Elk Lake logging GPS
 	
headingDatum = 180
 	
function headingInc(heading)
  if (heading > 180) or (heading < -180)
then
    error("too big")
  end
 	
  if headingDatum > 360 then
    error("bad datum")
  elseif headingDatum < 0 then
    error("bad datum")
  end
 	
  headingDatum = headingDatum +
heading
  if headingDatum > 360 then
    headingDatum = headingDatum - 360;
  elseif headingDatum < 0 then
    headingDatum = headingDatum +
360;
  end
  headingAbs(headingDatum)
end
 	
function surfaceNow()
  depthAbs(0.35)
  pitchAbs(0)
  twiddleThumbs(20)
end
 	
startLogFile("5mLake.log", 6)
 	
surfaceNow()
twiddleThumbs(30)
 	
--section 1
depthAbs(5)
headingAbs(90)
surgeDispInc(25)
	--section 2
	depthAbs(5)
	headingAbs(0)
	surgeDispInc(100)
	
	--section 3
	depthAbs(5)
	headingAbs(90)
	surgeDispInc(25)
	surfaceNow()
	
	--section 4
	depthAbs(5)
	headingAbs(180)
	surgeDispInc(200)
	
	--section 5
	depthAbs(5)
	headingAbs(90)
	surgeDispInc(25)
	surfaceNow()
	
	--section 6
	depthAbs(5)
	headingAbs(0)
	surgeDispInc(200)
	
	--section 7
	depthAbs(5)
	headingAbs(90)
	surgeDispInc(25)
	surfaceNow()
	
	--section 8
	depthAbs(5)
	headingAbs(180)
	surgeDispInc(200)
	
	--section 9
	depthAbs(5)
	headingAbs(90)
	surgeDispInc(25)
	surfaceNow()
		--section 10
		depthAbs(5)
		headingAbs(0)
		surgeDispInc(200)
		
		--section 11
		depthAbs(5)
		headingAbs(90)
		surgeDispInc(25)
		surfaceNow()
		
		--section 12
		depthAbs(5)
		headingAbs(180)
		surgeDispInc(200)
		
		--section 13
		depthAbs(5)
		headingAbs(90)
		surgeDispInc(25)
		surfaceNow()
		
		--section 14
		depthAbs(5)
		headingAbs(0)
		surgeDispInc(100)
		surfaceNow()
		
		--section 15
		depthAbs(5)
		headingAbs(270)
		surgeDispInc(175)
		surfaceNow()
		
		headingLoopOff()
		surgeDispLoopOff()
		
		stopLogFile("5mLake.log")
		
		twiddleThumbs(300)
		twiddleThumbs(300)
		twiddleThumbs(300)
		twiddleThumbs(300)

8.10 Halifax Mission Script File

```
--Halifax mission 15 m

headingDatum = 180

function headingInc(heading)
    if (heading > 180) or (heading < -180) then
        error("too big")
    end

    if headingDatum > 360 then
        error("bad datum")
    elseif headingDatum < 0 then
        error("bad datum")
    end

    headingDatum = headingDatum + heading
    if headingDatum > 360 then
        headingDatum = headingDatum - 360;
    elseif headingDatum < 0 then
        headingDatum = headingDatum + 360;
    end
    headingAbs(headingDatum)
end

function surfaceNow()
    depthAbs(0.35)
    pitchAbs(0)
    twiddleThumbs(30)
end

startLogFile("halifax15.log", 1)
commentLogFile("halifax15.log", "waypoint 18
4433.743 Long 6401.012 Lat")

surfaceNow()
twiddleThumbs(30)

-- first straight section
depthAbs(15)
headingAbs(232.0)
commentLogFile("halifax15.log", "ping")
ping()
surgeDispInc(68)
commentLogFile("halifax15.log", "ping")
ping()
surgeDispInc(68)
commentLogFile("halifax15.log", "ping")
ping()
surgeDispInc(68)
commentLogFile("halifax15.log", "ping")
ping()

-- third straight section
depthAbs(15)
headingAbs(50)
commentLogFile("halifax15.log", "ping")
ping()
surgeDispInc(67)
commentLogFile("halifax15.log", "ping")
ping()
surgeDispInc(67)
commentLogFile("halifax15.log", "ping")
ping()
surgeDispInc(67)
commentLogFile("halifax15.log", "ping")
ping()

commentLogFile("halifax15.log", "waypoint 21
4433.539 Long 6400.985 Lat")
surfaceNow()

-- fourth straight section
depthAbs(15)
headingAbs(323)
commentLogFile("halifax15.log", "ping")
ping()
surgeDispInc(62)
commentLogFile("halifax15.log", "ping")
ping()
surgeDispInc(62)
commentLogFile("halifax15.log", "ping")
ping()
surgeDispInc(62)
commentLogFile("halifax15.log", "ping")
ping()
surgeDispInc(63)
commentLogFile("halifax15.log", "ping")
ping()
surgeDispInc(63)
commentLogFile("halifax15.log", "ping")
ping()

commentLogFile("halifax15.log", "waypoint 18
4433.743 Long 6401.012 Lat")
surfaceNow()

-- fifth straight section
depthAbs(15)
headingAbs(175)
commentLogFile("halifax15.log", "ping")
ping()
surgeDispInc(63)
commentLogFile("halifax15.log", "ping")
ping()
```

```
commentLogFile("halifax15.log", "waypoint 19    surgeDispInc(63)
4433.675 Long 6401.134 Lat")                   commentLogFile("halifax15.log", "ping")
surfaceNow()                                   ping()
                                               surgeDispInc(63)
-- second straight section                     commentLogFile("halifax15.log", "ping")
depthAbs(15)                                    ping()
headingAbs(142.0)                              surgeDispInc(63)
commentLogFile("halifax15.log", "ping")        commentLogFile("halifax15.log", "ping")
ping()                                         ping()
surgeDispInc(64)                               surgeDispInc(64)
commentLogFile("halifax15.log", "ping")        commentLogFile("halifax15.log", "ping")
ping()                                         ping()
surgeDispInc(64)                               surgeDispInc(64)
commentLogFile("halifax15.log", "ping")        commentLogFile("halifax15.log", "ping")
ping()                                         ping()
surgeDispInc(64)
commentLogFile("halifax15.log", "ping")        commentLogFile("halifax15.log", "waypoint 20
ping()                                         4433.539 Long 6400.985 Lat")
surgeDispInc(64)                               surfaceNow()
commentLogFile("halifax15.log", "ping")
ping()                                         headingLoopOff()
surgeDispInc(64)                               surgeDispLoopOff()
commentLogFile("halifax15.log", "ping")
ping()                                         stopLogFile("halifax15.log")

commentLogFile("halifax15.log", "waypoint 20   twiddleThumbs(300)
4433.539 Long 6400.985 Lat")                   twiddleThumbs(300)
surfaceNow()                                   twiddleThumbs(300)
                                               twiddleThumbs(300)
```

Bibliography

[ALLEN] B. Allen, R. Stokey, T. Austin, N. Forrester, R. Goldsborough, M. Purcell and C. von Alt, "REMUS: A small, low cost AUV; System description, field trials and performance results," in Proceedings of the 1997 Oceans Conference. Part 2 (of 2), Oct 6-9 1997, 1997, pp. 994-100.

[BACCOU] P. Baccou, B. Jouvencel, V. Creuze and C. Rabaud, "Cooperative positioning and navigation for multiple AUV operations," in Oceans 2001 MTS/IEEE - An Ocean Odyssey, Nov 5-8 2001, 2001, pp. 1816-1821.

[BUTLER] B. Butler and V.d. Hertog, "Theseus: a cable-laying AUV," in Proceedings of the Conference on Oceans '93. Part 1 (of 3), Oct 18-21 1993, 1993, pp. 210-213.

[DAMUS] R. Damus, J. Manley, S. Desset, J. Morash and C. Chryssostomidis, "Design of an inspection class autonomous underwater vehicle," in Ocean's 2002 Conference and Exhibition, Oct 29-31 2002, 2002, pp. 180-185.

[DOSSO] S.E. Dosso, N.E.B. Collison, G.J. Heard and R.I. Verrall, "Experimental validation of regularized array element localization," *J.Acoust.Soc.Am.,* vol. 115, pp. 2129-2137, 2004.

[ERIKSEN] C.C. Eriksen, T.J. Osse, R.D. Light, T. Wen, T.W. Lehman, P.L. Sabin, J.W. Ballard and A.M. Chiodi, "Seaglider: A long-range autonomous underwater vehicle for oceanographic research," *IEEE J.Ocean.Eng.,* vol. 26, pp. 424-436, 2001.

[EVANS1] J.C. Evans, K.M. Keller, J.S. Smith, P. Marty and V. Rigaud, "Docking techniques and evaluation trials of the SWIMMER AUV: An autonomous deployment AUV for workclass ROVs," in Oceans 2001 MTS/IEEE - An Ocean Odyssey, Nov 5-8 2001, 2001, pp. 520-528.

[EVANS2] J. Evans, P. Redmond, C. Plakas, K. Hamilton and D. Lane, "Autonomous docking for intervention-AUVs using sonar and video-based real-time 3D pose estimation," in Celebrating the Past... Teaming Toward the Future, Sep 22-26 2003, 2003, pp. 2201-2210.

[FLETCHER] B. Fletcher, "Chemical plume mapping with an autonomous underwater vehicle," in Oceans 2001 MTS/IEEE - An Ocean Odyssey, Nov 5-8 2001, 2001, pp. 508-512.

[HEARD] G. Heard, *Autonomous Underwater Vehicle Array Element Localization,* statement of work, Defence Research and Development Canada, 2002.

[HOBSON] B. Hobson, B. Schulz, J. Janet, M. Kemp, R. Moody, C. Pell and H. Pinnix, "Development of a micro autonomous underwater vehicle for complex 3-D sensing," in Oceans 2001 MTS/IEEE - An Ocean Odyssey, Nov 5-8 2001, 2001, pp. 2043-2045.

[KEMP] M. Kemp, B. Hobson, J. Meyer, R. Moody, H. Pinnix and B. Schulz, "MASA: A multi-AUV underwater search and data acquisition system," in Ocean's 2002 Conference and Exhibition, Oct 29-31 2002, 2002, pp. 311-315.

[MARTHINIUSSEN] R. Marthiniussen, K. Vestgard, R.A. Klepaker and N. Storkersen, "HUGIN-AUV concept and operational experiences to date," in Ocean '04 - MTS/IEEE Techno-Ocean '04: Bridges across the Oceans - Conference Proceedings, Nov 9-12 2004, 2004, pp. 846-850.

[PATTERSON] M, Patterson, and J. Sias, *Modular Autonomous Underwater Vehicle System*. US patent 5,995,882, Patterson et al., Patent and Trademark Office, 1999.

[RISH] Rish J.W. III, S. Willcox, R. Grieve and I. Montieth, "Operational testing of the battlespace preparation AUV in the shallow water regime," in Oceans 2001 MTS/IEEE - An Ocean Odyssey, Nov 5-8 2001, 2001, pp. 123-129.

[SHERMAN] J. Sherman, R.E. Davis, W.B. Owens and J. Valdes, "The autonomous underwater glider "Spray"," *IEEE J.Ocean.Eng.*, vol. 26, pp. 437-446, 2001.

[SIBENAC] M. Sibenac, W.J. Kirkwood, R. McEwen, P. Shane, R. Henthorn, D. Gashler and H. Thomas, "Modular AUV for routine deep water science operations," in Ocean's 2002 Conference and Exhibition, Oct 29-31 2002, 2002, pp. 167-172.

[SINGH1] H. Singh, J. Catipovic, R. Eastwood, L. Freitag, H. Henriksen, F. Hover, D. Yoerger, J.G. Bellingham and B.A. Moran, "Integrated approach to multiple AUV communications, navigation and docking," in Proceedings of the 1996 MTS/IEEE Oceans Conference. Part 1 (of 3), Sep 23-26 1996, 1996, pp. 59-64.

[SINGH2] H. Singh, R. Eustice, O. Pizarro and C. Roman, "Optical and acoustic habitat characterization with the SeaBed AUV," in Celebrating the Past... Teaming Toward the Fututre, Sep 22-26 2003, 2003, pp. 332.

[SOUSA] J.B. Sousa, F.L. Pereira and E.P. da Silva, "General control architecture for multiple AUVs," in Proceedings of the 1996 IEEE Symposium on Autonomous Underwater Vehicle Technology, Jun 2-6 1996, 1996, pp. 223-230.

[STEVENSON] P. Stevenson, "Development of reliable sub systems for Autosub," in Proceedings of the 1996 MTS/IEEE Oceans Conference. Part 2 (of 3), Sep 23-26 1996, 1996, pp. 711-716.

[STOKEY] R. Stokey, T. Austin, B. Allen, N. Forrester, E. Gifford, R. Goldsborough, G. Packard, M. Purcell and C. Von Alt, "Very shallow water mine countermeasures using the REMUS AUV: A practical approach yielding accurate results," in Oceans 2001 MTS/IEEE - An Ocean Odyssey, Nov 5-8 2001, 2001, pp. 149-156.

[THOREIFSON] J.M. Thorleifson, T.C. Davies, M.R. Black, D.A. Hopkin, R.I. Verrall, A. Pope, I. Monteith, V.D. Hertog and B. Butler, "Theseus autonomous underwater vehicle - a Canadian success story," in Proceedings of the 1997 Oceans Conference. Part 2 (of 2), Oct 6-9 1997, 1997, pp. 1001-1006.

[TRIBLE] G.M. Trimble, "Cetus UUV/EOD robotic work package: A low-cost shallow-water UUV system for underwater search and intervention," in Proceedings of the 1998 Oceans Conference. Part 1 (of 3), Sep 28-Oct 1 1998, 1998, pp. 369-373.

[TRIPP] S.T. Tripp, *Autonomous Underwater Vehicles (AUV'S) A Look at Coast Guard Needs to Close Performance Gaps and Enhance Current Mission Performance*, whitepaper, U.S.C.G. research and Development Center, 2001.

[WEBB] D.C. Webb, P.J. Simonetti and C.P. Jones, "SLOCUM: An underwater glider propelled by environmental energy," *IEEE J.Ocean.Eng.*, vol. 26, pp. 447-452, 2001.

[WICK] C.E. Wick and D.J. Stilwell, "A miniature low-cost autonomous underwater vehicle," in Oceans 2001 MTS/IEEE - An Ocean Odyssey, Nov 5-8 2001, 2001, pp. 423-428.

[1] "Seaeye Cougar," http://www.seaeye.com/cougar.html (accessed June 16, 2005).

[2] "Theseus An Autonomous Underwater Cable Laying Vehicle," Jul. 2001; http://www.ise.bc.ca/theseus.html (accessed June 1, 2005).

[3] "Monterey Bay 2003 Experiment," March 2005; http://www.mbari.org/aosn/ (accessed May 10, 2005).

[4] "REMUS Autonomous Underwater Vehicle," http://www.hydroidinc.com/remus_brochure.pdf (accessed June 12, 2005).

[5] "Webb Research Corporation, The Electric Glider," http://www.webbresearch.com/electric_glider.htm (accessed June 3, 2005).

[6] "Seaglider," http://www.apl.washington.edu/projects/seaglider/images.html (accessed May 25, 2005).

[7] "CETUS," http://auvlab.mit.edu/vehicles/vehiclespecCETUS.html (accessed May 23, 2005).

[8] "Canadian Forces Auxiliary Vessel "QUEST"," April 2005; http://www.atlantic.drdc-rddc.gc.ca/factsheets/15_research_sea_e.shtml (accessed June 11, 2005).

[9] "GAVIA – The Great Northern Diver," Oct., 2003; http://www.gavia.is/products/index.html (accessed June 16, 2005).